GRAPHENATED ELECTRODE PROTOCOL FOR ELECTROCHEMICAL NANOSENSING OF 17β-ESTRADIOL AS AN ENVIRONMENTAL ESTROGENEOUS ENDOCRINE DISRUPTOR

By

NURALLI MOHAMED

MSc Chemistry (University of the Western Cape)

A thesis submitted in fulfilment of the requirements for the degree of

PHILOSOPHIAE DOCTOR

In the

Department of Chemistry

Faculty of Science

University of the Western Cape, South Africa

Supervisor: Prof. Emmanuel I. Iwuoha

Co-supervisor: Professor Nazeem Jahed

May 2016

ABSTRACT

17β-Estradiol can be defined as an endocrine disruptor chemical with estrogenic activity, which can bind to the estrogen receptor in the body and potentially alter the normal physiological function of the endocrine systems. Estradiol has come into veterinary use both to cure and to prevent animal infections. But owing to its anabolic properties it is also illegally used in livestock production for growth promotion purposes. The presence of low concentrations of estrogens in the environment can cause abnormal sexual development of animals and decrease the average number of human spermatozoa. Therefore, we must monitor the concentration of estradiol in aquatic environment to protect the health of humans and animals. Generally, the detection of estradiol includes the use of high performance liquid chromatography (HPLC), surface plasma resonance (SPR), gas chromatography (GC), liquid chromatography (LC) and electrochemical enzyme-linked immunosorbent assay (ELISA). Although these techniques are useful, many of them are expensive and time consuming.

The main objective of this study was to utilise the capabilities of nanostructured material for the detection of estradiol. In this thesis glassy carbon and screen printed carbon electrodes surfaces were modified with conducting films of nanostructured reduced graphene poly (2,5-dimethoxy aniline) nanoparticles (PDMA-GA) for the application as electrochemical sensors. The PDMA-GA nanocomposites were prepared by the Hummer's method. Sensors were constructed by drop coating on the surfaces of the carbon electrodes with PDMA-GA films followed by drying at room temperature. The nanocomposite material was characterised by: scanning and transmission microscopies; FT-IR, UV-vis, AFM and Raman spectroscopies; voltammetry and electrochemical and impedance spectroscopy. The electroanalytical properties of estradiol were first studied by cyclic voltammetry followed by square wave voltammetry. These studies involved the optimisation of experimental conditions such as selection of adequate supporting electrolyte, choice of pH, film thickness and deposition time.

The detection of estradiol was performed using Poly-(2,5-dimethoxy aniline) (PDMA), Poly-(2,5-dimethoxy aniline) graphene oxide (PDMA-GO) and Poly-(2,5-dimethoxy aniline) graphene (PDMA-GA) at the optimised experimental conditions. This study provides a promising analytical tool for estradiol detection.

KEYWORDS

17β-Estradiol

Endocrine disruptor

High performance liquid chromatography

Surface plasma resonance

Liquid chromatography

Electrochemical enzyme-linked immunosorbent assay

Graphene poly (2,5-dimethoxy aniline)

Cyclic voltammetry

Square wave voltammetry

Poly-(2,5-dimethoxy aniline)

Poly- (2,5-dimethoxy aniline) graphene oxide

LIST OF ABBREVIATIONS AND ACRONYMS

AFM	Atomic Force Spectroscopy
APS	Ammonium persulfate
ARPES	Angle-resolved photo emission spectroscopy
CI	Chemical interface
CME	Chemically modified electrode
CMOS	Complementary metal-oxide-semiconductor
CNTs	Carbon nanotubes
CV	Cyclic voltammetry
CVD	Chemical vapour deposition
DBSA	Dodecyl benzene sulfonic acid
DDT	Dichlorophenyl trichloroethane
DES	Diethylstilbestrol
DNA	Deoxyribonucleic acid
DPV	Differential pulse voltammetry
DPV	Differential pulse voltammetry
EB	Emeraldine
EDCs	Endocrine disruptors
EDX	Energy dispersive x-ray spectrum
EIS	Electrochemical impedance spectroscopy
ELISA	Electrochemical enzyme-linked immunosorbent assay
EMI	Electromagnetic interference shielding
ES	Emeraldine salt
FET	Field-effect transistors
FT-IR	Fourier Transform Infrared spectroscopy
GA	Graphene
GC	Gas chromatography
GICs	Graphite intercalation compounds
GO	Graphene oxide
HOMO	Highest occupied molecular orbital
HOPG	Highly oriented pyrolytic graphite
HPLC	High performance liquid chromatography

HR-SEM	High resolution scanning electron microscopy
HR-TEM	High resolution tunnelling electron microscopy
IC	Integrated circuit
ICPs	Intrinsically conducting polymers
IL	Ionic liquids
ISE	Ion selective electrode
ISFETs	Industrial ion-sensitive field effect transistors
ITO	Indium tin oxide
LC	liquid chromatography
LE	Leucoemeraldine
LEDs	Light emitting diodes
LOD	Limit of detection
LR	Linearity
LUMO	Lowest unoccupied molecular orbital
MBE	Molecular beam epitaxy
PA	Poly-acetylene
PAHs	Polyacyclic hydrocarbons
PANI	Polyaniline
PBDEs	Polybrominated diphenyl ethers
PCBs	Polychlorinated biphenyls
PCDDs	Polychlorinated dibezodioxins
PCE	Power conversion efficiency
PDMA	Poly-(2,5-dimethoxyaniline)
PDMA-GA	Poly-(2,5-dimethoxyaniline) graphene
PDMA-GO	Poly-(2,5-dimethoxyaniline) graphene oxide
PN	Pernigraline
PPP	Poly-paraphenylene
PPY	Polypyrolle
SPR	Surface plasma resonance
STM	Scanning tunnelling microscopy
SWCNTs	Single- walled carbon nanotubes
SWV	Square wave voltammetry
TI	Transducer interface

UNEP	United Nations Environmental Programme
USEPA	United States Environmental Protection Agency
UV-vis	Ultraviolet-visible spectroscopy
WHO	World Health Organization
XRD	X-Ray diffraction

DECLARATION

I declare that **Graphenated electrode protocol for electrochemical nanosensing of 17β-estradiol as an environmental estrogenous endocrine disruptor** is my own work, that it has not been submitted before for any degree or examination in any other university, and that all the sources I have used or quoted have been indicated and acknowledged as complete references.

Signature ----------

Nuralli Mohamed **May 2016**

DEDICATION

I dedicate this thesis to my father Abdullah and mother, Yasmina Osman, my wife Rehana and my family for their patience and understanding.

ACKNOWLEDGEMENTS

I would like to express my sincere gratitude and appreciation to my supervisors Prof E Iwuoha and Prof N Jahed. My deepest and immense gratitude goes to Prof E Iwuoha for encouraging me to pursue my PhD studies. I acknowledge his guidance and encouragement which made the completion of this work possible. He is truly a man of vision and an inspiration to all in the Sensor Lab may we benefit from his wise council for many years to come. My special thanks to Prof N Jahed for his guidance, support and encouragement during my study. I express gratitude to all my colleagues, the Sensor Lab group for the wholehearted support, encouragement and cooperation. Thanks to Dr F Ajayi, for her encouragement and for checking the thesis. Also to Mrs Wilma Jackson who is the driving force of the Chemistry Department and Mr Timothy Lesch for his support and assistance.

LIST OF PUBLICATIONS

Tovide, Oluwakemi, Nazeem Jahed, **Nuralli Mohamed**, Ezo Nxusani, Christopher E. Sunday, Abebaw Tsegaye, Rachel F. Ajayi et al. "Graphenated polyaniline-doped tungsten oxide nanocomposite sensor for real time determination of phenanthrene." *Electrochimica Acta* 128 (2014): 138-148.

Pokpas, Keagan, Salma Zbeda, Nazeem Jahed, **Nuralli Mohamed**, Priscilla G. Baker, and Emmanuel I. Iwuoha. "Electrochemically Reduced Graphene Oxide Pencil-Graphite in situ Plated Bismuth-film Electrode for the Determination of Trace Metals by Anodic Stripping Voltammetry." *Int. J. Electrochem. Sci* 9 (2014): 736-759.

Mohamed, Nuralli, Nazeem Jahed, Rachel Ajayi, Priscilla Baker and Emmanuel Iwuoha. "Synthesis and spectroelectrochemistry of graphene-poly(2,5-dimethoxyaniline) nano-composite. *Electroanalysis*, Under Review.

Mohamed, Nuralli, Nazeem Jahed, Keagan Pokpas, Priscilla Baker and Emmanuel Iwuoha. Response profile of graphenised poly(2,5-dimethoxyaniline) electrochemical nanosensor for 17-beta-estradiol. *Sensors and Actuators B*: Chemical, Under Review.

TABLE OF CONTENTS

LIST OF FIGURES

LIST OF TABLES

CHAPTER 1

INTRODUCTION

This chapter gives a brief background on the aspects involved in this project namely; endocrine disruptors, chemical sensors, conducting polymers and graphene. Also, included in this chapter are the project's rationale and motivation, the aims, the specific objectives of the study and finally the thesis outline.

1.1 Background

The number and the variety of chemicals to which man and his environment are exposed to are increasing every year. Over a hundred thousand chemicals are estimated to be commercially available in the markets [1-2]. Of these chemicals, many have the potential to pollute the environment and consequently, have an impact on human health. Thousands of these substances are of natural origin and may be present as pollutants and contaminants in food, environmental media and commercial products. Thus, environmental pollution is a problem of great concern to scientists, governmental and regulatory agencies as well as, the public in general because of the hazardous nature of chemicals when present even at minute levels in the environment [3]. The monitoring of, risk assessment and the prevention of adverse health effects of chemical pollutants is a major challenge even though thorough control and prevention systems regarding chemical hazards are well recognised worldwide. During the last forty years, much attention has been focused on the potential of xenobiotic chemicals that interact with the endocrine system of animals and human populations [4]. The endocrine system is one of the body's main communication networks and is responsible for controlling and coordinating numerous bodily functions such as body energy levels, reproduction, growth and development, internal balance of bodily systems and response to surroundings, stress, and injury.

Initially hormones are produced by the endocrine tissues, which include the ovaries, testes, pancreas, pituitary, and thyroid glands and then secreted into the blood to act as the body's chemical messengers. Whilst in the blood they direct communication and coordinate functions between other tissues throughout the body. Hormones work with the nervous, reproductive and respiratory systems to control body energy levels, reproduction, growth and the development of internal balance of bodily systems; also, referred to as homeostasis [5].

The term "endocrine disruptors" was coined in 1991 at a conference held at the Wingspread Conference Centre in Racine, Wisconsin [6]. This term was attributed to endocrine disrupting chemicals or compounds that interfere with the body's hormonal functioning. Endocrine disrupting compounds (EDCs) have the potential to elicit negative effects on the endocrine systems of humans and wildlife. Various natural and synthetic chemical compounds including pharmaceuticals, pesticides, industrial chemicals, and heavy metals have been identified to induce estrogenic-like responses [7]. These compounds can modulate both the endocrine and immune systems resulting in the alteration of homeostasis, reproduction, development and behaviour. Some of the effects of these chemicals on the endocrine and reproductive system include their ability to: mimic the effect of endogenous hormones, antagonize the effect of endogenous hormones and disrupt the synthesis and metabolism of the endogenous hormones and disrupt the synthesis of hormone receptors [8].

In 1996 the European Commission defined "endocrine disruptors as an exogenous substance that causes adverse effects on intact organism or its progeny and sub population [9]. A broader definition which includes all substances that affect endocrine functions via interference with natural hormone (e.g. estrogen, androgen or thyroid hormones) pathways was proposed by the United State Environmental Protection Agency (USEPA) where it was defined as an exogenous substance that interfere with the synthesis, secretion, transport, binding action or elimination of the natural hormones in the body that are responsible for maintenance of homeostasis,

reproduction, development and/ or behaviour. To date, approximately 60 chemicals have been identified as endocrine disruptors. Chemicals with hormonal activity fall into three broad classes namely: synthetic chemicals used in industry, agriculture and consumer products, synthetic chemicals used as pharmaceutical drugs and natural chemicals found in human and animal food (phytoestrogens). About half of these compounds are chlorinated, including dioxins (PCDDs), polychlorinated biphenyls (PCBs), Dichlorophenyl trichloroethane DDT, bisphenol A, polybrominated diphenyl ethers (PBDE's) and a variety of phalates [10].

This study was focused on the testing and monitoring of estrogenic EDCs, designated as e-EDCs, which are either hormonal estrogens or chemicals which mimic or induce estrogenic-like response in an organism. These compounds have varying degrees of potency, some being strongly active compounds, whilst others are of weak estrogenic activity. The aqueous solubility of hydrophobic endocrine disrupting compounds influences their distribution, bioavailability, and their persistence in the aquatic environments. Activity assays that evaluate the overall estrogenic potential as well as, concentration, cumulative effects, and potency of the chemical are essential for assessing the total environmental estrogenic potentials [11]. This broad class of chemicals includes both natural and synthetic estrogens (e.g. xenoestrogens and pseudo estrogens). The majority of e-EDCs are ubiquitous since they may be present in all compartments of the environment (water, air, soil and sediment) during imperfect manufacturing processes and /or leaching from the final end products. These contaminants are found in various environmental matrices, but they are mainly detected in the aquatic environment, particularly vulnerable to pollution, because of considerable intentional release of chemicals into rivers, lakes, and the sea (mostly through effluents from sewage treatment plants and factories), and accidental releases of chemicals through spills, run-off and atmospheric deposition [12].

These EDCs often occur in domestic' effluents, industrial wastewaters, landfill effluent and livestock wastes that are considered as main sources of endocrine disruptors to the aquatic environment [13-14]. It has been postulated that increase in the incidences of breast and testicular cancers in humans may be caused by exposure to e-EDCs especially via drinking water whose source is from surface water [14].

Different types of estrogeneous endocrine disruptors have been reported which include: 17β-estradiol, estriol, estrone which play a very important role in women's fertility and whose concentrations and changes are closely related to human's health status. EDCs have received increased attention in water quality management and healthcare due to their widespread presence in the environment and toxic activity even at low concentrations [13]. We will mainly focus on the determination of 17β-Estradiol (referred as estradiol hereafter) which can be defined as an endocrine disrupting chemical with estrogenic activity, which can bind to the estrogen receptor in the body and potentially alter the normal physiological function of the endocrine systems [14-16]. Estradiol has come into veterinary use both to cure and to prevent animal infections [17]. But owing to its anabolic properties it is also illegally used in livestock production for growth promotion purposes [18]. The presence of low concentrations of estrogens in the environment can cause abnormal sexual development of animals and decrease the average number of human spermatozoa [19]. Therefore, we must monitor the concentration of estradiol in aquatic environment to protect the health of humans and animals. Generally, the detection of estradiol includes the use of high performance liquid chromatography (HPLC) [20], surface plasma resonance (SPR) [21], gas chromatography (GC) [22], liquid chromatography (LC) [23] and electrochemical enzyme-linked immunosorbent assay (ELISA).

Although these techniques are useful, many of them are expensive or require time consuming derivation steps. In recent years, chemical sensors have attracted considerable interest because of their intrinsic advantages, such as low cost, high sensitivity and high compatibility with advanced micromachining technologies [24]. Here we propose a novel assay system based on specific receptor binding to detect estrogenic compounds using sensor technology.

A sensor is generally a device which transduces a physical or chemical parameter into an electrical or optical signal. Physical parameters which are commonly monitored with sensors are temperature, pressure, force, magnetic field etc. while chemical parameters of interest most often are the concentration of chemical substances. Chemical sensors differ significantly from physical sensors in the sense that the numbers of chemical parameters are almost infinite. The number of different gas pollutants in the air or the number of proteins in the human body is so high that selectivity or specificity becomes a crucial property of chemical sensors. While sensors for temperature, acceleration, etc. can be hermetically encapsulated, - the chemical sensor easily becomes affected by interfering substances as well as environmental effects such as light, corrosion, etc. [25]. Chemical sensors are finding more and more applications in chemical analysis, in environmental monitoring, in medicine and various other industries. A great number of chemical sensors have been developed and commercialized over the last decade [26-29].

Everyday clinical analyses are based on the use of ion-selective electrodes (ISE), - pH- sensitive electrodes are probably the most popular chemical sensor used in analytical chemistry, - and industrial ion-sensitive field effect transistors (ISFETs) are applied in food tests, to name a few of the successfully introduced sensors. Notably enough of the success of some of these chemical sensors relies on the use of conducting polymers which effectively ensure the relay of electrons required in chemical reactions.

Conducting polymers are a new class of materials with potent applications in several growing new technologies, such as energy storage [30-32], molecular recognition [33-34], electromagnetic interference (EMI) shielding [35-36] and opto-electronic devices [37-38]. All conducting polymers exhibit highly reversible redox behaviour with a distinguishable chemical memory and hence have been considered as prominent new materials for the fabrication of chemical sensors. Among all conducting polymers, polyaniline (PANi) has achieved widespread importance because of its wide unique conduction mechanism and high environmental stability. Conducting polyaniline has been used as a sensing material for different vapours like methanol, ethanol, acetone and benzene [39] where the effect of these vapours on the electronic properties of polyaniline has been investigated. Conducting polymers may also be used as sensitive layers in chemical micro sensors [40]. Selected functionality introduced into the polyaniline structure by appropriate counter ions leads to substantial changes in the chemical and biological sensing [41]. Polyaniline, the polymer resulting from the oxidative polymerization of aniline, is built up from reduced (B-NH-B-NH) and oxidized (B-N=Q=N-) repeat units, where B denotes benzoid and Q denotes quinoid ring. Thus, the ratio of amine and imine yields various structures, such as leucoemaraldine (reduced form), emeraldine base (50% oxidized form) and pernigraniline (fully oxidized form).

Unlike other phenylene-based conducting polymers, polymers based on aniline and its analogues can be doped/undoped on exposure to an acidic or alkaline environment. This type of doping mechanism is due to the presence of the –NH group in the polymer backbone, the protonation/deprotonation of which brings about a change in the electronic conductivity as well as the colour. This simple doping/undoping phenomenon makes polyaniline and its analogues highly suitable for industrial applications [42]. Recently, synthesis of some substituted polyanilines which are soluble in organic solvents as well as in water have been achieved [43-44].

To obtain materials with superior electrical and optical properties, for this study we have selected 2,5-dimethoxy aniline. To further improve these properties, we included graphene to create a highly conductive nanocomposite.

Graphene- based nanomaterials have captured great interest among physicist, chemists and materials scientists alike. Graphene is a two-dimensional (2-D) sheet of carbon atoms in a hexagonal configuration with atoms bonded by sp^2 bonds. These bonds and their electron configuration are the reasons for the extraordinary properties of graphene, which includes a very large surface area [at 2630 m^2/g, it is double that of single-walled carbon nanotubes (SWCNTs)], a tunable band gap, room-temperature Hall effect, high mechanical strength (200 times greater than steel), and high elasticity and thermal conductivity [45]. Graphene is an ideal material for electrochemistry [46-49] because of its very large 2-D electrical conductivity, large surface area and low cost. In comparison with carbon nanotubes (CNTs), two advantages of graphene are apparent. Firstly, graphene does not contain metallic impurities as CNTs do [50]. In many cases, such impurities dominate the electrochemistry of CNTs (so far, such negative influence is known for hydrazine [50-52], hydrogen peroxide [53-54], halothane [55], glucose [56], amino acids [57]). Secondly the production of graphene uses graphite, which is cheap and accessible.

1.2 Problem statement

The concern about the human health associated with the exposure to synthetic chemicals in the environment has brought about the interest in the development of a suitable method of analysis that is cheaper and easier to use in identifying and quantifying them. Despite the effectiveness of conventional methods in terms of high accuracy and low detection limit of the techniques which includes: high performance liquid chromatography (HPLC), surface plasma resonance (SPR), gas chromatography (GC), liquid chromatography (LC) and electrochemical enzyme-linked

immunosorbent assay (ELISA), that have been reported and adopted. However, they have limitations, in that, they are very costly, time consuming, laboratory borne, they need a lot of skill in the operation and sometime suffer from low detection limit. Apparently, there is the need to overcome all these challenges. Consequently, a cheaper, faster, easier to use low power consuming, and user friendly, and on site analytical device suitable to compliment or substitute for these classical methods is developed in the form of a graphenated polyaniline nanocomposite based electrochemical sensor for the detection and quantitative determination of estradiol.

1.3 Rationale and motivation

The increasing concern worldwide over the adverse effects of endocrine disruptors to the health of humans and wild-life has created a need for screening systems to detect xenoestrogens, a diverse group of environmental chemicals that mimic estrogenic actions and are hypothesized to decrease male fertility. The ability to detect xenoestrogens in environmental samples is a task that is being actively pursued by bioorganic chemists. Because of their ubiquitous nature, the need for the detection of trace amount of this chemical using simple, low cost, highly sensitive, low detection range, highly selective and easy to handle, electro analytical techniques become necessary.

The commonly used techniques such as chromatography and mass spectroscopy are very expensive and time consuming. For that reason, it has become extremely important to effectively monitor the hazardous nature of endocrine disrupting chemical in an environmental sample using new and simple analytical methods. Monitoring and evaluating the effects of these chemicals require new technologies that are capable of screening various chemicals in the field. For proper and effective screening and monitoring of these chemicals in environmental samples, an electrochemical technique which exhibit low detection limit and high sensitivity is necessary for this purpose.

1.4 Aim

The aim of this study was to develop nanocomposites based on graphenated polydimethoxy polyaniline nanosensors for the detection of selected environmental estrogens in water. The objectives of this study were as follows:

1. To prepare graphene from graphite

2. To chemically prepare poly (2,5-dimethoxyaniline) (PDMA)

3. To electrochemically and chemically prepare graphenated poly (2,5-dimethoxy aniline) (PDMA-GA)

4. To interrogate and model responses of the PDMA, PDMA-GO and PDMA-GA nanocomposites using High Resolution Scanning Electron Microscopy (HR-SEM), High Resolution Transmission Electron Microscopy **(**HR-TEM**),** Fourier Transform infrared spectroscopy (FT-IR), Ultraviolet Spectroscopy (UV-Vis), Raman spectroscopy, Atomic force spectroscopy (AFM), and X-ray diffraction (XRD).

5. To electrochemically characterize and model the responses of the graphenated PDMA (PDMA-GA) nanocomposites using Cyclic Voltammetry (CV), Differential Pulse Voltammetry (DPV) and Square Wave Voltammetry (SWV), and Electrochemical Impedance Spectroscopy (EIS).

6. To determine the detection limit, sensitivities and analytical linear range of the PDMA-GA sensor systems with respect to estradiol.

1.5 Thesis lay-out

This thesis consists of six chapters.

Chapter 1: This chapter gives a brief background on the aspects involved in this project namely; endocrine disruptors, chemical sensors, graphene and conducting polymers. Also included in this chapter are the project's rationale and motivation, the aim and specific objectives of the study as well as the thesis outline.

Chapter 2: The focus of this chapter is the discussion on estradiol, methods of detection, sensors, and the different types of sensors, electro-catalysis, polymers, and the different type of polymers with special emphasis on conducting polymers. Discussed here also, is the role of conducting polymers in chemical sensors. Finally, a brief background of the characterisation techniques used in the study is also discussed.

Chapter 3: This chapter gives information on materials and different experimental procedures employed for the chemical preparation of graphene oxide, graphene, poly-(2,5-dimethoxy aniline), poly-(2,5-dimethoxy aniline) graphene oxide (PDMA-GO) and poly-(2,5-dimethoxy aniline) graphene (PDMA-GA) modified electrodes and the fabrication of electrochemical sensors based on the graphenated-polyaniline derivative.

Chapter 4: This chapter presents results and discussion on the chemical synthesis of graphite oxide and graphene. The morphology and structural characterisation of the prepared materials studied using techniques such as HR-SEM, HR-TEM, FT-IR, XRD, AFM, RAMAN and UV-vis spectroscopy are discussed in this chapter.

Chapter 5: The results and discussion on the chemical polymerization of graphene-poly-dimethoxy aniline (PDMA-GA) modified electrodes, the morphology and structural characterisation of PDMA-GA are presented in this chapter. Electrochemical analysis by means of CV and SWV as well as the catalytic effect of the modified electrodes on estradiol are discussed.

Chapter 6: Conclusion and recommendations.

CHAPTER 2

LITERATURE REVIEW

The focus of this chapter is the discussion on estradiol, methods of detection, sensors, and the different types of sensors, electro-catalysis, polymers, and the different type of polymers with special emphasis on conducting polymers. Discussed here is also the role of conducting polymers in chemical sensors. Finally, a brief background of the characterisation techniques used in the study is also discussed.

2.1 Chemistry of the monitored Estrogen

2.1.1 Chemistry of Estradiol

Estradiol generally refers to the 17-beta isomer of estradiol, an aromatized C18 steroid with hydroxyl group at 3-beta and 17-beta position. Estradiol 17-beta is the most potent form of mammalian oestrogenic steroids. In humans, it is manufactured primarily by the cyclic ovaries and the placenta. It is also produced by the adipose tissue of men and postmenopausal women. The 17-alpha isomer of estradiol binds weakly to the oestrogen receptors and exhibit little oestrogenic activity in oestrogen-responsive tissues **Figure 1**. It is a white or slightly yellow odourless crystalline powder that is very soluble in acetone, ethanol and dioxane and other organic solvents. Exogenous oestrogens are metabolized in the same manner as endogenous oestrogens. Circulating oestrogens exist in a dynamic equilibrium of metabolic inter-conversions. These transformations take place mainly in the liver. Estradiol is converted reversibly to estrone, and both can be converted to estriol, which is the major urinary metabolite [58].

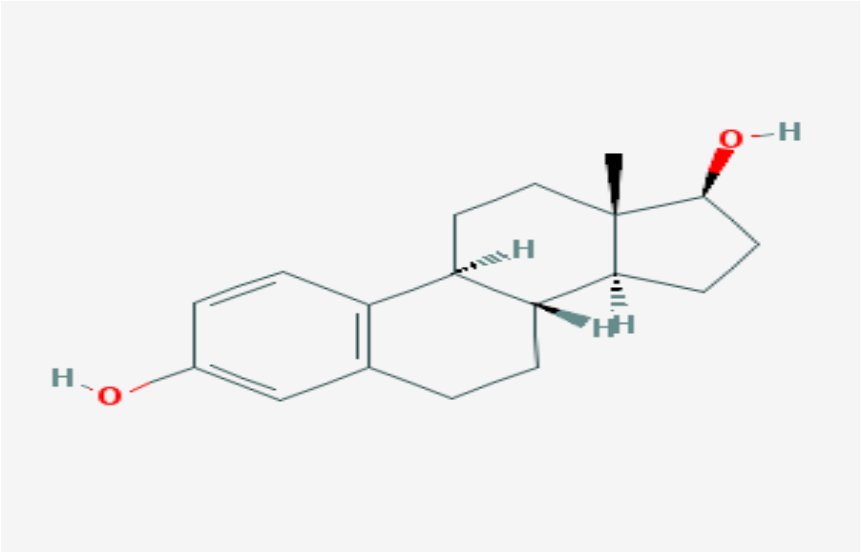

Figure 1: Chemical structure of Estradiol [58]

2.1.2 Method of detection of estradiol

There are a few instrumental analysis methods, such as high performance liquid chromatography (HPLC) [59], surface plasma resonance (SPR) [60], gas chromatography (CG) [61], liquid chromatography (LC) [62] and electrochemical enzyme-linked immunosorbent assay (ELISA) [63]. Many of these techniques are expensive or require time-consuming derivation steps. In recent years, electrochemical immunoassays have attracted considerable interest because of their intrinsic advantages, such as low cost, high sensitivity and high compatibility with advanced micromachining technologies [64].

The electrochemical detection of oestrogens has not been easy due to fouling of the electrode surface during estradiol detection. The phenolic group of the estradiol gets oxidized to the phenoxonium ion. However, coupling of the phenoxonium ions will form a dimer or a quinone, which is known to passivate or foul the electrode surface, leading to a weak, transient loss of estradiol detection signal at naked electrodes [65]. As far as electrochemical detection of estradiol goes, several people have detected estradiol electrochemically. Hu *et al* [65] detected estradiol using a nafion modified glassy carbon electrode in the presence of cetyltrimethylammonium bromide, Janegitz *et al* [66] detected estradiol using a thin film containing reduced graphene oxide

and dihecylphophate, and Liu *et al* [67] detected estradiol using a carbon nanotube [Ni(Cylam)] composite electrode based on two-factorial design, to name but a few. In this work, an electrochemical method for the detection of the selected oestrogens have been developed in the form of graphenated modified poly (2,5-dimethoxyaniline), constructed by deposition of poly (2,5-dimethoxyaniline) doped with graphene on the surface of a screen-printed electrode, which was then used as an electrochemical sensor.

2.2 Polymers

2.2.1 History of Natural and Synthetic Polymers

The polymer industry is a huge industry and is not very old. Natural polymeric products, e.g. pitch, milk, egg white, gum arabic and beeswax, were known to the ancient Egyptians and Greeks. They were combined with minerals to be used as preparation coating compositions for walls, burial chambers, etc. The Chinese developed wood lacquers by utilizing the sap from the Chinese tree, Rhus Vernicifera. While the painters in Europe began to use linseed oil (from flax). During the eleventh century, the monk, Theophilus, described how varnish was made (cooked) from linseed oil and tall oil (i.e. pine tree gum also called 'rosin'). Centuries ago, natives of South America gelled 'latex', a milky white sap of rubber trees, to form rubber balls that were utilized in the National Sport of the Mayan Indians. In 1839, Goodyear (US) vulcanized rubber by heating it with sulfur. Since the start of the twentieth century, not a lot had been done to improve on the natural materials (polymers) accessible to mankind. Nevertheless, the situation changed rapidly after that. When the Civil War ended in America there was a scarcity of ivory (used to make billiard balls and piano keys). In 1868, John Hyatt, a printer, developed the first commercial plastic, i.e. cellulose nitrate (gun cotton). Utilizing only natural materials, Hyatt manufactured a stiff polymer by treating cotton with HNO_3. Camphor oil (a whitish, terpene ketone, $C_{10}H_{16}O$, from the camphor tree) was added as a 'plasticizer' making the stiff gun cotton moldable. Hyatt patented cellulose nitrate plastic under the name 'celluloid' which up till today is still utilized in the making of combs and guitar picks. Celluloid products, such as photographic film and plastic collars, are now developed from other polymers due to the flammability of celluloid. Dr. Leo Bakeland discovered the first phenolic polymer made from phenol and formaldehyde, called 'Bakelite'. Shaping these ingredients under heat and pressure, led to a hard, heat resistant plastic being formed. Phenolic resins have been utilized in the production of pot handles, electrical plug outlets and adhesives for laminating plywood.

Herman Staudinger (Germany) suggested his 'macromolecular hypothesis', stating that substances like natural rubber were not colloidal, physical associations of small molecules but were truly long-chain molecules of extremely high molecular weight. Twenty years after Bakelite the next polymers were discovered, which got the ball rolling. In 1927, American scientist, Wallace Carothers, produced and characterized alkyd resins for paints. Carothers is regarded as the father of polymer chemistry, because his research explained polymerization and gave rise to the formation of many new polymers [68].

2.2.2 Conducting Polymers (Intrinsically conducting polymers, ICPs)

Traditionally polymers were used as insulators however this function has become redundant. Polymers are now being utilized as conductors with a host of novel applications. Scientists have since combined their abilities to study organic solids that display amazing conducting properties. Numerous organic compounds, which effectively transport charge, are generally divided into three groups, that is, charge transfer complexes/ion radical salts, organometallic species and conjugated organic polymers. A new class of polymers, known as intrinsically conducting polymers (ICPs) or electro-active conjugated polymers has since materialized. These materials display interesting electrical and optical properties which up to that time was only existent in inorganic systems. Electronically conducting polymers differed from inorganic crystalline semiconductors, e.g. silicon, with regard to two significant features; that polymers are molecular in nature and lack long range order [69]. A polymer becomes intrinsically conductive when there is an overlap of molecular orbitals to allow the formation of delocalized molecular wave function. Furthermore, the molecular orbitals must be partially filled so that there is a free movement of electrons throughout the lattice [70]. Conducting polymers have a π-electron backbone which is responsible for their extraordinary electronic properties, such as electrical conductivity, low energy optical transitions, low ionization potential and high electron affinity.

This extended π- conjugated system of the conducting polymers comprises of single and double bonds alternating along the polymer chain. The excellent electrical conductivity achieved in such organic polymers has caused them to being referred to as 'synthetic metals'. Numerous uses of conducting polymers, including analytical chemistry and bio sensing devices, have been reviewed by various researchers [71-75]. The result of their research has led to the modification of the surface of the conventional electrodes, giving rise to new and interesting properties. Some of which, were applied in electro-catalysis, membrane separation and chromatography. This also created novel technological possibilities in design of chemical and biochemical sensors [76].

2.2.3 Background of ICP's

Studies on conducting polymers increased soon after the discovery of poly (sulphur nitride) [$(SN)_x$] in 1975, which becomes superconducting at low temperatures [77]. Even though conducting polymer complexes in the form of tetracyano and tetraoxalato-platinates, the Krogman salts charge transfer complexes [78], had been known earlier, the significance lies in the rediscovery of poly-acetylene (PA) in 1977 by Macdiarmid and Heeger, University of Pennsylvania (initially discovered by Shirikawa *et al.* [79] 1977 using Ziegler Natta type polymerization catalyst). They improved the electrical conductivity of PA (10^{-9} Scm^{-1}) by several orders, i.e. 10^5 Scm^{-1}, by simply doping with oxidizing agents e.g. I_2, AsF_5, $NOPF_6$ (p-doping) or reducing agents (n-doping) e.g. sodium napthalide. Poly-paraphenylene was produced by Ivory *et al* (1979) [80], producing highly conducting charge transfer complexes with both n and p type dopants. Doping with AsF_5 increases its conductivity from 10^{-5} to 500 Scm^{-1}. Theoretical models and electron spin resonance measurements indicate that the charge transport in PPP is a polaron/bipolaron. PPS was the first non-rigid, but not fully carbon, backbone linked conducting polymer. This was a significant discovery, since its property of solution processability led to the viability for commercially conducting plastics [81].

The most studied of the polyheterocyclines was polypyrrole (PPY). The electrochemical oxidation of pyrolle in aqueous H_2SO_4 can be conducted on a platinum electrode. The product of this oxidation is a conducting polymer known as "Pyrrole Black". Kanazawa *et al* (1979) [82] manufactured coherent films of PPY with a conductivity 100 Scm^{-1} which displayed excellent air stability. Nonetheless, the biggest drawback is in its insolubility in any organic solvents. PTH displayed significant stability of both its oxidized (p-doped) conducting form and its neutral (undoped) insulating form in both air and water. It exhibited high doping levels up to 50% which may be ascribed to its partially crystalline nature that has been confirmed by X-ray photoelectron spectroscopy studies [83]. Numerous conducting polymers, such as polyfuran, polyindole, polycarbazole, polyanile etc. have also been synthesized.

2.2.4 Conduction mechanism

Conducting polymers exhibit improved electrical conductivity by several orders of doping magnitude. The concepts of solitons, polarons and bipolarons have been used to explain the electronic phenomena in these systems [84]. Conductivity in conducting polymers is affected by a number of factors, including polaron length, the conjugation length, and overall chain length and by charge transfer to adjacent molecules [85]. This can be explained by large numbers of models based on intersolition hopping between localized states assisted by lattice vibrations, intra-chain hopping of bipolarons, variable range hopping in three-dimensions and charge energy limited tunnelling between conducting domains [86].

2.2.4.1 Polarons

The polaron is a radical ion (spin ½) associated with a lattice distortion, and the presence of localized electronic states in the gap referred to as polaron states. The capacity of a charge to significantly cause deformation around the lattice is the manifestation of a strong electrophonon coupling, which is thus denoted as p+ or p- depending on the sign of the charge. The level of polarons is within the upward shift of the highest occupied molecular orbital (HOMO) and the downward shift of the lowest unoccupied orbital (LUMO). As a result, the charge localization process is favourable relative to the band process, thus a localized electronic state in the gap [87]. This is different compared to a case of inorganic semiconductor as shown in **Figure 2**. In the **Figure 2 (a)**, the level of the mid gap is the level of the distorted region and is effectively added to the undistorted states described as the HOMO and LUMO. The formation of these distorted levels is favourable since it gives rise to an overall reduction in energy, which is referred to as binding energy, associated with the formation of a polaron. However, there could also be bipolaron being formed at this stage, as shown in **Figure 2 (b).**

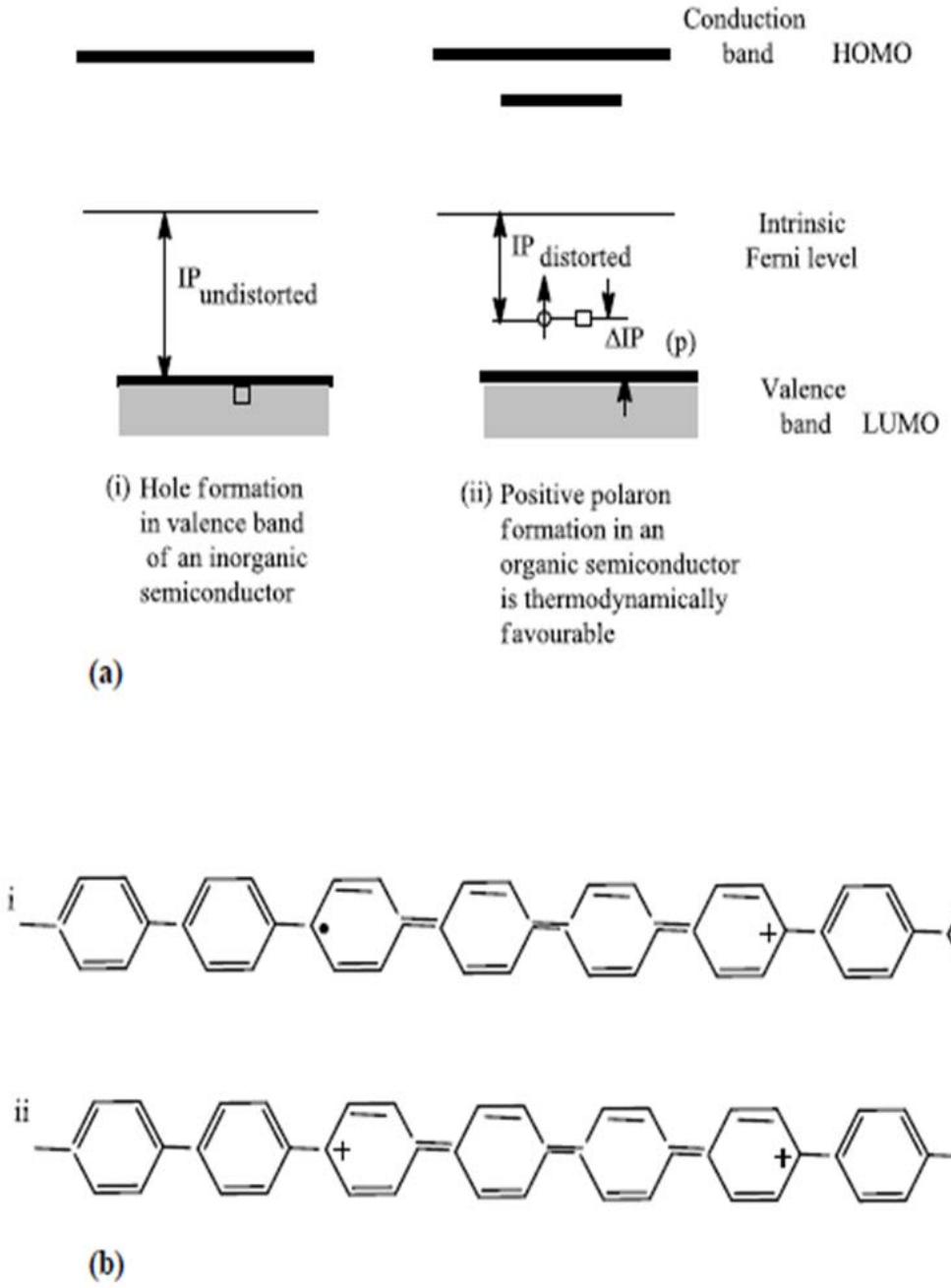

Figure 2: Distorted geometry of the excited state (lattice relaxation) results in a reduction of the ionization potential Δ IP (a) (i) Accommodation of charged within two' polaron' states within the semiconductor gap (ii) (b) and a geometrical representation of (i) a single polaron and (ii) a doubly charged polaron having a spin 0 and charged ±2e (b) [87]

2.2.4.2 Bipolarons

A bipolaron is a bound pair of polarons, formed when two polarons (i.e. the combination of electron distortion) of like charges come to interact in a conjugated system. Of course, the two polarons must be close enough to share the same distortion and develop a lower energy, which effectively leads to attraction between the two polarons. If the interaction is large enough, then a bound polaron will be formed. This can be related to theory of conductivity of a material consisting of two electrons coupled through lattice vibration, i.e. a phonon. The formation of a bipolaron implies that the energy gained by the interaction with the lattice is larger than the coulomb repulsion between the two charges of the same sign confined in the same location. Bipolarons and polarons processes lead to carrier mobility which results in high conductivity of the polymers i.e. in doped conducting polymers such as polythiophene [88].

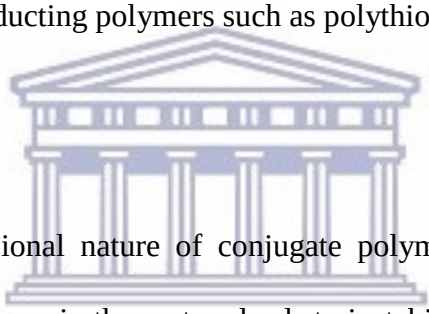

2.2.4.3 Solitons

Due to the quasi one-dimensional nature of conjugate polymers, the interaction between the electron and the carbon backbones in the system leads to instability in relation to the dimerization of the lattice, which is usually portrayed as an alteration of single and double bonds. Resulting in an excitation state referred to as solitons occurred. Solitons can be referred to as mobile charges or neutral defects or “kinks” in the polymer chain that propagate down the chain and reduces the barrier of interconversion. Compared to a polaron, a soliton has an unusual spin charge separation: a neutral soliton has ½ spin, while a charge soliton is spinless. Polarons, Bipolarons and solitons are commonly believed to play a major role in doping [89-90]. The formation of the charge carriers in doped polyaniline shows that controlling the concentration of dopant can lead to an enhancement in conductivity due to the formation of charge carriers i.e. polarons/bipolarons which are facilitated through manipulation from the external potential and the coulomb field of a counterion distributed along the chains [91].

Figure 3 shows the schematic illustration of doped polyaniline showing the formation of charge carrying polarons (radical cations) and bipolarons (di-cations)

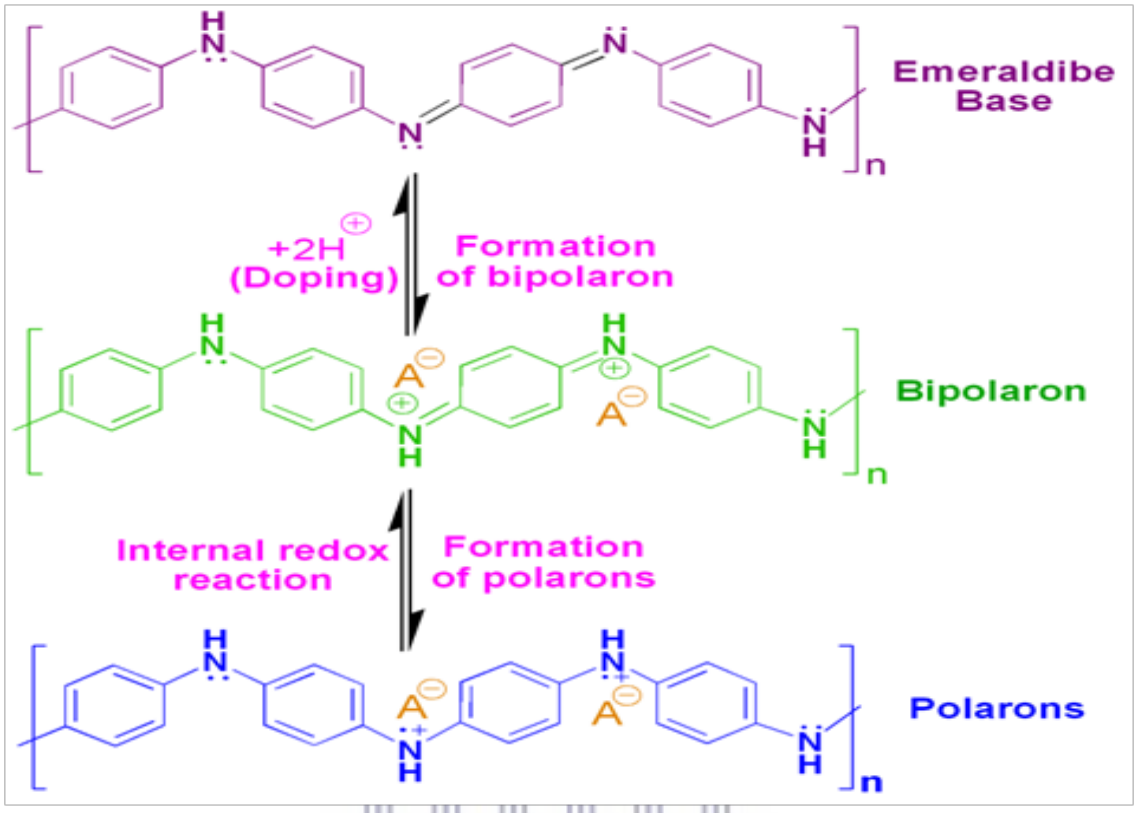

Figure 3: Schematic illustration of doped polyaniline showing the formation of charge carrying polarons (radical cations) and bipolarons (di-cations) (Intech Science, Technology and Medicine)

The foundation of conductivity in heterocyclic conjugated polymers can be accredited to the nearby sp^2 hybridised carbon centres in the polymer backbones. A valence electron on each centre resides in a p_z orbital, which is orthogonal to the three sigma bonds. During doping, by oxidation, the electron in these delocalized orbitals attained high mobility and some of these electrons were removed. Therefore, a conjugated p-orbital is formed as a one-dimensional electronic band. In this case, the electrons within this band are partially emptied and are mobile. Theoretically, an unfilled band can accept electrons if the same material is doped by reduction. The fact of the matter is that most organic conductors are doped oxidatively to give p-type materials.

Delocalisation is restricted by both disorder and coulombic interactions between electrons and hole, and generally, materials with conductivities less than 10^{-8} Scm^{-1} are deemed insulators, while those between 10^{-8} and 10^{3} cm^{-1} are semiconductors and those with conductivities greater than 10^{3} Scm^{-1} are considered conducting [92-94]. The conducting properties of conjugated polymers are derived from the delocalisation of p-electron bonding along the polymer chain. The ease with which the polymer can be oxidized or reduced is very significant and this accounts for the choice of π- bonding system which can readily be twisted without much interference of the σ (sigma) bonds which is mainly the dependable bond holding the polymer together. Different from poly-acetylene and deliberately because of its limitations, heterocyclic conjugated polymers in the form of polyaniline, polypyrolle, polythiophene, polyfuran and their derivatives, which are known to be thermally stable due to their aromaticity, can be easily produced by electrochemical or chemical oxidation of their neutral polymers. The mechanism of the two types of preparation leads to the polymers in their doped (oxidized) state. The neutral polymer can thus be obtained when they are reduced by electrochemical or chemical methods. Various types of conducting polymers, structures, conductivities (S cm^{-1}), and types of doping (n or p) for some conducting polymers are presented in **Figure 4** [91].

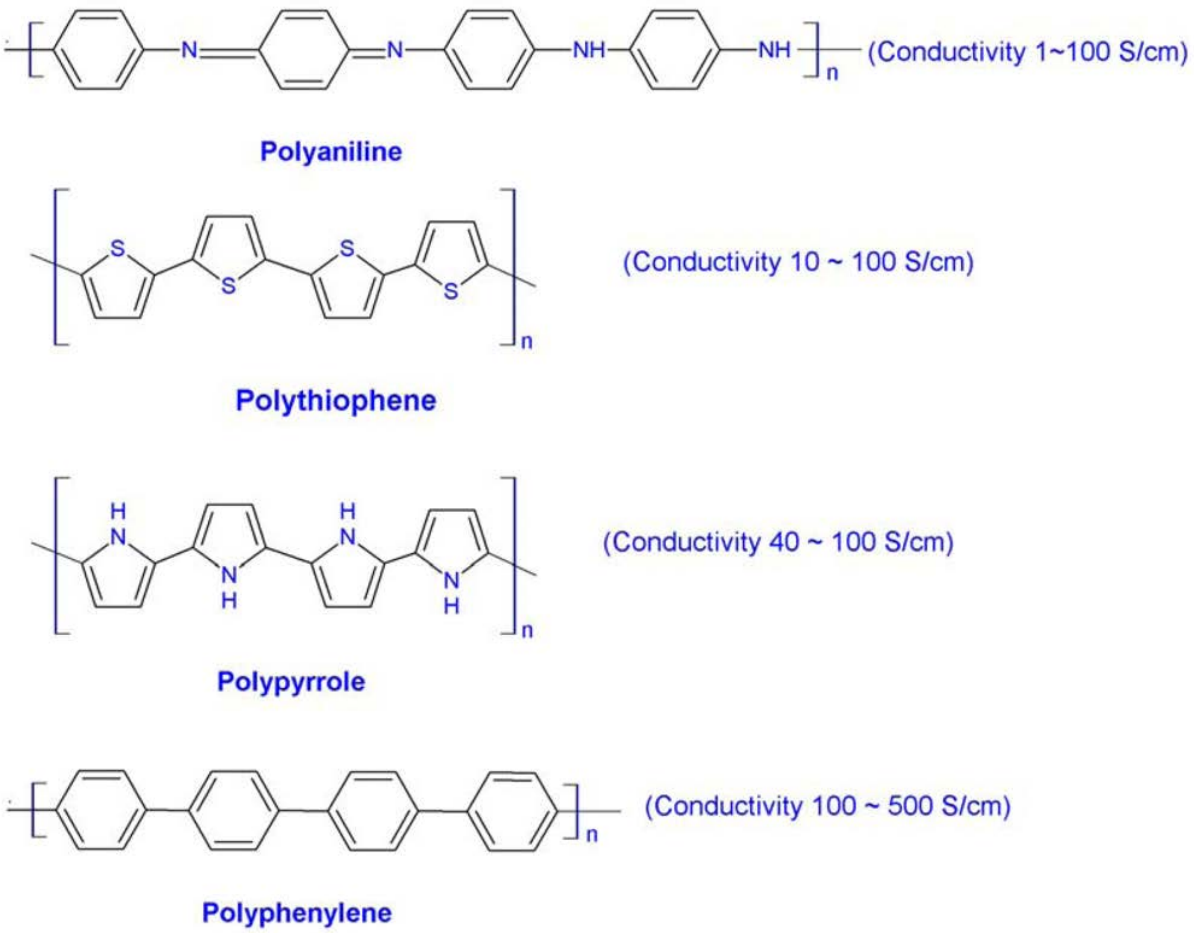

Figure 4: Chemical structures of some conducting polymers. [91]

2.2.5 Synthesis of conducting polymers

Numerous methods are available for the synthesis of conducting polymers. Still, the most extensively used method is the oxidative coupling involving the oxidation of monomers to form a cation radical followed by coupling to form di-cations. Replication of these methods leads to the polymer **Figure 5**. Electrochemical synthesis is rapidly becoming the preferred technique for the synthesis of electrically conducting polymers because of its ease and reproducibility. The benefit of electrochemical polymerization is that reactions can be carried out at room temperature. The thickness of the film can be regulated by changing either the potential or current with time.

Electrochemical polymerisation of conducting polymers is generally employed by: (i) constant current or galvanostatic; (ii) constant potential or potentiostatic; (iii) potential scanning/cycling or sweeping methods. The basic electrochemical technique used is that which utilizes a divided cell containing a working electrode, a counter electrode and a reference electrode, and usually yields the best films. The generally used anodes are chromium, gold, nickel, palladium, titanium, platinum and indium-tin oxide coated glass plates. Semi-conducting materials, such as n-doped silicon [95], gallium arsenide [96], cadmium sulphide and semi-metal graphite [97], are also used for the growth of polymer films. Electrochemical synthesis can be employed to prepare free standing homogeneous and self-doped films. Moreover, it is possible to obtain copolymers and graft polymers. Polyazulene, polythiophene, polyaniline, polycarbazole and several other polymers have been synthesized using this approach.

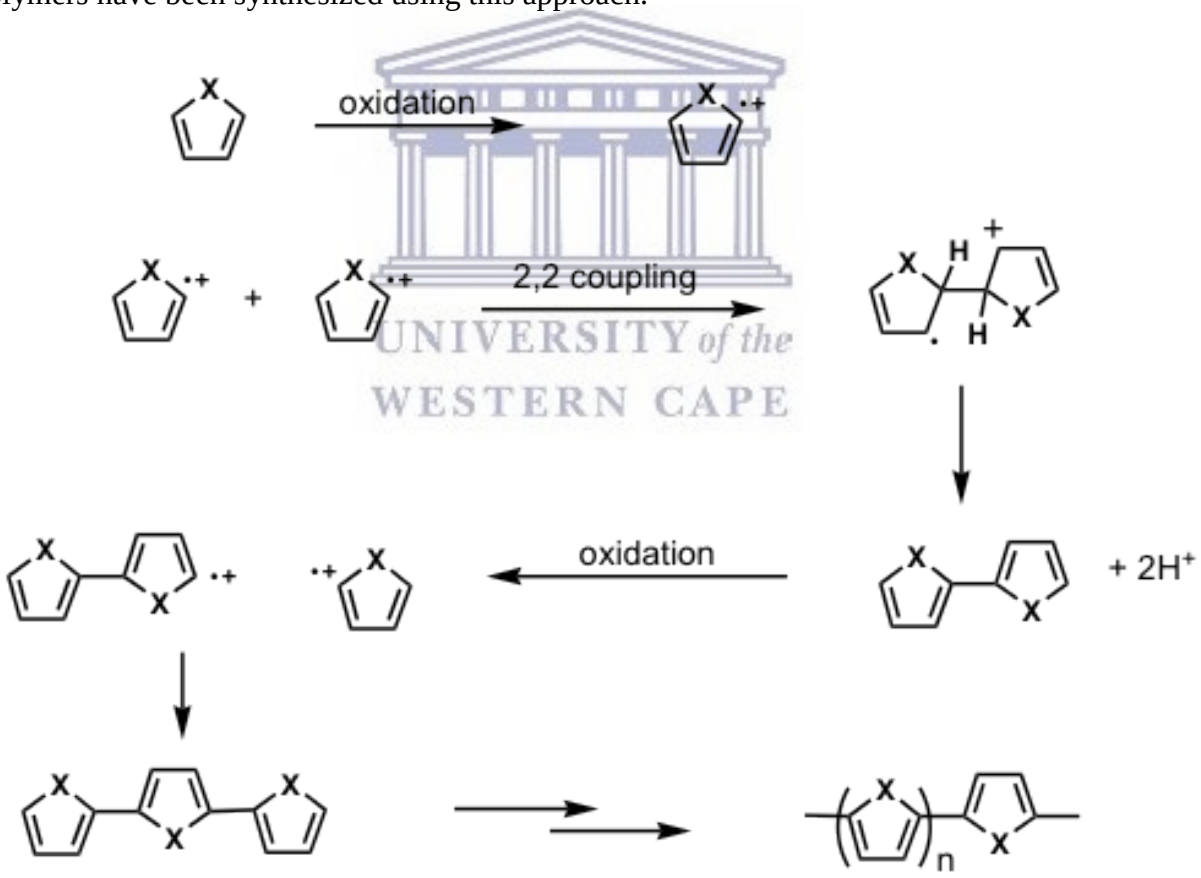

Figure 5: Schematic illustration of oxidation of monomer showing initial product of oxidation to resulting polymer [91]

2.2.6 Applications of conducting polymers

Conducting polymers have been the focus of much attention primarily because of their numerous anticipated applications in solar cells, light weight batteries, electrochromic devices, sensors and molecular electronic devices. Polymeric heterojunctions (solar cells) have been constructed by electrochemical deposition of PPY on n-silicon [98]. Numerous conducting polymers such as polyacetylene, polthiophene, polyindole, polypyrolle, polyaniline etc. have been reported as electrode materials for rechargeable batteries [99-101]. It has been stated [102] that the conducting polyheterocycles are good candidates for electrochromic displays and thermal smart windows. Scientists have PPY films in a neurotransmitter as a drug release system into the brain [103]. The possibility of the use of conducting polymers in electronics and photonics (non-linear optics) is huge and has been used to fabricate diodes, capacitors, field-effect transistors (FET) and printed circuit boards. Polyaniline (PANi) is used by Hitachi-Maxell for anti-static coating of 4 MB barium ferrite disks [104]. The issue of selectivity is of utmost importance in analytical chemistry, especially at low analyte concentration and in the presence of interfering substances. The manufacturing of sensors, which are highly selective and easy to handle, solves many a problem encountered in analysis. Conducting polymers have enough potential for the development of various sensors. During the production of chemical or biological sensors, the electrical properties of these conducting polymers also undergoes changes. Biochemical and morphological processes are on the rise in fields such as pharmaceutical manufacturing, food manufacturing, waste water treatment and energy production [86].

2.2.7 Polyaniline

Polyaniline (PANi) is one of the most scrutinised conducting polymers [105-108]. The reason for this is due to its good environmental stability, optical and electrochemical properties. Because of its light weight, flexibility and acceptable facile processibility, PANi is being utilised in the production of electromagnetic interference shielding materials and in broadband microwave absorbing materials [109]. PANi has also warranted applications in numerous areas, including biosensor technology, electrochromic devices, energy storage systems and anticorrosion materials. The biggest obstacle related to polyaniline, is its poor processibility, both in melt and solution forms due to its rigid backbone and insolubility in most solvents. A number of techniques have been utilised to make PANi more processible. One such method involves the introduction of substituents [110-112] on the aromatic ring or aromatic nitrogen which distorts the rigid π-electron system and boosts organic/aqueous solubility depending on the substituent type. Co-polymerization with aliphatic monomers and the preparation of PANi blends/composites with other conventional polymers [113-115] have given rise to more soluble PANi. PANi colloidal dispersions have also found various applications in many areas. PANi colloidal dispersion has been synthesised by several methods. The polymerisation of aniline monomers in a micelle [106], emulsion [116], and reversed micro-emulsion media [117] or in the presence of polymeric stabilisers has produced colloidally stable PANi with submicrometer/nanometer-sized particles. Since then it has been shown that the morphology of PANi can be as diverse as there are synthetic methods and reaction conditionality. PANi with needle-like or spherical shapes has been obtained through the dispersion polymerisation technique in the presence of stabilizers. Also, microporous PANi has been produced by means of colloidal assemblies as templates [118]. In another place [aniline]: [β-NSA] micelles play a pseudo template role of facilitating the formation of PANi-β-NSA nano and microstructure [119].

Wei and Wan [120], synthesised polyaniline hollow microspheres with diameter ranges of 450-1370 nm on aniline emulsion templates making use of β-NSA and ammonium persulfate as oxidant. Polyaniline dodecyl benzene sulfonic acid (DBSA) complex showed micro tube morphology and camphor sulfonic acid-doped PANi exhibited fibrillar morphology. These sulphonic acids exhibited both surfactant and dopant roles [121].

2.2.7.1 Synthesis of polyaniline

Essentially, PANi and derivatised PANi can be made through chemical or electro synthetic routes [122]. Chemical synthesis is easy, inexpensive and preferred method for mass production [123]. The electrochemical method is expensive and inefficient for large scale technological applications, it is the preferred method to produce films for use in small geometric systems such as sensors, micro-electronics, optical devices and batteries [124]. The electro synthetic method also allows for easy control of polymer properties such as film thickness and by-product formation. Chemical synthesis encompasses the oxidative polymerisation of the requisite monomers in an acidic medium by utilising strong oxidants such as ammonium persulfate (APS), potassium persulfate, potassium dichromate, ferric ions or hydrogen peroxide in the presence or absence of templates. These compounds are then able to oxidize the monomers leading to chemically active cationic radicals of the respective monomers. The cationic radicals react with more monomer molecules producing oligomers or insoluble polymers [124]. Through chemical synthesis, polymerisation occurs in bulk and the resultant polymers precipitate as insoluble solids. Electro synthetic techniques make use of the electro-oxidation of monomers to commence the formation of the polymer without chemical oxidants. The potential of the working electrode is scanned anodically, within a potential window where the oxidation of the monomer occurs, followed by a reverse scan. Anodic scanning of the potential applied at the electrode raises the electrode Fermi level. At an appropriate positive potential, the electrode Fermi level can interact with the frontier molecular orbitals of the monomer.

The movement of electrons from the monomer's highest occupied molecular orbital (HOMO) to the lowest unoccupied molecular orbital (LUMO) comprises oxidation and yields highly reactive nitrenium cations. Dimerization or deprotonation of these cationic radicals may give rise to various products depending on the electro synthetic conditions. 4-Aminidiphenylamine, p-bezoquinone, and benzidine are possible products [125]. It is commonly concurred that the mechanisms for the oxidative polymerisation of aniline and aniline-related monomers are alike. **Figure 6** shows the reaction mechanism for the polymerisation of anilines as suggested by Benjan and Duca [126].

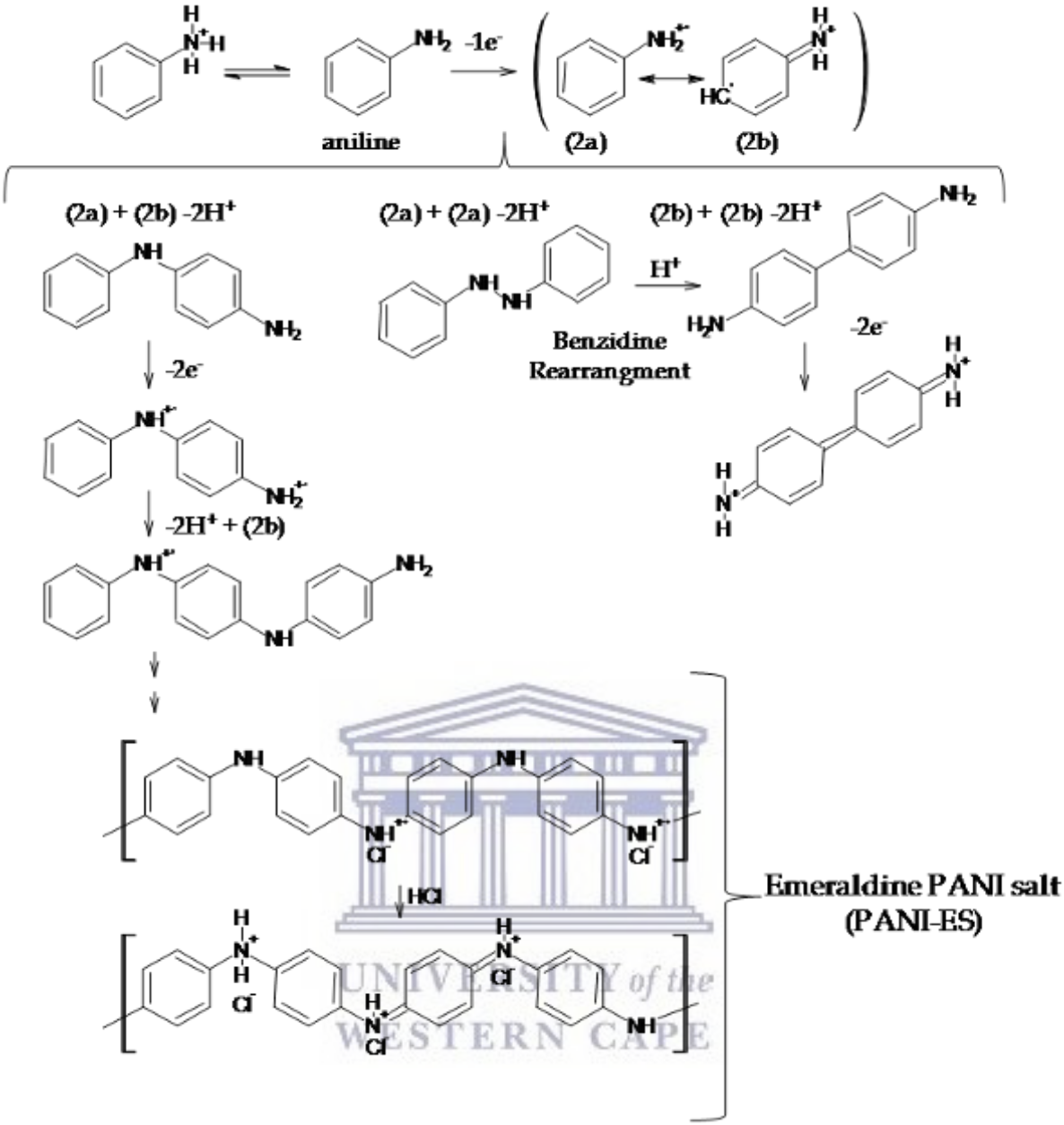

Figure 6: Schematic representation of the polymerization steps present during the aniline polymerization. The structure of PANI is shown with radical cations (or polarons) and dications (bipolaron) segments [166].

Polymerisation of aniline or substituted anilines (e.g. o-methoxy aniline and 2,5-dimethoxyaniline) in acidic media proliferates through a chain of steps commencing with the removal of an electron from the bonding π-orbital of the monomer yielding highly reactive cations. These cations then promptly undergo deprotonation and electron loss with 'head to tail' coupling to form dimers. During the anodic oxidative process, the dimer formation is the rate determining step. In the chain propagation step, dimer/dimer or dimer/monomer cation 'head to tail' coupling, amidst deprotonation or de-electronation, leads to lengthening of the polymer chain.

2.2.7.2 Structure of polyaniline and its derivatives

PANi has been known to display more complex chemistry than other conducting polymers. The wide spread work of MacDiarmid [127] on polyanilines has shown that they usually have one basic structure made of alternating reduced and oxidized repeated units **Figure 7**. Even though polyaniline can, in principle, exist in a continuum of oxidation states between y = 0 and y = 1, there are generally three permitted oxidation states **Figure 7**. These oxidation states are; the fully reduced leucoemeraldine (LE, y = 1), the half oxidized emeraldine form (EB, y = 0.5) and the fully oxidized pernigraniline (PN, y = 0) [128-129]. Protonation of EB or oxidation of the leucoemeraldine (LE) gives rise to the production of a polysemiquinone radical cation which forms the emeraldine salt (ES) with solvent anion. The emeraldine salt comprises of a half filled broad polaron energy band and is the only conductive form of PANi.

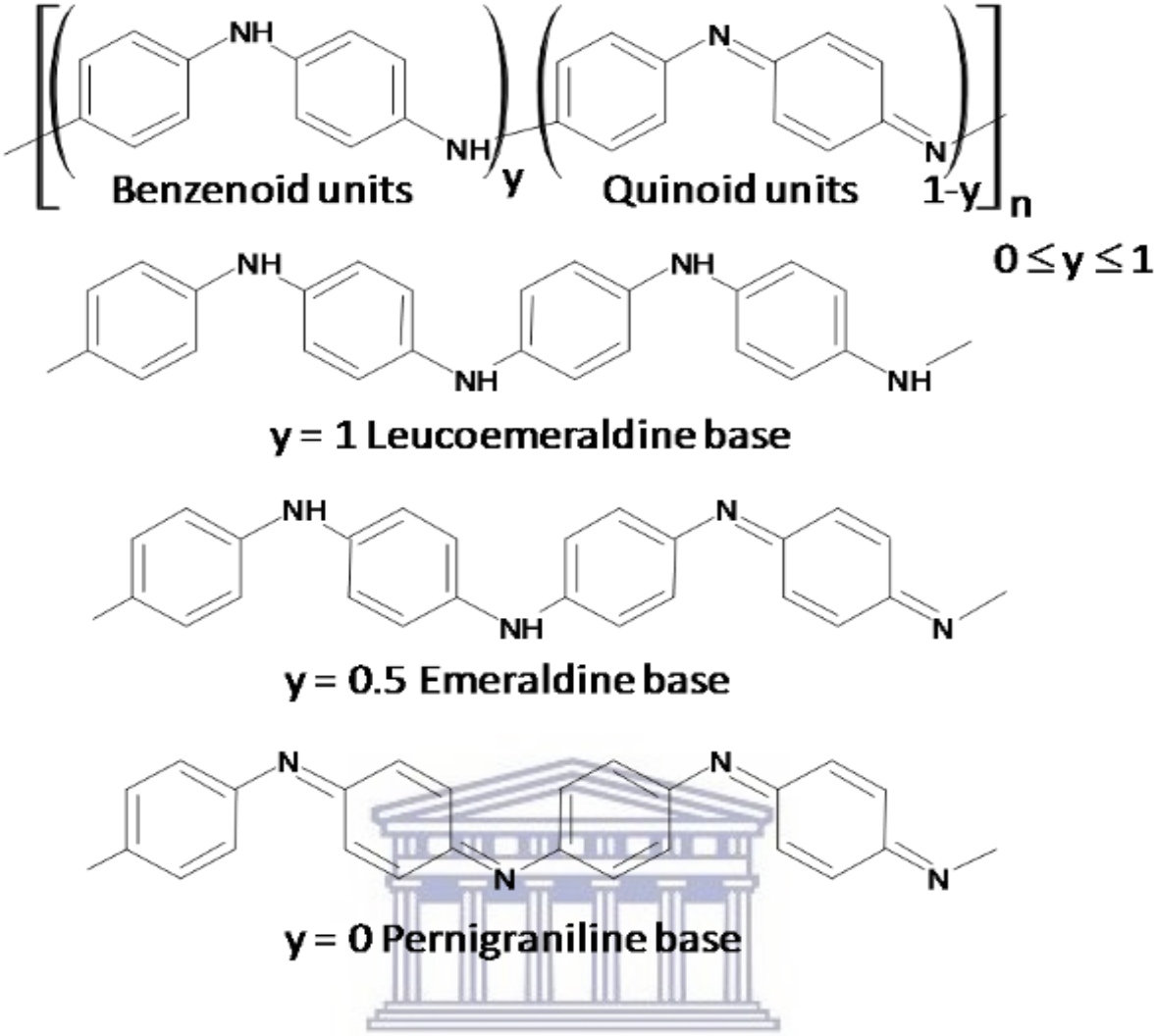

Figure 7: **Structure of polyaniline in its different oxidation states [166]**

2.2.7.3 Poly (2,5 dimethoxy aniline) (PDMA)

As mentioned earlier, more work has been dedicated to the study of substituted polyanilines to affect the optical properties of the polymer material and increase the solubility in organic solvents. Even though substitution of PANi often causes a decrease in conductivity, when aniline is substituted with two methoxy groups to form 2,5-dimethoxy aniline (DMA), it is reported to produce a soluble polymer with conductivity similar to that of PANi. The structure of poly (2,5-dimethoxyaniline) (PDMA) is presented in **Figure 8**. As for PANi, the properties of its derivatives, e.g. PDMA, also depend on the synthesis conditions, such as the type of supporting electrolyte, monomer concentration, applied potential, the type of solvent and pH [130-132].

The reason why polyanilines displays more complex chemistry than other conducting polymers, is due to their dependence on both the pH value and the oxidation states. These oxidation states are described by three different forms of the polymer known as leucoemeraldine base (LB) (fully reduced form), emeraldine base (EB) (50% oxidised form), pernigraniline base (PB) (fully oxidised form). The emeraldine (EB) form is the most significant one and its protonation by means of H^+ ions produced from protic acids gives the emeraldine salt form (ES), which is responsible for the strong increment of conducting properties. As PDMA is more soluble and has conductivity similar to that of PANi, the anion present in the electrolyte medium effects the degradation of PDMA. In this respect PDMA has shown redox transitions for leucoemeraldine to more oxidised PANi-forms at lower potentials in comparison with PANi. The probability for converting PDMA to its fully oxidised state was found to be much less than in the case of PANi and has been shown to be 0.27 V for PDMA as compared to 0.70 V for PANi [133-136].

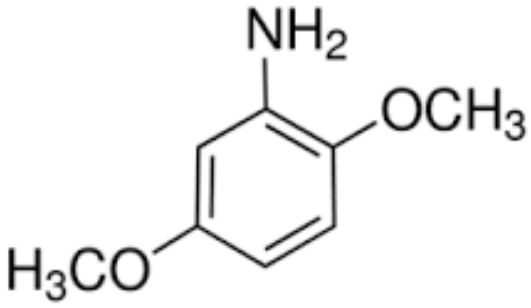

Figure 8: Chemical Structure of 2,5 dimethoxy aniline [130]

2.2.7.4 Conductivity in polyaniline

The mechanism of polyaniline conductivity differs from other electro conducting polymers, since a nitrogen atom is involved in the formation of the radical cation, unlike most of the electro conducting polymers whose radical cation are formed at carbon. Conversely, nitrogen is also involved in the conjugated double bond system. Consequently, electrical conductivity of polyaniline is dependant both on the oxidation and protonation degrees [137-140]. As previously stated, polyaniline is characterized by the existence of various oxidation forms.

Polyaniline in the form of emeraldine can be doped (protonated) to conducting form of emeraldine salt. Emeraldine base, half oxidized form, consisted of equal amounts of amine (-NH-) and imine (=NH-) sites. Imine sites are subjected to protonation to form bipolaron or dication (emeraldine salt form). Bipolarone is further dissociated by insertion of two electrons both from electron pairs of two imine nitrogen, into quinidiimine ring, and the third double bond of benzenoid ring is formed [141]. Unpaired electrons at nitrogen atoms are cation radicals, but essentially, they represent polarons. The polaron lattice, responsible for high conductivity of polyaniline in the form of the emeraldine salt, is formed by the redistribution of polarons along the polymer chain, according to the schematic representation given in **Figure 9** [140]. Though both bipolarons and polaron theoretical models of emeraldine salt conductivity were proposed [142], it was lately confirmed that, beside the few spineless bipolarons that exist in polyaniline, formation of polarons as charge carriers explained the high conductivity of polyaniline [143].

As mentioned, a unique property of polyaniline is conductivity dependence on the doping (proton) level [144]. The maximal conductivity of polyaniline is attained at a doping degree of 50%, which corresponds to polyaniline in the form of emeraldine salt [145]. For higher doping degrees, some of the amine sites were left unprotonated, explaining why, in the light of the polaron conductivity model, reduction of emeraldine salt to leucoemeraldine and perninggraniline

states decreases the conductivity. The order of magnitude for conductivity varies from 10^{-2} Scm^{-1}, for undoped emeraldine, up to $10^{3}Scm^{-1}$ for doped emeraldine salt [146]. As well as doping degree having the noticeable effect on the conductivity, various other factors were also found to influence the polyaniline conductivity, such as: moisture [147], morphology [148], temperature [149] etc.

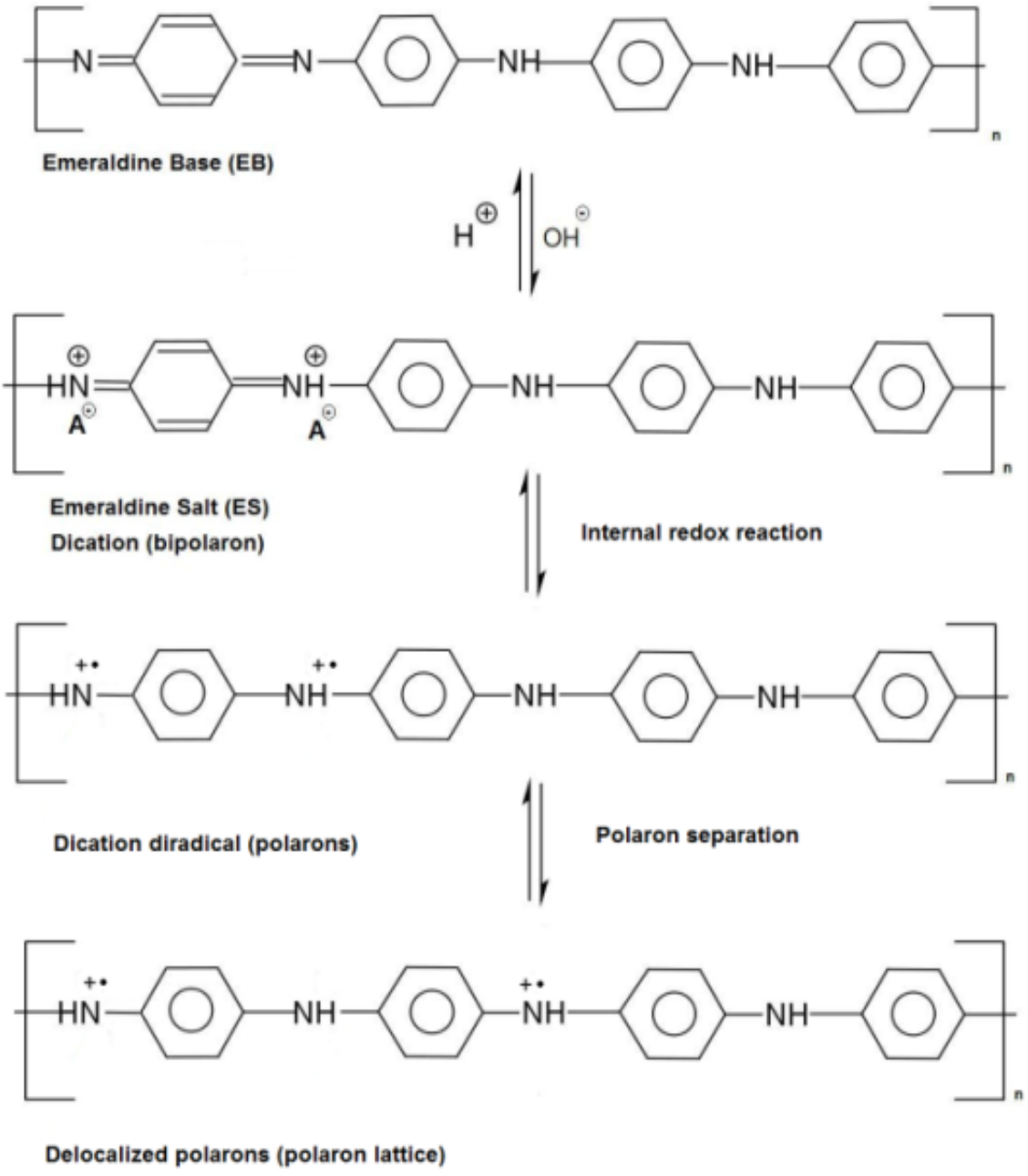

Figure 9: Schematic representation of polyaniline conductivity [166]

2.2.7.5 Nucleation and growth of polyaniline

The kinetics of the nucleation and growth process during electrochemical synthesis of electro-conducting polymers generally depend on the metal deposition theory [150]. According to this theory, two types of nucleation methods exist, instantaneous and progressive, with three types of growth referring to: one- (1D), two- (2D), and three- (3D) dimensional processes. Instantaneous nucleation indicates a regular number of nuclei, growing without further formation of the nuclei. In the case of progressive nucleation, nuclei are constantly generated. One-dimensional growth suggests growth in only one direction, e.g. perpendicular to the electrode surface. In 2D growth, the nuclei have preference to grow parallel to the electrode surface, while 3D growth is characterized by the similar rates, for these processes perpendicular and parallel to the electrode are quite similar [129].

Based on potentiostatic experiments it was shown, that a number of stages of polyaniline growth during electrochemical polymerization of aniline were involved, taking place through a different mechanism [151]. Cyclic voltammetry studies showed that polyaniline growth was greatly dependent on the type and concentration of anion in the electrolyte [152]. Research on the early stages of the polyaniline growth pointed toward progressive nucleation of the polyaniline film, with 2D or 3D growth mechanism or 3D instantaneous nucleation, depending on, electrolyte concentration and composition [153-154]. The mass transfer regulated the early stage of polyaniline growth which in turn leads to formation of a compact layer [155]. In the instance of perchloric acid, depending on monomer concentration, the nucleation process proceeds from progressive, at lower, to instantaneous nucleation to higher concentration [72]. At the advanced stage, characterized by exponential current increase, 1D growth was assumed, resulted in continual branching and formation of the open structure [156].

2.2.7.6 Factors influencing the electrochemical polymerization of aniline

Electrochemical synthesis of electro-conducting polymers is greatly dependent on a number of parameters, for instance the nature of the doping anion (affecting morphology), order of the polymer rate growth, nature and the components of the solvent (nucleofilic solvent would react with cation radicals formed by monomer oxidation on the anode), electrode material (regulates the simplicity of the desired polymer deposition, depending on its surface energy) and temperature of the electrochemical polymerization, etc. [139].

2.2.7.6.1 Doping anions

Electrochemical polymerization of aniline, as mentioned before, is essentially always carried out in strong acidic aqueous electrolytes. Doping anions contained in polyaniline originate from acid, and represents its conjugated base. The dopant anions are placed in during electrochemical polymerization, fulfilling the request of electroneutrality, and therefore their concentrations are on the stoichiometric levels, it is for this reason that their presence has a strong influence on, polyaniline morphology, conductivity, and electrochemical activity and the polymerization process itself [157-158]. Polyaniline obtained in the presence of so called “large dopant ions” originated from hydrochloric acid, sulphuric acid, nitric acid, p-toluensulfonic acid, and sulfosalicyclic acid, and stimulated creation of a more swollen and open structured film, while the presence of “small ions” such as ClO_4^- or BF_4^-, resulted in formation of a more compact structure [159]. The order of the polyaniline growth was shown to increase with the size of the dopant anion [136]. The addition of polyelectrolytes in polymerization leads to the insertion of these molecules as dopants [139]. It was also possible to obtain optically active polyaniline by electrochemical polymerization in the presence of (+) or (-) camphorsulfonic acid, leading to insertion of chiral dopants [160].

2.2.7.6.2 Nanostructured polyaniline

The synthesis of nanostructured PANi, particularly as nanofibers, can increase its electrical, thermal and mechanical stabilities. These nanostructured polyanilines can have an important impact for applications in electronic devices and molecular sensors, owing to their extremely high surface area, synthetic versatility and low-cost. The usual synthesis of polyaniline, based on the oxidative polymerization of aniline in the presence of a strong acid dopant, typically results in an irregular granular morphology that is accompanied by a very small percentage of nanoscale fibres. Nevertheless, different methods have been developed in order to produce PANi and many other polymers with nanostructured morphology. The nanostructured PANi has been prepared by various synthetic methods. Nonetheless, these techniques can be grouped into two general synthetic routes, as presented in **Figure 10**. Uniform nanofibres of pure metallic PANi (30-120nm, depending on the dopant) have also been synthesised by polymerization at an aqueous-organic interface [161-162].

During the first step (see item 'a') of the interfacial polymerization, the oxidant and monomers (aniline) dissolve in immiscible solvents in the interfacial region between the two solutions, forming some oligomers (see item 'b') of the interfacial polymerization. It is theorized that movement of the product into the aqueous phase can supress unrestrained polymer growth by separating the fibres from the excess of reagents. Subsequently, the initial chains grow up and more PANi chains are formed (see step 'c'). Interfacial polymerization can thus be regarded as a non-template approach in which high local concentrations of both monomer and dopant anions at the liquid-liquid interface might be expected to promote the formation of monomer-anion (or oligomer-anion) aggregates. These aggregates can act as nucleation sites for polymerization, resulting in powders with fibrillar morphology. It has since been shown that the addition of certain surfactants to such an interfacial system allows further control over the diameters of the nanofibers. A vital part that is frequently neglected or not explained in detail is the isolation of the nanostructured PANi from the solution.

However, generally, the nanofibers are isolated by filtration in a nanoporous filter, the isolated polymer being washed with different solutions with the aim to clean it up. The solution can also be dialyzed and the clean solution containing the nanofibers is centrifuged to separate the nanofibers from the solution.

Polyaniline nanofibers or nanotubes can be acquired by making use of large organic acids **Figure 10**. These acids form micelles upon which aniline is polymerized and doped (**Figure 10** steps (a), (b) and (c) of micellar polymerization). Fiber diameters are observed to be as low as 30-60 nm and are highly affected by reagent ratios [163-166]. Ionic liquids (ILs) have also been used as synthetic media for the preparation of nanostructured conducting polymers [167-168]. Ionic liquids are organic salts with low lattice energies, which lead to low melting points. Many ILs are liquid at room temperature [169]. There is a large assortment of ionic liquids and the most used ones are derived from imidizolium ring, pyridinium ring, quaternary ammonium and tertiary phophonium cations. The normal differentiation between conventional molten salts and ionic liquids are based on the melting point. While most molten salts have melting points higher than 200ºC, ionic liquids normally melt below 100ºC [170]. The most uncommon characteristics of these systems are that although they are liquids, they display features similar to solids, such as structural organization at intermediate distances [171] and negligible vapour pressure [172]. This structural arrangement can act as a template like system, and PANi nanofibers are obtained when the aniline is polymerized in these media. Consequently, the template-free methods, such as interfacial, seeding and micellar, can be utilised as different “bottom up” approaches to obtain pure PANi nanofibers. The synthesise of nanostructured PANi by self-assembly with reduced post-synthesis processing warrants further study and applications of these materials, especially in the field of electronic nanomaterials [173].

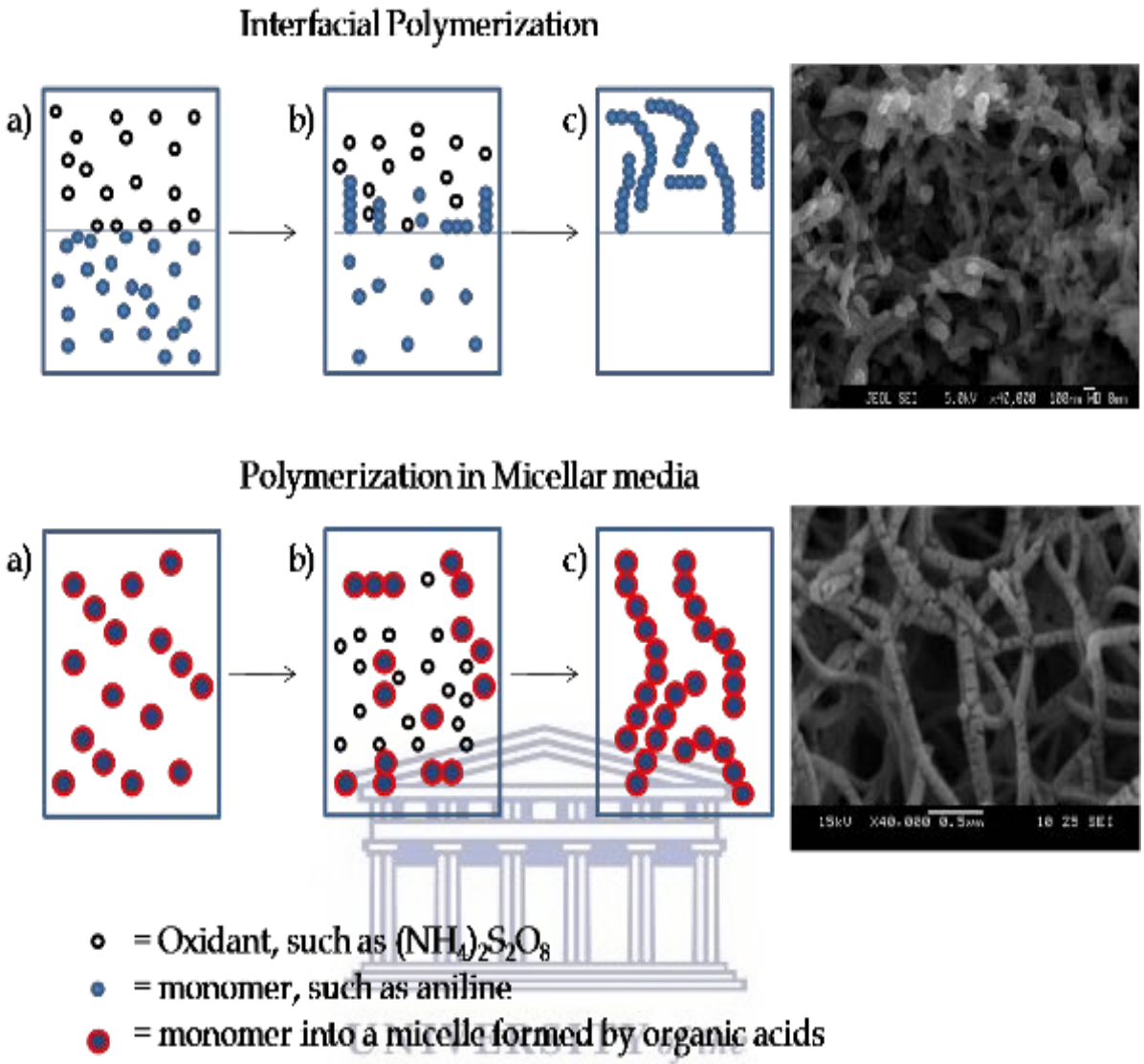

Figure 10: Schematic representations of the two polymerization ways that are commonly employed in the preparation of PANi with nanofiber or nanotube morphology [173].

2.3 Sensors and Sensor devices

The 21st century is being proclaimed as the age of information: escalating capabilities for computer-assisted organization of information, increased competences in decision making and process control, and automated health care will add to the pace and quality of life in this new age. The ability to simultaneously manage numerous information sources as well as infinitely more well-organized methods for categorizing, organizing and recovering information will put increasing demands on the technologies and instruments used for obtaining information in a well-timed manner. This capacity is demonstrated by physical sensing and measurement systems i.e. systems that have the capability to detect measured parameters such as temperature, pressure, electrical viscosity and light intensity. During the past two decades, it became obvious that other more sophisticated measuring devices were required to collate the information which could be processed in new management systems. Chemical and biological sensors have materialized because of this. Chemical and biological sensors having near –infinite abilities of analyte detection were developed and will become an essential part of collection and control systems in nearly every industry and market place [174].

2.3.1 Definition of sensors and the type of sensors

A device which transduces a physical or chemical parameter into an electrical or optical signal is defined as a sensor. Physical parameters which are usually measured with sensors are temperature, pressure, force, magnetic field, etc. while chemical parameters of interest most often are the concentration of chemical substances [175]. There seems to be a natural separation between chemical and physical sensors. Nevertheless, some sensors do not classify easily, for example relative humidity sensors, a chemical sensor conventionally lumped with physical sensors. Physical sensors measure physical quantities such as length, mass, temperature, and electricity for their own sakes [176].

2.3.2 Chemical Sensors

Chemical sensors are devices that transmute chemical information, varying from concentration of a specific sample component to total composition analysis, into analytically useful signals. This chemical information may stem from a chemical reaction of the analyte or from a physical property of the system studied. A chemical sensor is an important component of an analyser. In addition to the sensor, the analyser may contain devices that perform sampling, sample transport, signal processing and data processing functions. An analyser may be an indispensable part of an automated system. The analyser working according to a sampling plan as a function of time acts as a monitor [177]. This definition is presented in **Figure 11 (a)** and compared to two other sensor devices, specifically, the micro instrument **Figure 11 (b)** and the" lab-on-a chip" sensor concept **Figure 11(c)** [176].

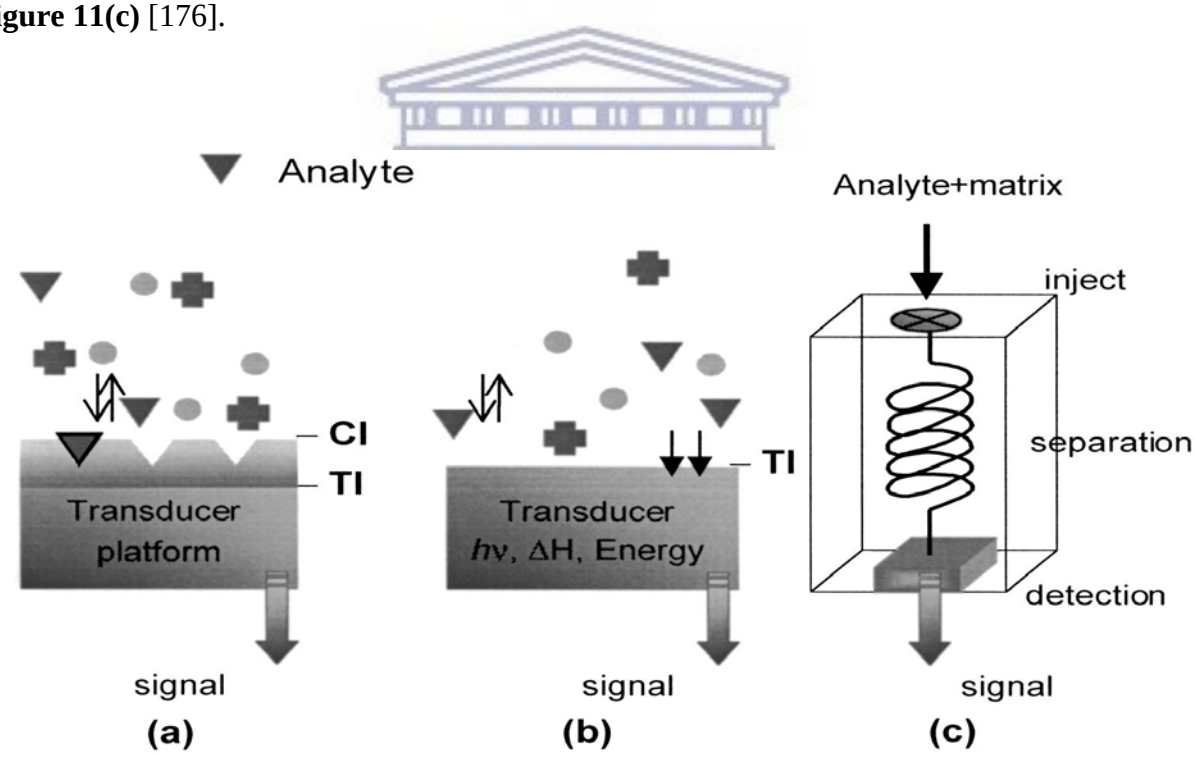

Figure 11: Three types of sensor design and operating principle. CI: chemical interface, TI: transducer interface. (a) Chemical or biochemical sensor (analyte reacts at interface). (b) Physical sensor for chemical analysis, e.g., molecular or atomic spectroscopy(c) Micro-Total Analytical System, µ-TAS (lab-on-a chip technologies) [176].

2.3.3 Components of Chemical Sensors

Chemical sensors usually contain two rudimentary components connected in series: a chemical (molecular) recognition system (receptor) and a physico-chemical transducer. Certain sensors may include a separator which is, for example, a membrane. The receptor part of the sensor transforms the chemical information into a form of energy which may be determined by the transducer [177].

2.3.3.1 Transducers

A transducer is a device that can convert an observed change (physical or chemical) into a measureable signal. With chemical sensors, the measureable signal is generally an electronic signal whose magnitude is proportional to the concentration of a particular chemical or set of chemicals. Analytical techniques in chemistry have mainly been fashioned on photometric transducers, as in spectroscopic and colorimetric techniques. Nonetheless, most sensors have been developed around electrochemical transducers, because of ease of construction and cost-effectiveness. While electrons drive microprocessors, the directness of an electrical device will tend to have maximum appeal. The increase in devices using fiber optic technology can lead to the obsoleteness of electrical appliances starting with the telephone. Also, the utilisation of micro-mass-controlled devices, constructed mainly on piezo-electric crystals, may become competitive in the near future.

Transducers can be subdivided into the following four main types.

1. Potentiometric – These transducers are involved the measurement of the emf (potential) of a cell at zero current. The emf is proportional to the logarithm of the concentration of the substance being determined.

2. Voltammetric – An increasing (decreasing) potential is applied to the cell until oxidation (reduction) of the substance to be analysed occurs and there is a sharp rise (fall) in the

current to give a peak current. The height of the peak current is directly proportional to the concentration of the electroactive material.

If the correct oxidation (reduction) potential is known, one may step the potential directly to that value and observe the current. This method is known as amperometric.

3. Conductometric- Most reactions encompass a change in the composition of the solution. This change usually results in a change in the electrical conductivity of the solution which can be measured electrically.

4. FETs (field-effect transistors) - based sensors- Miniaturization are sometimes achieved by constructing one of the above types of electrochemical transducers on a silicon-chip-based field-effect transistor. This technique has been mainly used with potentiometric sensors, but could also be used with voltammetric or conductometric sensors.

Table 1: **Type of electrochemical transducers for classified type of measurements, with corresponding analytes to be measured [178].**

Measurement type	Transducer	Transducer analyte
1. *Potentiometric*	ion-selective electrode (ISE) glass electrode gas electrode metal electrode	K_, Cl_, Ca2_, F_ H_, Na_... CO_2, NH_3 redox species
2. *Amperometric*	metal or carbon electrode Chemically modified electrodes (CME)	O_2, sugars, alcohols... sugars, alcohols, phenols, oligonucleotides...
3. *Conductometricimpedimetric*	interdigitated electrodes, metal electrode	urea, charged species oligonucleotides
4. *Ion charge or field effect*	ion-sensitive field effect transistor (ISFET), enzyme FET (ENFET)	H_, K_...

2.3.3.2 Receptors

The receptor part of chemical sensors is based upon several principles:

1. Physical, where a chemical reaction does not occur. Which those based upon measurement of absorbance, refractive index, conductivity, temperature or mass change.

2. Chemical, in which a biochemical reaction with involvement of the analyte gives rise to the analytical signal.

3. Biochemical, in which a biochemical process is the source of the analytical signal. Typical examples are microbial potentiometric sensors or immune sensors. They may be regarded as a subgroup of the chemical ones. Such sensors are called biosensors.

It is not always possible to decide whether a sensor functions on a chemical or physical principle. As in the case when the signal is due to an adsorption process [177]. The biological recognition system (receptor) interprets information from the biochemical domain, generally an analyte concentration, into a chemical or physical output signal with defined sensitivity. The recognition system in return is responsible for a sensor with a high degree of selectivity for the analyte to be measured. Even though all chemical sensors are selective (non-specific) for a particular analyte, some are, by design and construction, only class-specific, since they use class enzymes, e.g. phenolic compound biosensor, or whole cells, e.g. used to measure biological oxygen demand. In sensing systems present in living organisms systems, such as olfacation, taste and neurotransmission pathways, the word receptor or bio receptor is also often used for the recognition system of a chemical biosensor because the actual recognition is performed by the cell receptor. Examples of single and multiple signal transfers are listed in **Table 2**. These examples are limited to the most common sensor principles, excluding the existing laboratory instrumentation systems [178].

Table 2: **Types of receptors used in sensors and the electrochemical measurement techniques, linked to them that recognize specific species [178].**

Analytes	Receptor/Chemical Recognition Technique	Measurement Transduction System
1. *Ions*	mixed valence metal oxides permselective, ion-conductive inorganic crystals trapped mobile synthetic or biological ionophores ion exchange glasses enzyme(s)	potentiometric, Voltammetric
*2. Dissolved gases v*apours, *odours*	bilayer lipid or hydrophobic membrane inert metal electrode enzyme(s)	in series with 1 amperometric amperometric or potentiometric amperometric, potentiometric or impedance
3. Substrates	enzymes(s) whole cells membrane receptors plant or animal tissue	amperometric or potentiometric in series with 1, or 2, or metal or carbon electrode, conductometric, piezoelectric, optical calorimetric
4. Antibody/Antigen	antigen/antibody oligonucleotide duplex, aptamer enzyme labelled chemiluminescent or fluorescent labelled	amperometric, potentiometric or impedimetric
5. Various proteins and low molecular weight substrates ions	specific ligands protein receptors and channels enzyme labelled	amperometric, potentiometric or impedimetric

2.3.4 Characteristics of an ideal sensor.

1. *Selectivity:* The most essential characteristic of sensors is the ability to discriminate between different substances. Such behaviour is principally a function of the selective component, although sometimes the operation of the transducer can contribute to the selectivity.

2. *Sensitivity range:* This generally needs to be sub-millimolar, but in special cases can go down to the femtomolar (10^{-15}) range.

3. *Accuracy:* This needs to be better than ±5%.

4. *Nature of solution:* Conditions such as pH, temperature and ionic strength must be considered.

5. *Response time:* This is usually much longer (30s or more) with biosensors than with chemical sensors.

6. *Recovery time:* This is the time that elapses before the sensor is ready to analyse the next sample – it must not be more than a few minutes.

7. *The working lifetime:* is usually determined by the stability of the selective material. For biological materials, this can be as short as a few days, although it is several months or more.

2.3.5 Film Depositions

The selective element must be connected to the transducer. This presents specific problems if the element is biological in nature. Several methods of connection have been developed namely:

1. The simplest method is adsorption to the surface.
2. Microencapsulation is the term used for trapping between membranes – one of the earlier methods to be employed.
3. Entrapment, where the selective element is trapped in a matrix of a gel, paste or polymer – this is a very popular method.
4. Covalent attachment, where covalent chemical bonds are formed between the selective component and the transducer.
5. Cross-linking, where a bifunctional agent is used to chemically bond the transducer to the selective component – this is often used in conjunction with other methods such as adsorption or microencapsulation [179].

2.3.6 Types of Chemical Sensors

The evolvement of sensors which utilizes most of the known chemical, physical and biological properties used in chemistry is mainly due to the development of instrumentation, microelectronics and computers. Chemical sensors are usually categorized according to the operating principle of the transducer.

2.3.6.1 Electrochemical Sensors

These sensors make use of the development of an electrical charge (potential/current/impedance) at the surface of a solid material when it is placed in a solution containing ions which can exchange with the surface. The magnitude of the electrical charge (potential/current/impedance) is related to the number of ions in the solution. Among all the chemical sensors reported in literature, electrochemical are the most attractive because of their remarkable sensitivity, experimental simplicity and low cost.

2.3.6.2 Optical sensors

These involve a system wherein the reagents are immobilized in or on a solid substrate which changes colour in the presence of a solution of the analyte.

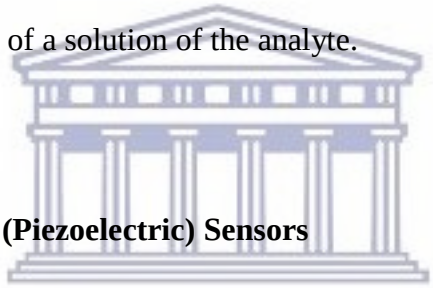

2.3.6.3 Mass sensitive (Piezoelectric) Sensors

When a chemical reaction takes place at the surface of a sensor, their heat evolves, but there is also a change in mass. The mass change is very small but if a sensitive microbalance is used, it can be detected and be related to the amount of analyte reacting with surface.

2.3.6.4 Heat Sensitive Sensors

When a chemical reaction produces heat, the quantity of heat produced depends on the amount of the reactants. Then the measurement of the reaction can be related to the amount of a particular reactant.

2.3.6.5 Biosensors

Biosensors are chemical sensors in which the recognition system uses a biological mechanism or entity (enzyme/substrate, antibody/antigen, receptor/hormone, etc.) as a fundamental part of the sensing process, instead of a chemical process. In a biosensor, the species recognition reagent is often a macromolecule which is immobilized into a membrane or chemically bound to a surface in contact with analyte solution. A specific chemical reaction then takes place between the reagent and the analyte. A transducer transforms the response measured at the receptor into a detectable signal [180].

2.4 Electroanalytical techniques

Electrochemical techniques in which a potential is imposed upon an electrochemical cell and the resulting current is measured are generally categorized as voltammetric methods. An assortment of such methods has been developed. They vary in the type of waveform applied upon the cell, the type of electrode used and the state of the solution in the cell (quiescent or flowing). Voltammetry has proved to be very useful for the analyses of dilute solutions, quantitatively and qualitatively, as well as for evaluating inorganic, organic and biological components.

2.4.1 Voltammetry

The name voltammetry refers to a group of electroanalytical methods in which we obtain information about the analyte by measuring current in an electrochemical cell as a function of applied potential. This information is acquired under circumstances that promote polarization of a minute indicator, or working electrode. When a current proportional to analyte concentration is monitored at a fixed potential, the technique is called amperometry. To enhance polarization, working electrodes in voltammetry and amperometry have surface areas of a few square millimetres at most and, in some applications, a few square micrometers or less.

Voltammetry is extensively used by inorganic, physical and biological chemists for fundamental studies of oxidation and reduction processes in various media, adsorption processes on surfaces, and electron transfer mechanisms at chemically modified electrode surfaces. During the application of the voltammetry technique a current develops in an electrochemical cell which is measured under conditions of complete concentration polarization. A polarized electrode is one to which we have applied a voltage in excess of that predicted by the Nernst equation to cause oxidation or reduction to occur. In potentiometry measurements are made at currents approaching zero in the absence of polarization.

Voltammetry are different from coulometry since with coulometry, measures are taken to minimize or compensate for the effects of concentration polarization. What's more, in voltammetry, there is a minimal consumption of analyte, while in coulometry essentially all the analyte is transformed to another state.The field of voltammetry was developed from polarography, which is a specific type of voltammetry that was invented by the Czechoslovakian chemist, Jaroslav Heyrovsky, in the early 1920s. Polarography is different from other types of voltammetry because the working electrode is the unique dropping mercury electrode. Polarography used to be an important tool utilised by chemists for the determination of inorganic ions and certain organic species in aqueous solutions. The utilization of polarography as an electro analytical tool has been on the decrease. This is mainly due to the apprehensions about the usage of mercury in the laboratory which can lead to the possible contamination of the surroundings notwithstanding the cumbrous nature of the equipment, as well as the extensive availability of faster and more expedient (predominantly spectroscopic) techniques. As polarograhy has declined in prominence the other electroanalytical techniques (voltammetry and amperometry) have grown at an astounding rate. Furthermore, voltammetry and amperometry coupled with liquid chromatography have become powerful tools for the investigation of complex mixtures.

These voltammetric techniques continues to be an exceptional tool in diverse areas of chemistry, biochemistry, materials science and engineering, and the environmental sciences for studying oxidation, reduction and adsorption processes [181].

2.4.1.1 Cyclic voltammetry

Cyclic voltammetry is a very resourceful electrochemical technique which allows investigation into the workings of the redox and transport properties of a system in a solution. This is achieved by applying a three electrode system, whereby the potential relative to some reference electrode is scanned at a working electrode, while the resulting current flowing through a counter (or auxiliary) electrode is monitored in a quiescent solution.

This technique is preferably suitable for a quick search of redox couples present in a system; on locating the redox couple it may be further investigated by a more careful analysis of the cyclic voltammogram. The governing electronics are constructed in such a way so that the potential between the reference and the working electrodes can be modified, however the big impedance between these two components effectually forces any resulting current to flow through the auxiliary electrode. The potential is scanned back and forth linearly with time between two extreme values – the switching potentials using triangular waveform **Figure 12 (a)**. The moment the potential of the working electrode becomes more positive than that of a redox couple present in the solution, the equivalent species may be oxidized (i.e. electrons going from the solution to the electrode) and an anodic current is obtained. Correspondingly, as the scan is reversed the working electrode potential becomes more negative than the reduction potential of a redox couple, reduction (i.e. electrons flowing away from the electrode) may transpire causing a cathodic current. By IUPAC convention, anodic currents are positive and cathodic currents negative.

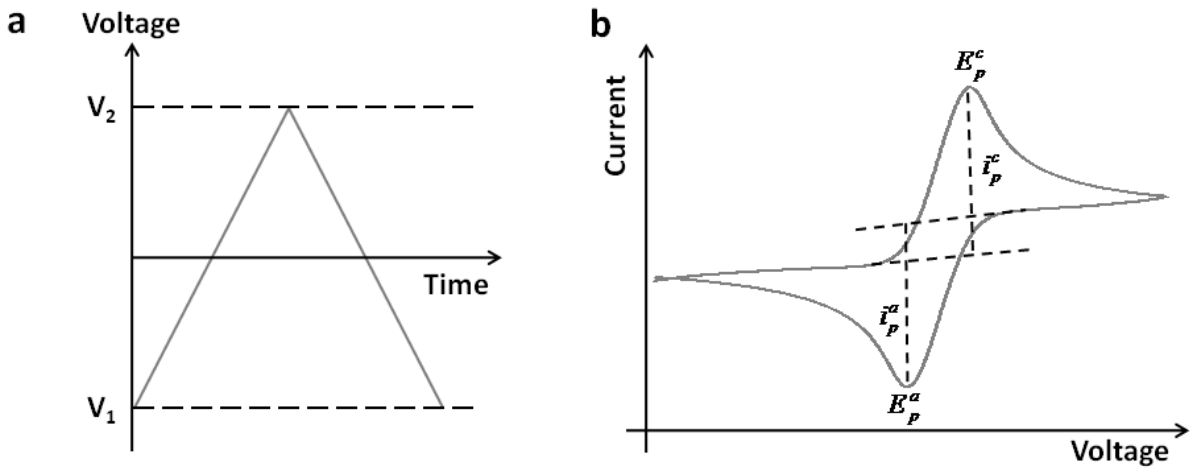

Figure 12: (a) A cyclic voltammetry potential waveform with switching potentials.
(b) The expected response of a reversible redox couple during single potential cycle [181].

Information of the numerous reactions taking place at the working electrode surface can be gathered by the magnitude of the faradaic current observed. And what is usually expected of any reaction occurring in more than one step, the overall rate is determined by the slowest step. Therefore, for any redox reaction occurring at the working electrode, the rate determining step may be anyone of the following individual steps depending on the system under investigation:

1. Rate of mass transport of electro-active species.
2. Rate of adsorption or desorption at electrode surface.
3. Rate of the electron transfer between the electro-active species and the electrode.
4. Rates of the individual chemical reactions which are part of the overall reaction scheme.

For the oxidation reaction involving n electrons

$$Red \longleftrightarrow Ox + ne^-$$

The Nernst equation provides the connection between the potential and the concentrations of the oxidized and reduced form of the redox couple at equilibrium (at 298 K):

$$E = E^{0\prime} + \frac{0.059}{n} log_{10} \frac{[Ox]}{[Red]} \quad (1)$$

Where E is the applied potential and $E^{0'}$ the formal potential; [Ox] and [Red] represent surface concentrations at the electrode/solution interface, not bulk solution concentrations. The Nernst equation may or may not be obeyed depending on the system or on experimental conditions. **Figure 12 (b)** shows a presentation of a typical voltammogram. The voltammogram depicted starts at a slightly negative potential (A) to some positive value (D) where the scan is reversed back to the starting potential.

The current is first perceived to peak at E_{pa} (with value i_{pa}) indicative of an oxidation reaction taking place then decreases due to depletion of the reducing species from the diffusion layer. During the return scan, the processes are reversed (reduction is now occurring) and a peak current is observed at E_{pc} (with value i_{pc}). If the charge-transfer reaction is reversible, and there is no surface interaction between the electrode and the reagents, as well as the redox products being stable (at least in the time frame of the experiment), the ratio of reverse and forward current i_{pr}/i_{pf}=1.0 (in **Figure 12 (b)** $i_{pa}= i_{pf}$ and $i_{pc}= i_{pr}$).

For such a system, it can be shown that:

1. The corresponding peak potentials E_{pa} and E_{pc} are independent of scan rate and concentration.

2. The formal potential for a reversible couple $E^{0'}$ is centred between E_{pa} and E_{pc}:

$$E^{\circ\prime} = \frac{E_{pa}+E_{pc}}{2} \quad (2)$$

3. The separation between peaks is given by:

$$\Delta E_p = E_{pa} - E_{pc} = \frac{59}{n}\ mV \quad (3)$$

(For an n electron transfer reaction) at all scan rates (nevertheless, the measured value for the reversible process is generally higher due to uncompensated solution resistance and non-linear diffusion. Larger values of ΔEp, which increase with increased scan rate, are characteristic of slow electron transfer kinetics). It is possible to relate the half-peak potential ($E_{p/2}$, where the current is half of the peak current) to the polarographic half-wave potential, $E_{½}$: $E_{p/2}= E_{½} \pm 29mV/n$ (the sign is positive for a reduction process). For multi-electron transfer (reversible) processes, the cyclic voltammogram consists of several distinctive peaks, if the E^o values for the individual steps are successively higher and are well separated.

An example of such a mechanism is the six-step reduction of fullerenes C_{60} and C_{70} to yield hexa-anion products C_{60}^{6-} and C_{70}^{6-} where six successive peaks can be observed. Differentiation between reversible (diffusion-controlled) and irreversible (charge-transfer controlled) kinetics of an electrode is achieved by using process potential scan-rate as a diagnostic tool – the rate of reagent transport is proportional to square root of scan-rate. Consequently, in one experimental set a shift in reversibility might be executed and analysis of ΔE_p vs $\upsilon^{½}$ gives information on the reversibility and applicability of further calculations. In straightforward conditions the working electrode may be viewed as a "reagent" of modifiable oxidising or reducing strength. Nevertheless, this is a purely conceptual image. The fact of the matter is that electrochemical processes are occurring at the interface of two distinctive phases, the electrode and the electro-active species in solution. Therefore, the processes under studies are heterogeneous in nature.

Electron transfer will only occur when the molecules in solution move towards the electrode. During a cyclic voltammetry experiment, the solution is kept unstirred; in this state of affairs, mass transport can occur only by diffusion due to concentration gradients generated around the electrode surface. The diffusion properties of the system will be related to the magnitude of the observed signal. Automatically, the current intensity (i.e. the flow of electrons) is anticipated to depend on the surface area of the working electrode and the concentration of the electro-active species. As expected the scan rate affects the concentration profile surrounding the electrode which directly affects the rate of charge transport, and for this reason, the diffusion coefficient appears explicitly. The expression of the peak current (A) for the forward sweep in a reversible system at 298 K is given by the Randles-Sevcik equation:

$$i_{pf} = (2.69 \times 10^5) n^{\frac{3}{2}} A D^{\frac{1}{2}} \upsilon^{\frac{1}{2}} C^* \qquad (4)$$

Where

i_{pf}	=	peak current, A
C	=	concentration, mol/cm^3
n	=	electron stoichiometry
A	=	electrode area, cm^2
D	=	diffusion coefficient, cm^2/s
υ	=	scan rate, V/s

For irreversible processes (those with slow-moving electron exchange), the individual peaks are reduced in size and extensively disjointed. Completely irreversible systems are characterized by a shift of the peak potential with the scan rate:

$$E_p = E^\circ - \left(\frac{RT}{\propto n_a F}\right)\left[0.78 - \ln\left(\frac{k^\circ}{(D)^{\frac{1}{2}}}\right) + \ln\left(\propto \frac{n_a F \upsilon}{RT}\right)^{½}\right] \qquad (5)$$

Where α = transfer coefficient

n_a = the number of electrons involved in the charge transfer step.

Thus, E_p occurs at potentials higher than E°, with the over-potential related to k^o (standard rate constant) and α. Independent of the value k^o, such peak displacement can be compensated by a suitable change in scan rate. The peak potential and the half-peak potential (at 25ºC) will differ by 48/αn mV. Hence, the voltammogram becomes drawn-out as αn decreases.

The peak current, given by:

$$i_p = (2.99 \times 10^5) n(\propto n_a)^{½} A C D^{½} \upsilon^{½} \quad (6)$$

is still proportional to the bulk concentration, but will be lower in height (depending on the value of α). Supposing α = 0.5, the ratio of the reversible current peaks is 1.27 (i.e. the peak current for the irreversible process is about 80% of the peak for the reversible one). For quasi- reversible systems (with $10^{-1} > k^o > 10^{-5}$ cm/s) the current is regulated by both the charge transfer and mass transport. The profile of the cyclic voltammogram is a function of the ratio $k^o/(\pi \upsilon n F D/RT)^{½}$. As the ratio increases, the process approaches the reversible case. For minute values of it, the system exhibits an irreversible behaviour. Generally, the voltammograms of quasi reversible systems are more drawn out and display a larger separation in peak potentials as compared to a reversible system. For a quasi-reversible reaction (ΔE_p up to 200mV) a numerical approach brings values of function Ψ:

$$\Psi = k_s \left(\frac{D_{ox}}{D_{red}}\right)^{\frac{\propto}{2}} \div \left[D_{ox} \pi \left(\frac{nF}{RT}\right)\right]^{½} \quad (7)$$

2.4.1.2 Square wave pulse voltammetry

Square wave voltammetry is a electroanalytical technique whereby a square wave modulation is applied to a constant or nearly constant dc potential, and current is sampled at the end of successive half cycles of the square wave. This technique is convenient primarily because: sensitivity is as good as or usually better than any other differential technique, voltammograms are promptly attained, background currents are efficiently differentiated against, the slope and position of the net current response are largely independent on convective mass transport, and the total charge passed can be insignificant. **Figure 13** depicts an Osteryoung Square Wave Voltammetry (OSWV), the perturbation of the potential with time involves an in-phase combination of a staircase waveform of small and constant step height ($1< \Delta E_{base}< 40mV$) with periodic square wave pulses ($1\leq \Delta E_{sw}$ (= ½ square wave amplitude) ≤ 250 mV). This last perturbation comprises of pulses alternating in direction, i.e. succession of forward (reduction or oxidation) and reverse (oxidation and reduction) cycles ($1\leq$ frequency SW ≤ 2000 Hz). The complete result obtained is a sequence of equally spaced steps: the forward step of height: $2\ \Delta E_{sw} + \Delta E_{base}$; the reverse step of height: $-2\Delta E_{sw}$ [182].

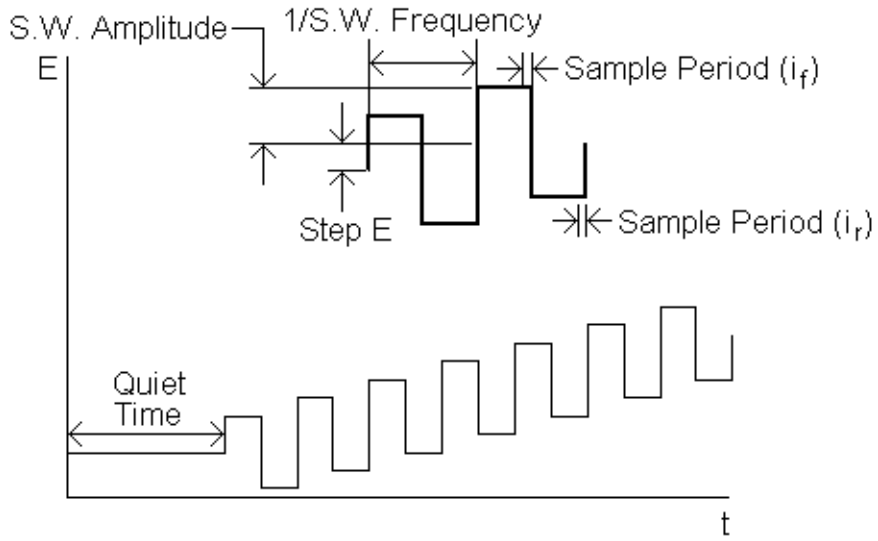

Figure 13: Potential-time perturbation on Osteryoung square wave voltammetry [182].

In SWV, the current is sampled at the end of each forward and reverse pulse. The result of this, is three curves being produced **Figure 14**: forward current (if), the reverse current (ir) and the net current. In a reversible system, the reverse pulse produces re-oxidation of the species produced on the forward pulse back to the original state, resulting in anodic current. Consequently, the net current at the current-voltage peak is larger than either the forward or reverse current, since it is the difference between them. The peak height is directly proportional to the concentration of the electrochemical species.

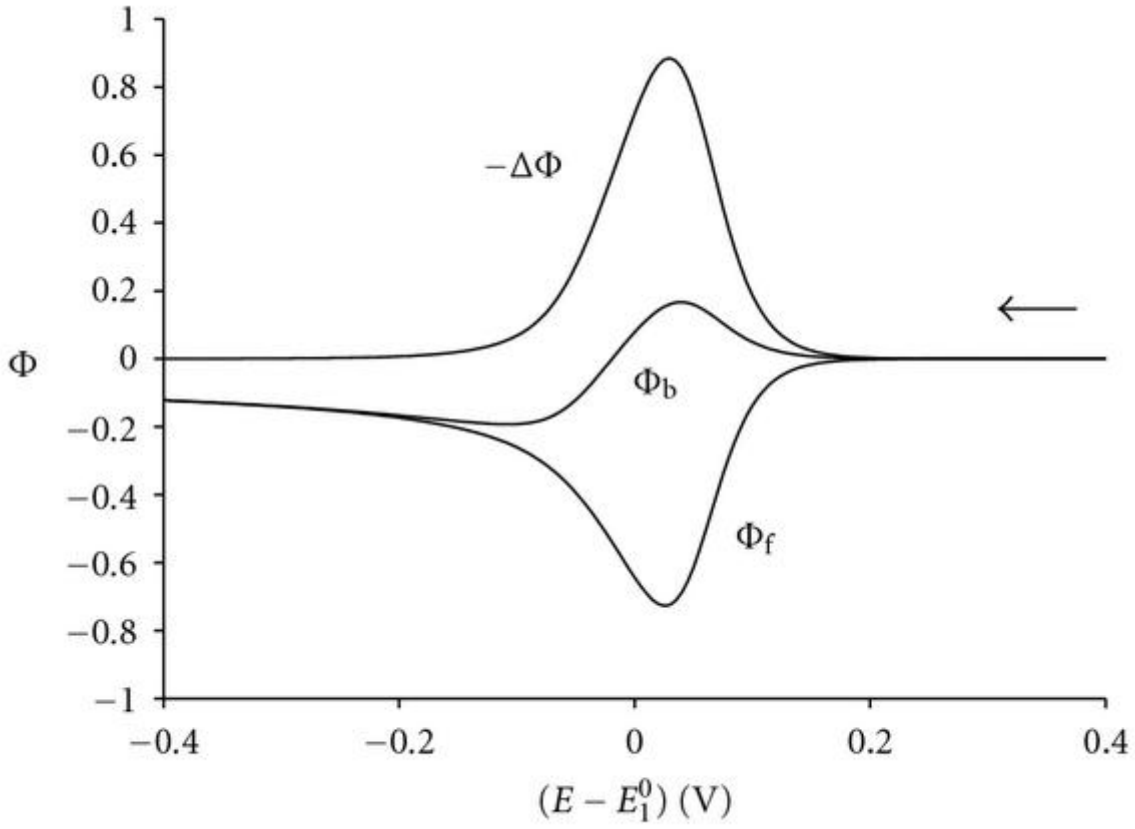

Figure 14: Osteryoung square wave voltammogram [182].

For a reversible electrochemical process, it was shown that the peak-potential almost corresponds with the formal electrode potential if ΔE_{sw} is small (about 50/n mV). In addition to this, with regards to a reversible process the width of the peak at half height, $\Delta E_{p/2}$ is given by the following two equations:

$$\Delta E_{\frac{p}{2}} = 4.90 \frac{RT}{nF} \quad (8)$$

or at a temperature of 25°C:

$$\Delta E_{\frac{p}{2}} = \frac{126}{n} mV \quad (9)$$

Therefore, OSWV can be very successfully used in solving most overlapping processes. In OSWV higher scan rates than in Differential Pulse Voltammetry (DPV) are attained from a few hundreds of mv/s to a few V/s. The value of the scan rate (obtained by the product SW frequency × ΔE_{base}) is around 0.2 V/s, a typical value for the scan rate of cyclic voltammetry. This also enables one to contend with the subsequent presence of chemical complications associated with the electron transfers. Square wave voltammetry is mainly utilised during the electrochemical investigations of selective polymeric nano-structures as a way of validating redox processes detected in preliminary cyclic voltammetry (CV). Square wave voltammetry can often clear up discrepancies in cyclic voltammograms, which results in the merging of the redox signals, producing individual sharp peaks [182].

2.4.2. Electrochemical impedance spectroscopy

Electrochemical reactions at the electrode-electrolyte interface cannot be fully comprehended using conventional electrochemical techniques. These conventional techniques afford only currents made of faradaic and non-faradaic components. A comprehensive description necessitates impedance measurements made over a broad frequency range at various potentials and determination of all electrical characteristics of the interface, which can be thought of as a thin capacitor that forms between the charged electrode and the counter ions lined up parallel to it [183-184]. Illustrations of the electrified interface have progressively changed from repeated adjustments **Figure 15(a)** of the model first proposed by Hemholtz [185]. In a simple case, the interface can be displayed by a corresponding circuit **Figure 15 (b)**, also called a Randles circuit [186], consisting of a double-layer capacitor in parallel with a polarization resistor (also known as a charge transfer resistor with definite constraints) and a Warburg impedance, connected in series with a resistor that measures the resistance of the electrolyte solution.

The equivalent circuit can be much more intricate, subject to the types of electrochemical reactions occurring at the interface. The representation in **Figure 15(b)** envisages that a faradaic current, which is due to the redox reactions, is always coupled with a capacitive component. Capacitance is considered as noise, and substantial attempts have been made to eradicate or reduce it, resulting in sampling, normal pulse, and differential pulse voltammetry [183]. The reduction or minimization of the effects of the non-faradaic currents is considered a submissive way to solve the problem. The separation of the faraidic currents from the non-faradaic signals would signify a more functional approach [187], which is conceivable with electrochemical impedance (EIS) because it provides all the information about the interface and the electrolyte solution. The removal of the noise and the reconstruction of the voltammograms of only the faradaic currents may solve another problem of conventional voltammetric measurements - the need to increase sensitivity, which is normally addressed by stripping voltammetry.

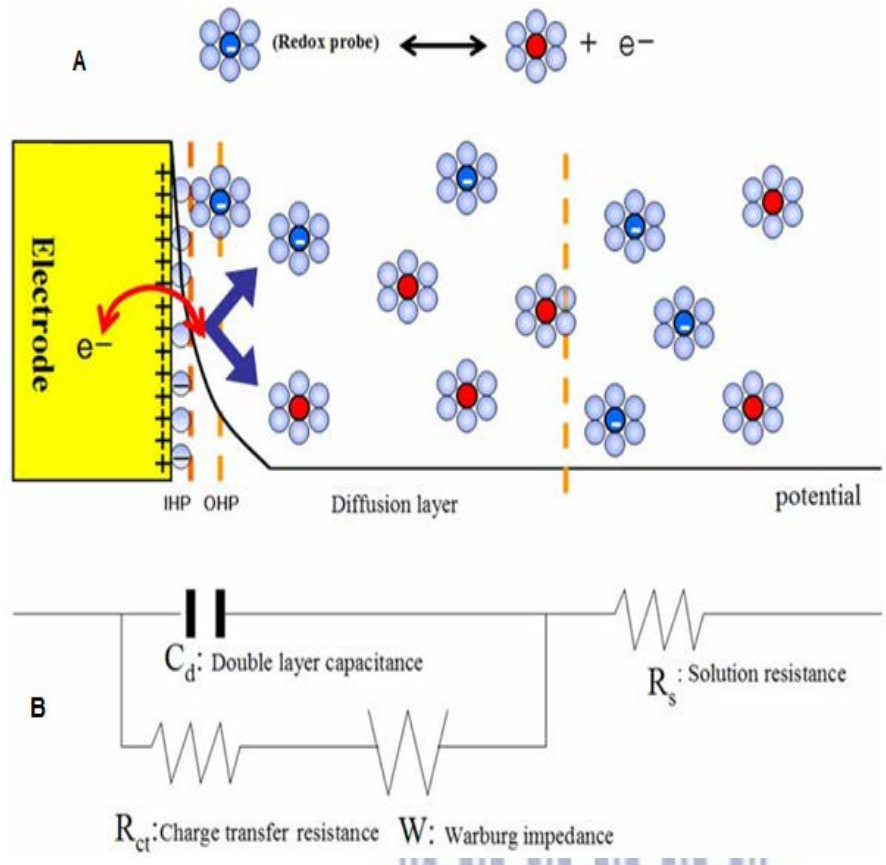

Figure 15: (a) and (b) A simple electrified interface, in which the vertical dotted lines in (a) are represented by the electronic components in (b) [184].

Impedance is an intricate resistance encountered when a current flow through a circuit which consisting of resistors, capacitors or inductors, or any permutation of these. The determination of the magnitude and the phase shift of an ac is dependant on the configuraton of the electronic components. Since an inductive effect is not ordinarily encountered in electrochemistry, we ruminate only the simple equivalent circuit shown in **Figure 15 (b),** in which no inductor is present.

However, first contemplate an experiment in which a series of increasing dc potentials (a ramp) are applied to a working electrode in an electrochemical cell containing an electroactive species.

A current-potential curve **Figure 16** is obtained, which is described by the Butler-Volmer equation (solid line)

$$\boldsymbol{i = i_0 \left[e^{\frac{-\propto nF}{RT}\eta} - e^{\frac{(1-\alpha)nF}{RT}\eta} \right]} \qquad (10)$$

in which η is the over-potential defined as E-E_{eq}, with E and E_{eq} representing the applied and equilibrium potentials, respectively; i_0 is the exchange current at η =0; n is the number of electrons transferred; F is the Faraday constant; R is the gas constant; T is the absolute temperature; and α is the transfer coefficient for electron transfer. The faradaic current *I* is limited by the mass transfer, (dashed line curving to the right) when the rate of electron transfer becomes large enough. At a given potential η_{bias}, the slope of the curves, $di/d_{\eta bias}$, is $1/R_p$, in which R_p is the polarization resistance. When a small ac voltage wave of frequency ω at η_{bias} **Figure 16** is superimposed, the ac of the same frequency will be flowing on top of the dc. Because the interface has resistors and a capacitor **Figure 15(b)**, the flowing ac will experience a phase shift, expressed as i_{bias}, caused by the ac wave perturbation.

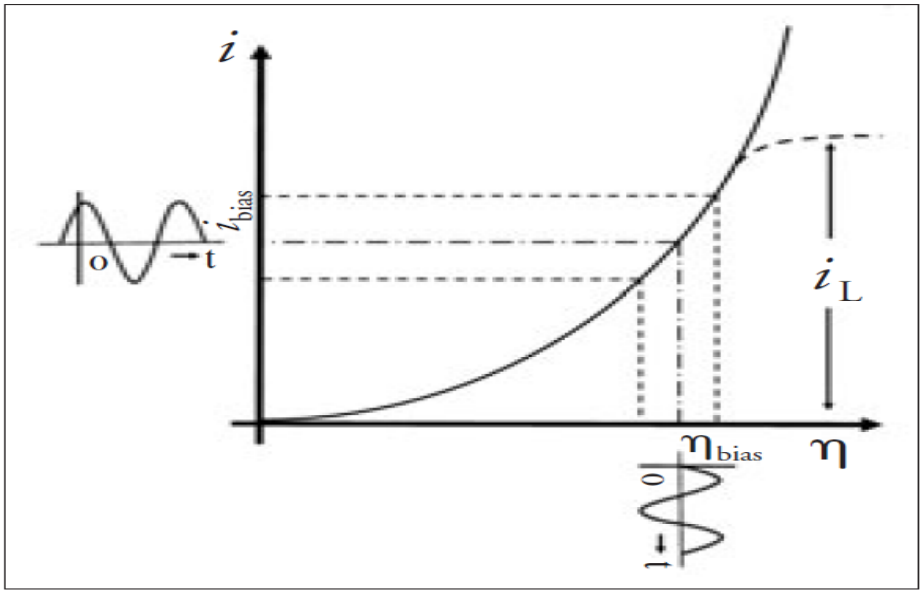

Figure 16: The dc plotted as a function of over-potential according to Butler-Volmer equation (solid line), which is limited by mass transport at large over-potentials (dashed line curving to the right), an ac voltage (broken line) superimposed on the dc bias potential, η_{bias} (dot-dashed line), shown on the *i* axis [$\eta_{bias} + \Delta\eta \sin(\omega t + \phi)$]. R_p is obtained by taking $\Delta\eta_i/\Delta i$, in which *I* is obtained after applying the ac voltage wave at a given η [184].

For a corresponding circuit, **Figure 16(b)**, a direct impedance expression can be derived by applying Ohm's law to two components connected in parallel. One of these is R_p, and the other is $1/(j\omega C_d)$, in which C_d is the double layer capacitance.

$$Z(\omega) = R_s + \frac{R_p}{1+j\omega R_p C_d} = R_s + \frac{R_p}{1+\omega^2 R_p^2 C_d^2} - \frac{j\omega R_p^2 C_d}{1+\omega^2 R_p^2 C_d^2} = Z' + jZ'' \qquad (11)$$

The derivation of the equation and its interpretation is simplified when we neglected the contribution of the Warburg component. Therefore, the impedance of the interface is made up of two parts, a real number Z' and an imaginary number Z'' with a complex representation, $Z(\omega) = Z'(\omega) + j\,Z''(\omega)$ with ϕ (the phase angle) $= \tan^{-1}[Z''(\omega)/ Z'(\omega)]$.

Even though the capacitance is comparatively uniform over the potential at a given electrode, the R_p varies as a function of η_{bias} applied to the electrode. A series of $Z(\omega)$ data is acquired in a range of frequencies of a given dc bias potential, typically between 100kHz-1×10^{-4} Hz. The impedance can vary, depending on frequencies being used, and is often plotted in a variety of ways as a function of frequency (making it a spectroscopic technique), consequently the name EIS [188]. Conversely, this is an inaccuracy since the frequencies do not represent energy levels and accordingly the impedance has nothing to do with quantum states in spectroscopic transitions. Consideration of the impedance data in such a frequency range results in the determination of system characteristics for the electrochemical reaction (i.e. R_s, R_p, and C_d). R_p is a function of potential; however, at $\eta=0$, it becomes the charge transfer resistance R_{ct}.

Two appropriate ways of handling the impedance data are the Nyquist plot **Figure 17(a)** according to equation 2. At high frequencies, the frequency-dependant term of equation 2 vanishes, resulting in $Z(\omega) = Z'(\omega) = R_s$, which is an intercept on the $Z'(\omega)$ axis on the high-frequency side ($\phi=0$ or $Z''(\omega)=0$). For $\omega\rightarrow0$, equation 2 becomes $Z(\omega) = R_s + R_p$ which is an intercept on the $Z'(\omega)$ axis on the low-frequency side. At the frequency where a maximum $Z''(\omega)$ is observed, the clear-cut relationship $R_p\times C_d = 1/\omega_{max} = 1/(2\pi f_{max}) = \tau_{rxn}$, which is the time constant of the electrochemical reaction can be shown and is an indication of how fast the reaction takes place. Also, if $R_p\times C_d$ is known, C_d can be obtained because R_p is already known from the low –frequency intercept on the $Z'(\omega)$ axis. The Nyquist plot provides all the information about the electrode-electrolyte interface and the reaction. Analogous information is obtained by scrutinizing the Bode plot **Figure 17(b)** using equation 2: log R_s and log $(R_s + R_p)$ are acquired from the $Z(\omega)$ versus log ω plot at high and low frequencies using the same reasoning as in the case of the Nyquist plot. In the intermediate frequency region, an almost straight line with a slope of ~ -1.0 can be observed. The equation for this line is determined by ignoring the frequency-independent terms, R_s and 1 in the denominator of equation 2 to yield

$$Z(\omega) = R_s + \frac{R_p}{1+j\omega R_p C_d} \quad (12)$$

If the logarithm is taken on both sides of the subsequent equation log Z (ω) = -log ω –log C_d is produced, which says that log |Z (ω)| versus log ω would have a slope of -1, and C_d can be obtained from the intercept of this line with the Z (ω) axis when –log ω = 0 at ω = 1. Thus, the Bode plot gives the same information as the Nyquist plot. A comprehensive description of an electrochemical system can be constructed with data obtained from impedance studies. The Randle circuit can be determined by fitting the experimentally acquired impedance data to the theoretical behaviour of the postulated corresponding circuit; this fitting supplies all the required parameters. Impedance measurements are most advantageous for examining complex systems such as anodic behaviour of metals and other composite materials [189-192], corrosion [193], states of electrodes during charging/discharging cycles of batteries [194-197], surface characterization of polymer-modified electrodes [198-200], and many other intricate electrochemical phenomena [201].

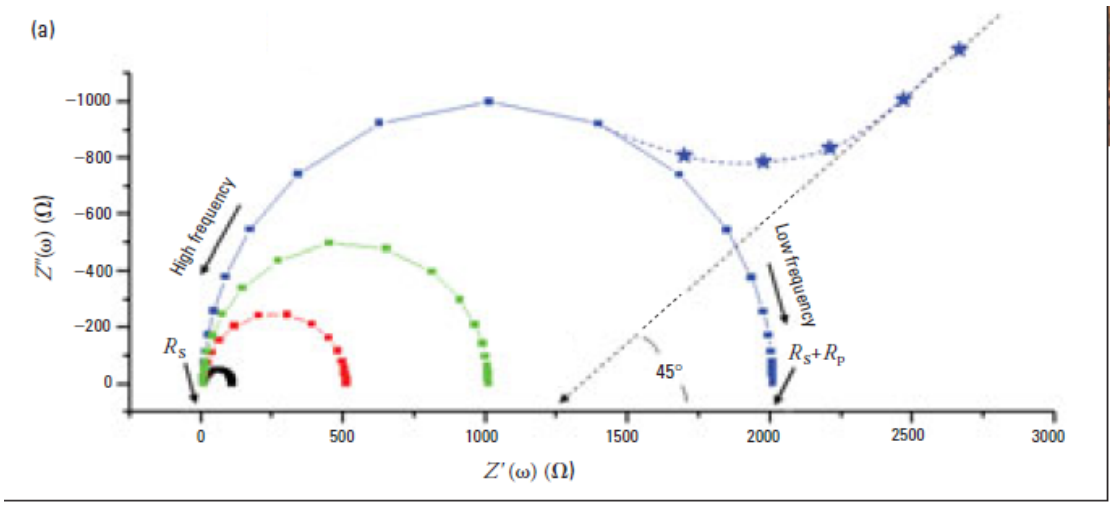

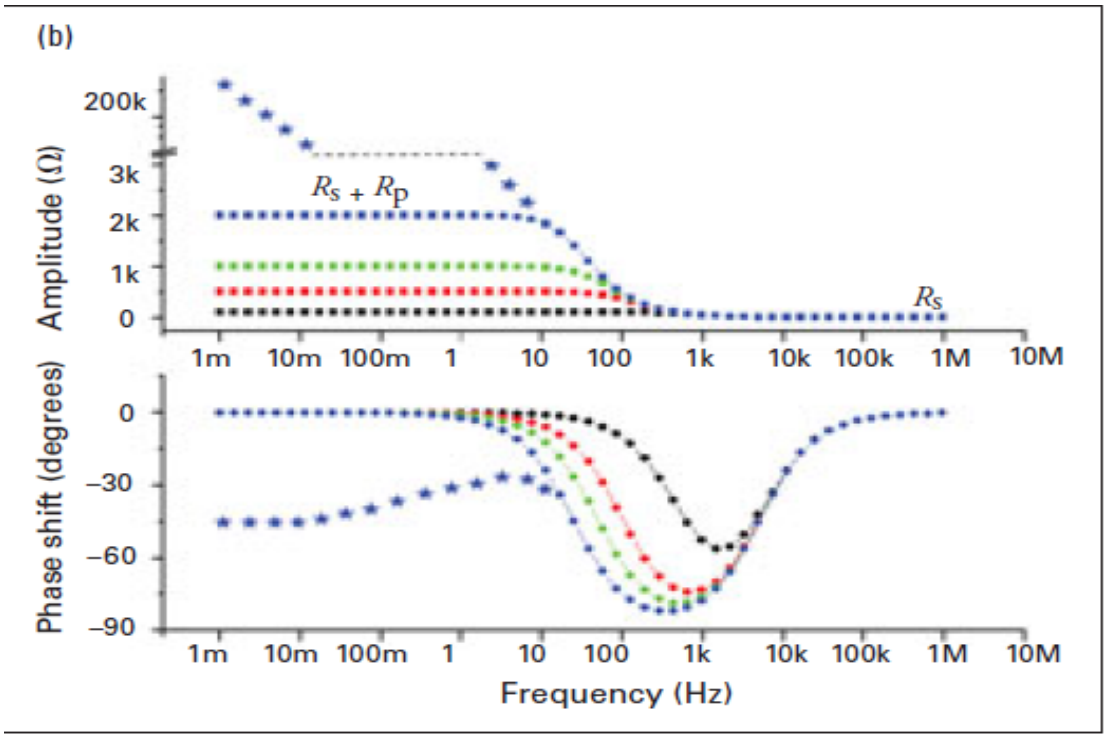

Figure 17: (a) Nyquist and (b) Bode plots [184]

2.5 Microscopy and Spectroscopy techniques

2.5.1 Ultraviolet-visible (UV-vis) spectroscopy

Most organic molecules and functional groups are translucent in the portions of the electromagnetic spectrum which we call the ultraviolet (UV) and visible (vis) regions – that is, the region where wavelengths range from 190 nm to 800 nm. Accordingly, absorption spectroscopy is of some degree of usefulness in this range of wavelengths. However, in some cases we can derive beneficial information from these sections of the spectrum. That information, when pooled with information provided by infrared and nuclear magnetic spectra, can lead to valued structural proposals [181]. The principle of molecular absorption spectroscopy is based on the measurement of transmittance T or the absorbance A of solutions enclosed in transparent cells having a path length of b centimetres. Normally, the concentration of an absorbing analyte is linearly related to absorbance as given by Beer's law

$$A = -\log T = log\frac{P_o}{P} = \varepsilon bc \qquad (13)$$

A is the Absorbance, T is the transmittance, P_0 is the incident radiant power, P is transmitted radiant power, b is the path length, c the concentration of the absorber and ε molar absorptivity.

Normally transmittance and absorbance cannot be measured in a laboratory because the analyte solution must be held in a transparent container, or cell. Reflection occurs at the two air-wall interfaces as well as the two wall-solution interfaces. The resulting beam attenuation is substantial. The attenuation of the beam may occur because of scattering by large molecules and occasionally from absorption by container walls. To compensate for these effects, the power of the beam transmitted by the analyte solution is usually compared with the power of the beam transmitted by an identical cell comprising of solvent only. An experimental transmittance and absorbance that closely approximate the true transmittance and absorbance are then obtained with the equations [181].

$$T = \frac{P_{solution}}{P_{solvent}} \approx \frac{P}{P_o} \quad (14)$$

$$A = log \frac{P_{solvent}}{P_{solution}} \approx log \frac{P_o}{P} \quad (15)$$

2.5.2 Fourier Transform infrared spectroscopy (FT-IR)

The application of Infra- Red (IR) technology as a characterisation tool in biology began as early as the 1910s, when the use of IR spectroscopy for the investigation of biological samples was first proposed. By the late 1940s, this diagnostic tool was being efficaciously explored for the study of biological materials and, in fact, IR spectroscopy had become an acknowledged tool for the characterization of biomolecules [202]. In fact, some of the earlier usages of FT-IR in micro-organisms date back to the 1950s [203-206]. Using IR-spectroscopy as a means of differentiating and identifying bacteria was extensively reported at nearly this year. In 1995 a critical review was published which stated that, although bacteria exhibit IR-spectra that are unique for individual strains, the identification of bacteria via IR-techniques cannot be regarded as a useful scheme, as it is an unfeasible procedure [206-207]. However, it was not until 1988 that Naumann *et al* [208] introduced this technique again as a useful tool in microbial identification [209]. This resurgence of IR-spectroscopy as a means for characterizing microbial samples was initiated after the development of modern interferometric IR-spectroscopy, the obtainability of low-cost mini computers and powerful new algorithms for multivariate statistical investigation and pattern recognition methodologies [207]. During the past four decades, it has been evidently verified by several authors that infrared spectra from bacteria can be used for identification [210] and differentiation [211]. The last decade has shown that FT-IR spectroscopy can be a powerful technique for the study of biological macromolecules [212] and of complex biological systems such as tissues and cells [213-215].

2.5.2.1 Methodological properties of FT-IR

FT-IR spectroscopy is a method of vibrational spectroscopy, and the FT-IR spectrum mirrors both molecular structure and molecular surroundings. The application of this technique, involves the irradiation of the sample with infrared radiation from an infrared source, and the absorption of the radiation excites vibrational motions by depositing quanta of energy into vibrational modes [216]. Consequently, the molecule in question, when exposed to radiation produced by the thermal emission of a hot source (a source of IR energy), absorbs only at frequencies conforming to its molecular modes of vibration in the region of the electromagnetic spectrum between visible (red) and short waves (microwaves) [202]. These vibrational motion changes cause the rising of bands in the vibrational spectrum; each spectral band is characterized by frequency and amplitude [216].

The IR region (1 to 100μ M) is sectioned in three zones far-(100 to 25μM), mid-(25 to 2.5μM), and near IR (2.5-1μM). The mid-IR depicts primary molecular vibrations and is the most common and extensively employed region for the investigations of substances in chemistry and forensics. Characteristic absorbance of all molecules exhibit peaks in a segment of this region (1350 cm^{-1} to1000 cm^{-1}; NB: by convention, the frequency is generally expressed as wave numbers using the reciprocal cm as its unit: 1μM= 10^4 cm^{-1}); accordingly, this physical property is considered a molecular fingerprint. The far and near IR zones are not frequently employed because only skeletal and secondary vibrations (overtones) occur in these regions, generating spectra that are difficult to construe [192 413]. Several of the infrared bands of biological concern transpire in the frequency range between 4000 and 1000 cm^{-1}. The FT-IR spectrum of a cell will reveal contributions from all cellular macromolecules, including protein, lipid, carbohydrates, and DNA. Even though the spectra of macromolecules are complex, protein, lipids, and DNA provide characteristic, non-overlapping contributions to the FT-IR spectrum. These non-overlapping spectral contributions permit the determination of macromolecular concentration from the band's amplitude [216-217].

To understand FT-IR spectra of biological samples, some fundamental knowledge on cell composition and the structures of the building blocks in biological samples is essential. The infrared spectra of complex biological molecules do not only refer to the composition of the cell, but also afford a number of definite bands that are sensitive to structural or conformational variations. The physical state of the sample (hydration or aggregation state, etc.) has a severe effect on FT-IR results. Thus, one has to be rigorous in standardizing sampling, preparation and data acquisition procedures when using this technique [217]. IR spectroscopy was significantly enhanced using a new component: the interferometer and by the application of a mathematical transformation, the Fast Fourier Transform algorithm, which allows for the concurrent detection of all the transmitted energy. Generally, for the identification of non-fastidious bacteria to be successful, growth conditions, such as the length of the growth period and the composition of the culture medium, should remain constant [218]. A benefit of FT-IR spectroscopy is that this method can be applied to powdered, dehydrated or aqueous samples. The FT-IR spectrometer can also be modified to facilitate the study of very small samples, such as tissue sections and single colonies, likelihood. This technique is intricately sensitive [219].

2.5.3 Raman spectroscopy

Raman spectroscopy is a vital technique for studies of pharmaceutically and medically pertinent molecules. This technique is used in numerous fields where non-destructive microscopic chemical analysis and imaging is necessary. Raman spectroscopy is used by biologists and chemists alike in identifying chemical compounds and their functional groups, and to determine the conformation of complex biomolecules, such as proteins and DNA. The chemical composition and structure of a sample, whether solid, liquid, gas, gel, slurry or powder can be promptly determined using this method of characterisation. It is primarily pliable to *in vivo* measurements. Raman spectroscopy and the infrared absorption spectroscopy are the most extensively used techniques which give information about the structure and properties of molecules by providing comprehensive characteristics of their vibrational transitions.

Raman analysis can afford key information without difficulty and rapidly. The Raman spectroscopy is centered on an inelastic light scattering by molecule (the Raman Effect). During the Raman scattering process, a photon interacts briefly with a molecule and is then scattered into surroundings in all directions. During the fleeting interaction with the molecule, a photon loses or gains energy which is then detected and analysed.

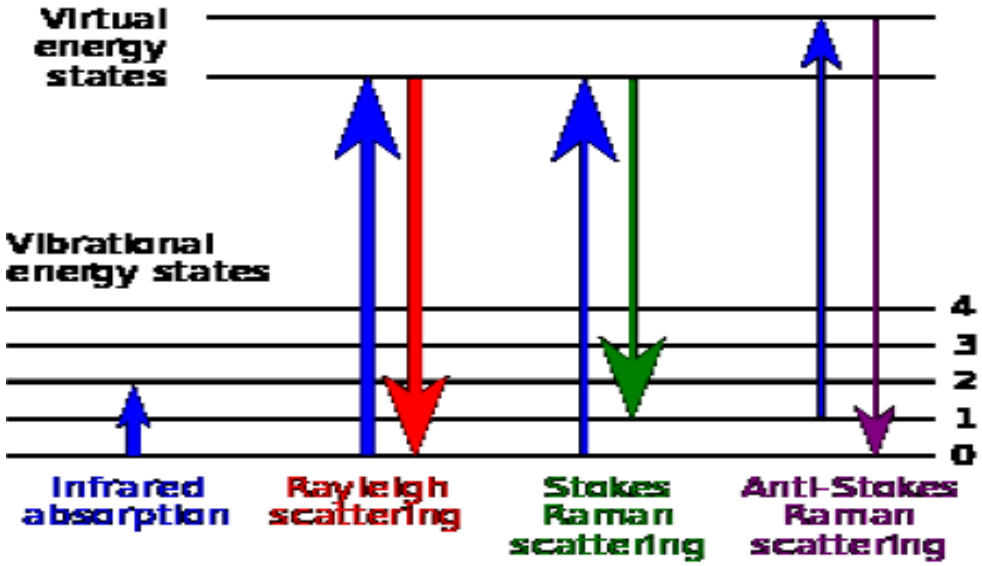

Figure 18: Energy-level diagram showing the states involved in Raman signal [220].

The Raman effect transpires when electromagentic radiation encroaches on a molecule and interacts with the polarizable electron density and the bonds of the molecule in the phase (solid, liquid or gaseous) and surroundings in which the molecule finds itself. The Raman effect, is a method of inelastic light scattering, a photon (electromagnetic radiation of a specific wavelength) excites (interacts with) the molecule in either the ground rovibronic state or an excited rovibronic state. The result of this interaction causes the molecule to be in a so-called virtual energy state for a brief period before an inelastically scattered photon results. The resulting inelastically scattered photon which is “discharged”/” scattered” can be either of higher (anti-Stokes) or lower (Stokes) energy than the inbound photon.

This interaction results in the molecule being in a different rovibrinic state than the one in which the molecule was originally, before interacting with the incoming photon (electromagnetic radiation). The change in energy between the original rovibronic state and this resulting rovibronic state leads to a shift in the emitted photon's frequency away from the excitation wavelength, the so-called Rayleigh line. The Raman effect is due to inelastic scattering and should not be mixed up with emission (fluorescence or phosphorescence) spectroscopy where a molecule in an excited electronic state emits a photon and returns to the ground electronic state, in many cases to a vibrationally excited state on the ground electronic state potential energy surface.

Raman spectroscopy, is a molecular spectroscopy which is perceived as inelastically scattered light, permitting for the interrogation and identification of vibrational (phonon) states of molecules. Thus, Raman spectroscopy affords an invaluable analytical tool for molecular finger printing as well as monitoring changes in molecular bond structure (e.g. state changes and stresses and strains). When comparing Raman to other vibrational spectroscopy methods, such as FT-IR and NIR, Raman has numerous major advantages. These advantages stem from the fact that the Raman effect displays itself in the light scattered by a sample as opposed to the light absorbed by a sample. The consequence of this is that Raman spectroscopy needs little to no sample preparation and is insensitive to aqueous absorption bands. And consequently, enables the Raman method to facilitate the measurements of solids, liquids and gases not only directly, but also through transparent containers such as glass, quartz, and plastics [220].

2.5.4 Atomic force spectroscopy (AFM)

Atomic force microscopy (AFM) is one of the leading tools for imaging used in materials science and has subsequently found many applications in biological sciences. This technique is used to image the topography of soft biological materials in their innate surroundings. The measuring of the mechanical properties of cells and extracellular matrices, including their intrinsic elastic modulus and receptor-ligand interactions can also be attained using this technique. And accordingly, the number of references to AFM in the physical sciences has affectedly increased. The AFM technique has several advantages over electron microscopy in the study of biological materials; one of them includes the ability to image in liquid with minimal sample preparation. This method also permits the topographic characterisation of surfaces at resolutions which could not be attained by optical microscopy. Optical microscopy is limited to the diffraction limit of light while; the achievable lateral resolution of the AFM is limited by the tip size and shape and is typical on the order of a few nanometers. The height (z) resolution of the AFM is approximately 1Å, limited only by electronic and thermal noise in the system. High-resolution imaging, therefore allows molecular scale features to be identified in the innate surroundings of the sample and in real time. The high- resolution images of typical and diseased states can be equated, giving insight into molecular reorganization which is not observed by other techniques. Adding to the high-resolution imaging, the AFM is capable of exerting and measuring forces of the order of pico-newton's. This feature affords the ability for investigation of mechanical properties, as well as obtaining a local elastic modulus of the surface, measuring modulus variations across a sample surface, and measuring ligand-receptor interactions. The ability to be able to explore the mechanical properties of biological materials and surfaces in their innate surroundings is indispensable for complete characterisation of the material [221].

2.5.5 X-ray diffraction (XRD)

X-ray diffraction (XRD) is the foremost characterisation techniques to be used when one has a sample of an unknown solid compound [222]. This technique involves taking a dry ground up sample, which could be a mixture, and bombards it with electron emissions from a cathode ray tube at a fixed wavelength. Bragg's law is then applied with the measured angle of reflection and the inner atom spacing is determined [223].

$$n\lambda = 2dsin\theta \qquad (16)$$

This was all started by a man named Max von Laue. In 1912, he came up with the idea that crystalline substances act as 3D diffraction grating for x-rays [213 434]. Subsequently W.H. Bragg and his son W.L. Bragg formulated the law now used. They did three diffractions on sodium chloride (NaCl), zinc sulphide (ZnS), and diamond (C). These experiments and the formulation of the law led them to receive a Nobel Prize for their work in 1915 [224].

Bragg's law is one of the most important features of XRD. The equation is $n\lambda=d\sin\theta$. Where n is an integer, λ is the wavelength in nm, d is the inner spacing, and θ is the angles of the diffractions. This equation is used to generate a graph that plots the angles versus intensity. From this graph three prominent spikes are observed which is used to identify the sample. The XRD technique allows for any crystalline substance to be identified. When classifying a mineral, one looks at the resulting graph of the d-spacing found with Bragg's law and then uses the three most prominent spikes from its angles that produce the most diffraction. XRD began using a cathode ray to shoot electrons at a crystalline substance, then the inner atomic spacing (d) is determined using Bragg's law to draw a graph. Now most laboratories have a machine that is fully automatic. These machines can perform multiple tests and create any number of graphs and average them for very fine precision [225].

2.5.6 High Resolution Transmission Electron Microscopy (HR-TEM)

High resolution transmission electron microscope is an imaging technique of the transmission electron microscope that allows for direct imaging of the atomic structure of a sample. The properties of material such as semiconductors, metals, nanoparticles and sp-bonded carbon (e.g. graphene) can be conveniently studied by using HR–TEM [226]. Imaging in HR–TEM is based on phase contrast with a scale (presently around 0.5 angstroms) enough to resolve individual atoms of a crystal and its defects. The process of contrast of a HR–TEM image occurred from the interference in the image plane of the electron wave with itself, a large part of the structural information of the sample which is contained in the phase of the electron wave is then recorded using the amplitude in the image plane. However, the phase contrast mode of operation is prone to some limitation, as image in phase contrast is influenced by aberration (e.g. defocus) of the imaging lenses in the microscope, which may not allow an instinctive interpretation. Also, problems may arise from the high magnification imaging which requires a high electron dose therefore, specimens need to be comparatively beam insensitive to avoid any damage of specimen, however, compounds with a high thermal stability and especially high melting inorganic material can be investigated at atomic resolution.

Analysis in HR-TEM requires a very thin specimen, because, the thinner the better for the technique normally smaller than 50nm, depending on acceleration voltage used [227]. HR-TEM is more applicable and useful in the distribution and structure of defects, interfaces and grain boundaries in samples, nano-crystalline features in amorphous films, small particle analysis in heterogeneous catalyst, sub-micron morphological and device features and in thermodynamic decompositions, diffusion and phase transformations [228-229]. Jiang *et al* [230] have employed high-resolution transmission electron microscopy (HR-TEM) to examine nano defects at shear bands (main microstructural effect of plastic deformation in amorphous alloys) in both the tensile and compressive regions, and the results have been used to interpret the mechanism of mechanically-induced nano-crystallisation.

They have been able to determine from the difference in crystallization at shear bands in compression versus tension, that the effect of the adiabatic heating on nanocrystallisation at shear bands is much less significant than enhancement of atomic mobility by deformation. HR-TEM has been employed by Yuk *et al* [231] and reported that direct atomic-resolution imaging allowed visualized critical steps in the process. Site-selective coalescence, surface faceting as well as structural reshaping after coalescence can also be achieved [232]. A typical representation of an HR-TEM instrument and sample of an image of graphene from the instrument is shown in **Figure 19** below [94].

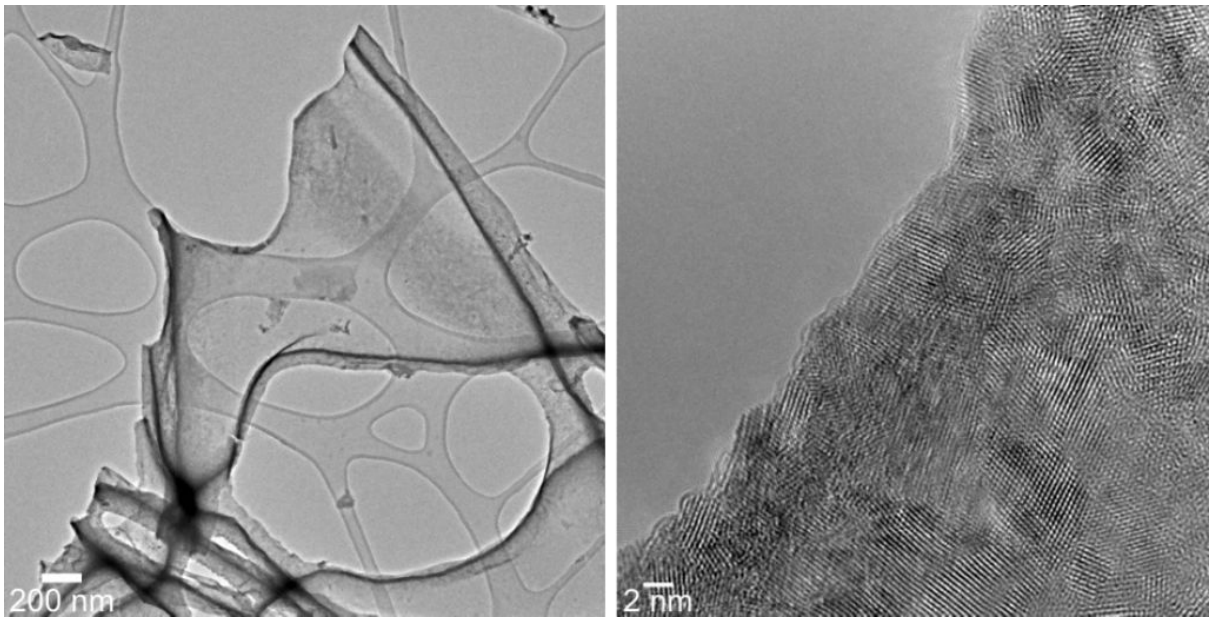

Figure 19: An example of HR-TEM image [88]

Figure 20: A typical HR-TEM [88]

2.7.7. High resolution scanning electron microscope (HR – SEM)

A scanning electron microscope is a powerful type of electron microscopic technique in the examination of materials. Images of a sample are produced in HR – SEM when samples are scanned with a focused beam of electron, the electrons then interact with atoms of the sample which resulted in the production of various signals that can be detected and that contain information about the surface topography of the sample and composition. Usually, the electron beams scan in a raster scan pattern, and position is combined with the detected signal to produce an image. High modification of images can also be obtained, with a good depth of field, as well as analysis of individual crystals or other features. A high-resolution SEM image has been reported to show detail down to about 20 to 25 Angstroms, or even higher [232].

When used in conjunction with the closely-related technique of energy-dispersive x-ray microanalysis (EDX, EDS, and EDAX), the composition of individual crystals or features can be determined. The magnification of the image is the ratio of the size of the screen to the size of the area scanned on the specimen, for example, if the screen is 300mm across and the scanned area is 3mm across on the specimen, then the magnification is x 100, also if the scanned area is 0,3mm across on the specimen, the magnification is x 1000 which serves as a higher magnification [92 181]. **Figure 21(a)** showed a typical MEB –FEG Low voltage and high resolution scanning electron microscope: Hitachi S -4700 (cold FEG) – EDS – back scattered electrons detector. LEO 1530 (Schottky source) - EDS - CL and EBIC at ambient and cryogenic temperature for high resolution imaging and high spatial resolution elemental analysis and an image sample of graphene **Figure 21(b)** that was taken [232].

Figure 21 (a) MEB –FEG Low voltage and high resolution scanning electron microscope: Hitachi S -4700 (cold FEG) – EDS – back scattered electrons detector. LEO 1530 (Schottky source) - EDS - CL and EBIC at ambient and cryogenic temperature for high resolution imaging and high spatial resolution (b) HR-SEM of graphene [88].

CHAPTER 3

MATERIALS AND METHODS

This chapter provides an in depth description of the materials and the different experimental procedures employed for the chemical preparation of graphene oxide, graphene, poly (2,5dimethoxyaniline), graphene-poly (2,5dimethoxyaniline). Also, included in this chapter are the procedures used for the fabrication of electrochemical sensor based on graphene-poly (2,5dimethoxyaniline) nanocomposite.

3.1 Reagents

Natural graphite powder (microcrystal grade, 99.9995 %) (Metal base) UCP-1-M grade, ultra F" purity purchased from Alfa Aesar was used for graphene oxide preparation. 2,5-dimethoxy aniline, estradiol, estrone, estriol, ammonium persulphate (APS, $(NH_4)_2S_2O_8$, 98 %), ferric chloride ($FeCl_3$), hydrochloric acid (HCl, 37 %), hydrogen peroxide (H_2O_2, 30 wt % water solution), sulphuric acid (H_2SO_4, 98 %), sodium nitrate ($NaNO_3$) and potassium permanganate ($KMnO_4$), were all obtained from Sigma-Aldrich. All chemicals used in this study were analytical reagent grade and used without further purification. 0.01 M phosphate buffer and ethanol (96.4 %) were used as supporting electrolytes. And deionised water (18.2 mΩ) purified by a milli-QTM system (Millipore) was used in all sample preparations. Analytical grade nitrogen, purchased from Afrox Company, South Africa was used in analyses. Polishing pads obtained from Buehler, IL, USA and Alumina micro powder (1.0, 0.3 and 0.05μm alumina slurries) were used for polishing the electrodes used in this study. The screen-printed electrodes used as additional tools for comparative studies were all obtained from Metrohm SA.

3.2 Measurements and instrumentation

Cyclic (CV) and square wave voltammetric measurements were carried out using a 797 VA COMPUTRACE interfaced with a personal computer. A conventional three-electrode system consisting of glassy carbon disk and screen printed working electrode (GCE 0.071cm^2), Ag/AgCl (saturated KCl) and platinum acting as a reference and counter electrodes respectively were used. All the experiments were carried out in a 20 ml volumetric cell at room temperature (25 °C). The reaction media in the volumetric cells were de-aerated prior to the voltammetric determination by bubbling high purity nitrogen gas through the solutions. The infrared spectra of graphite, graphene oxide, graphene, poly (2,5-dimethoxy aniline), poly (2,5-dimethoxy aniline) containing graphene oxide and graphene were evaluated using Fourier Transform Infrared spectrometer (FT-IR, Perkin Elmer Spectrum 100). The structural properties were also evaluated using X-ray diffraction (XRD, Phillips X-ray diffractometer with Cu-Kα radiation). A tapping-mode atomic force microscope (AFM) (Veeco Nanoman V) was employed to evaluate the morphology of graphene oxide and graphene, with special emphasis on estimating its thickness. The silicon tip [antimony (n) doped] had a curvature radius of 2.5 - 3.5 μM, a force constant of 1 - 5 Nm^{-1} and a resonance frequency of 60 - 100 kHz. The samples for AFM were prepared by drop coating a graphene/water (5μL) dispersion onto a silicon wafer. Transmission electron microscopy images were taken on a Tecnai F20 HR-TEM and the scanning electron microscopy images were taken using LEO 1450 HR-SEM 30KV instrument equipped with energy-dispersive X-ray spectroscopy (EDX) and wavelength-dispersive spectroscopy (WDS). The Raman spectra were recorded on a Dilor XY Raman spectrometer with a Coherent Innova 300 Argon laser with a 514.5 nm laser excitation. Electrochemical impedance spectra (EIS) measurements were performed using Volta-Lab PGL402 from Radiometer Analytical (Lyon, France. UV-Vis spectra measurements were recorded over a range of 200-900 nm using 3 cm^3 quartz cuvettes with Nicolette Evolution 100 Spectrometer (Thermo Electron Corporation, UK).

3.3 Preparation of materials

3.3.1 Synthesis of graphene oxide

Graphene oxide (GO) was chemically prepared from natural graphite using the modified Hummers method [233]. Two grams of graphite flakes and 2 g of sodium nitrate ($NaNO_3$) were mixed in 90 ml of sulphuric acid (H_2SO_4, 98 %) in a 250 ml volumetric flask. The mixture was maintained under ice-bath and strong magnetic stirring for 15 minutes. After this, 12 g of $KMnO_4$ was slowly added to the reaction mixture while stirring was maintained, for 75 minutes. Excess purified water (18.2 mΩ) was slowly added to the resultant paste with vigorous stirring for 10 more minutes followed by the addition of 280 ml of hot distilled water (~ 100 °C). Then 50 ml of 30 % hydrogen peroxide (H_2O_2) was added to reduce the unreacted potassium permanganate and the system was maintained under stirring for 30 minutes. For purification, the mixture was washed by rinsing and centrifugation with 5 % HCl and after that with de-ionised water (DI) for several times. After filtration and drying under vacuum, the graphene oxide (GO) was obtained as a grey powder [234].

3.3.2 Preparation of graphene

The chemical conversion of graphene oxide (GO) to reduced graphene oxide (RGO) has two intended goals: the elimination of functional groups and the healing of structural defects. This was achieved according to the method reported by Shen *et al* [235]. 0.1 g of the prepared graphene oxide was dispersed in 100 ml of deionised water to be exfoliated into graphite oxide (GO) sheets by ultra-sonication for 1 hour where a stable aqueous dispersion was formed. Thereafter 0.1 ml of hydrazine monohydrate was added, and the mixture was heated to 95 ºC for 1 hour. Once the reaction was completed, the graphene was collected by filtration as a black powder. The obtained cake was washed with de-ionised water several times to remove the excess hydrazine and the final product was dried in a vacuum oven at 80 ºC for 24 hours [235].

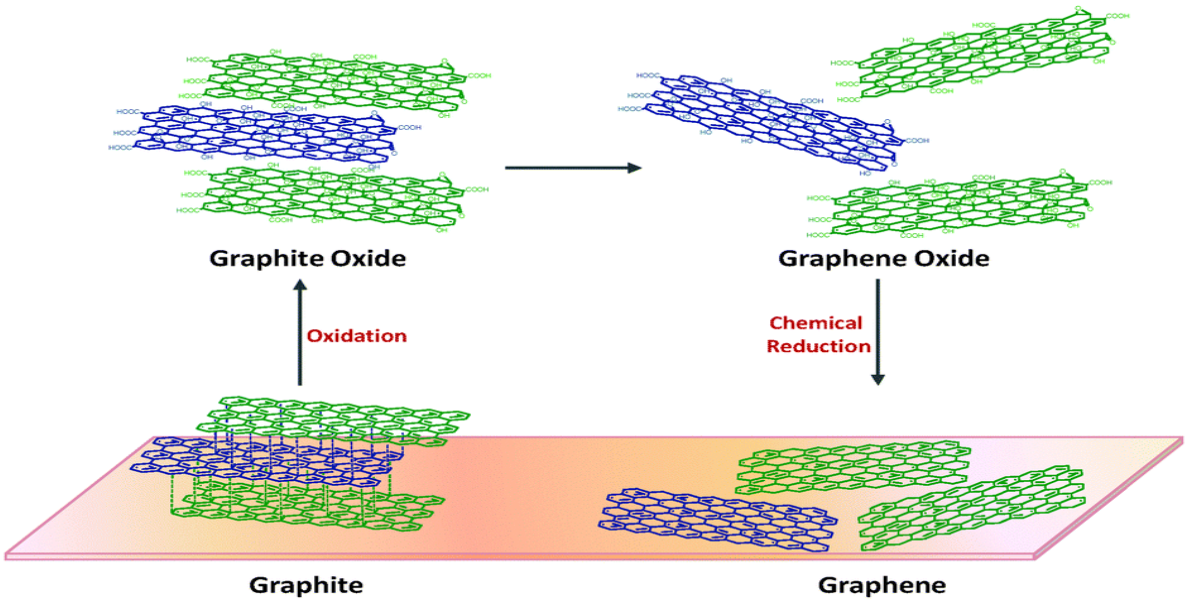

Figure 22: Schematic illustration of the synthesis of graphene (Chemical Society Reviews Chua *et al*)

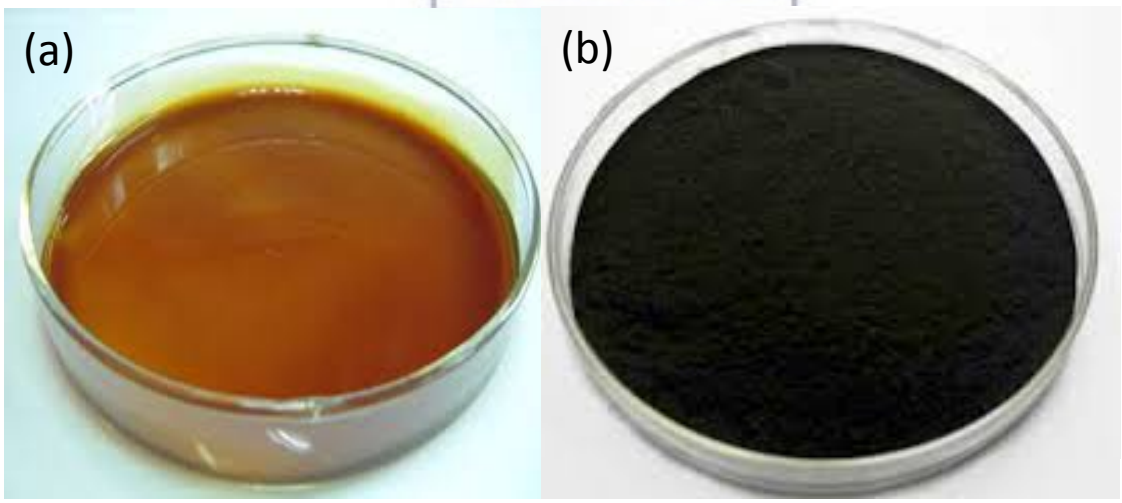

Figure 23: Sample of synthesised solution of (a) graphene oxide and (b) graphene (ES Nano Supplier of aminated graphene in China)

3.3.3 Preparation of poly (2,5-dimethoxyaniline) (PDMA) by chemical polymerization

The chemical polymerization of 2.5-dimethoxyaniline was achieved using the method prescribed by Mavundla *et al* [236]. In a 50 ml flask 0.2 g of 2,5-dimethoxyaniline was dissolved in a solution of 2 ml HCl in 20 ml of distilled water. The solution was stirred for 30 minutes at 50 °C after which 0.48 g of ammonium persulphate (APS) and 0.375 g of ferric chloride ($FeCl_3$) was added respectively in the reaction. The resultant mixture was stirred for another three hours at 50 °C. The contents of the reaction were then put in the oven at 70 °C overnight to evaporate the solvents. The remaining contents were washed with ethanol (96.4 %) and dried at 70 °C [236].

3.3.4 Chemical polymerization of 2,5-dimethoxyaniline with graphene oxide (GO)

The doping of poly (2,5-dimethoxyaniline) with graphene oxide was prepared by the in situ polymerisation of 2,5-dimethoxyaniline in a suspension of graphene oxide through the chemical oxidation of 2,5-dimethoxyaniline with ammonium persulphate (APS) in an acidic medium according to literature [236]. In a typical preparation, 0.2 g of 2,5-dimethoxyaniline and 0.2 g of the prepared graphene oxide was dissolved in a solution of 2 ml HCl in 20 ml water and the solution was stirred for 30 minutes at 50 °C followed by the addition of 0.48 g of APS and 0.375 g of ferric chloride respectively into the solution. The resultant mixture was stirred for another three hours at 50 °C and the contents of the reaction were put in the oven at 70 °C overnight to evaporate the solvents. The remaining contents were washed with ethanol and dried at 70 °C.

3.3.5 Reduction of poly (2,5-dimethoxyaniline) with graphene oxide

0.1 g of the prepared poly (2,5-dimethoxyaniline) graphene oxide composite was dispersed in 100 ml of distilled water and sonicated for 1 hour to form a stable aqueous dispersion. 0.5674 g of sodium borohydrate ($NaBH_4$) was added to the dispersion under magnetic stirring, and the mixture was maintained as such at 125 °C for 3 hours.

The reduced precipitate solid was obtained and isolated by filtration, then re-dispersed in 1M aqueous HCl containing ammonium persulfate (APS), and stirred at room temperature overnight for reoxidation and reprotonation to occur to recover the PDMA crystallinity. The resulting graphene-PDMA nanocomposite was collected by filtration and dried in vacuum at 70 °C [237].

3.3.6 Preparation of the graphene-PDMA modified electrode

Before commencing with the modification of the electrode the bare glassy carbon electrode (GCE) was polished with 1.0, 0.3 and 0.05 μM alumina powder then rinsed with distilled water. Thereafter the electrode was sonicated with deionised water, and dried at room temperature. The GR-PDMA nanocomposites (1 mg) was dispersed in ethanol (1 ml) and ultra-sonicated for 20 min to obtain a homogeneous suspension. Then 10 μL of the suspension was drop coated onto the surface of the glassy carbon electrode (GCE) and dried at room temperature, resulting in a graphene-PDMA modified electrode. A PDMA modified electrode was also prepared in the absence of graphene, and a graphene modified electrode in the absence of PDMA to compare the results. This electrode modification process was repeated using screen printed electrodes.

3.4 Characterisation of graphene-polyaniline derivative modified electrode

3.4.1 Electrochemical characterisation

3.4.1.1 Cyclic voltammetry (CV)

The electrochemical measurements and behaviour of the bare electrode and the modified electrodes namely graphene oxide, graphene, poly (2,5-dimethoxy aniline), graphene-oxide poly (2,5-dimethoxy aniline) and graphene-poly (2,5-dimethoxyaniline) were studied in 0.01 M phosphate buffer over a potential range of -1000 to +1000 mV at different scan rates and different concentrations.

3.4.1.2 Electrochemical impedance spectroscopy (EIS)

Electrochemical impedance spectroscopy (EIS) of the graphene-oxide, graphene, poly (2,5-dimethoxy aniline (PDMA), PDMA-GO and the PDMA-GA were performed in 0.01 M phosphate buffer containing ethanol. These results were then plotted in the form of Nyquist plots at perturbation amplitude of 10 mV and a frequency range of 100 kHz for each of the electrodes.

3.5 Morphological characterisation

The morphology of graphite, graphene-oxide graphene, poly (2,5-dimethoxyaniline), and graphenated-PDMA was characterised using HR-SEM, HR-TEM, FT-IR, UV-Vis spectroscopy, XRD, AFM and Raman spectroscopy as described in chapter 4.

3.6 Application of PDMA-GA- nanocomposite as an estrogen nanosensor

3.6.1 Electrolyte

Choosing a suitable solvent for the dissolution of estrogens is necessary because of its hydrophobic nature in water. Ethanol was chosen as a suitable solvent because of its reported ability to dissolve most estrogens. However, ethanol is a non-aqueous electrolyte and non-conducting, and usually requires the support of an electrolyte that can facilitate the conductivity and migration of current.

Another contributing factor to the choice of electrolytes are the fact that the estrogens are in aqueous form in the aquatic environment (wastewater). Taking these facts into consideration we needed to choose an electrolyte that is aqueous, more conductive and capable of detecting estradiol in the aqueous environment. Choosing a phosphate buffer as the working electrolyte in the detection of estrogens satisfied all the above-mentioned criteria. Phosphate buffer can ionize in water, is electronically conductive and has the affinity for the electroactive species. [238].

3.6.2 Preparation and determination of Estrogens

0.1 M solutions of estradiol was prepared by dissolving 0.2724 g of estradiol in 100 ml of ethanol. Thereafter dilution of this solution was made to get 1×10^{-5} M of the initial estradiol solution and from this solution, aliquot solutions (in μL) were added to the supporting electrolyte. For the electrochemical oxidation of these estrogens, 10 ml solution of 0.1 M phosphate buffer was placed in the electrochemical cell consisting of the nanocomposite modified electrodes. Cyclic, and square wave voltammetry characterisation of the modified electrodes were carried out at the scan rate of 150 mVs^{-1}, at the initial potential of -1000 mV to a final potential of 1000 mV, and the response in the absence and presence of the estrogens were monitored. The solution was stirred for 300 s after each addition of estrogen and the change in the current and the potential at which the oxidation reaction occurred was then monitored after each addition of the analyte.

3.7 Interferences, stability and reproducibility studies

The reproducibility and the stability of the modified electrodes were studied in the presence of each analyte of interest by performing cyclic voltammetry experiment five times with each of the electrodes. Changes in sensitivity were monitored to determine the reproducibility of the chemical sensors. In this study the results of other organic compounds on the peak current of estradiol was investigated. Compounds such as ascorbic acid, caffeine, vitamin B, estrone and estradiol were considered. Mixtures of the selected substances was prepared and mixed with estradiol and the cyclic voltammetry responses measured.

CHAPTER FOUR

RESULTS AND DISCUSSION –PART 1

SUMMARY

This chapter presents the results and discussion on the chemical synthesis of graphene oxide and graphene from graphite. Discussed herein are the morphology and structural characterisation of the prepared materials where techniques such as HR-SEM, HR-TEM, FT-IR, XRD, UV-vis spectroscopy, AFM and RAMAN were used to study them.

4.1 Introduction

In the preparation of graphene, the modified hummer's method has shown to be one of the most effective ways of producing a fairly large amount of graphene [233]. In the Hummers method graphite reacts with sulphuric acid, potassium permanganate, sodium nitrite and hydrogen peroxide to produce graphene oxide (GO). Graphene oxide is a layered stack of oxidized graphene sheets with different functional groups and can be completely exfoliated upon the addition of mechanical energy. The exfoliation process is possible due to the hydrophilicity of the oxygen-containing (i.e. epoxide and hydroxyl) functionalities introduced during the oxidation of the graphite. Thus, GO can easily be dispersed into single sheets in water at low concentrations (less than 1 mg/mL) [237]. Oxidation diminishes graphene's excellent conducting properties, so reduction of graphene oxide (GO) is desirable to partially restore its sp^2 network [239]. A solution of hydrazine is then added to graphene oxide as a reducing agent which results in agglomerated graphene-based nanosheets. When dried, an electrically conductive black powder with a C/O ratio of around 10 will be obtained. The mechanism of the synthesis is shown in F**igure 24**.

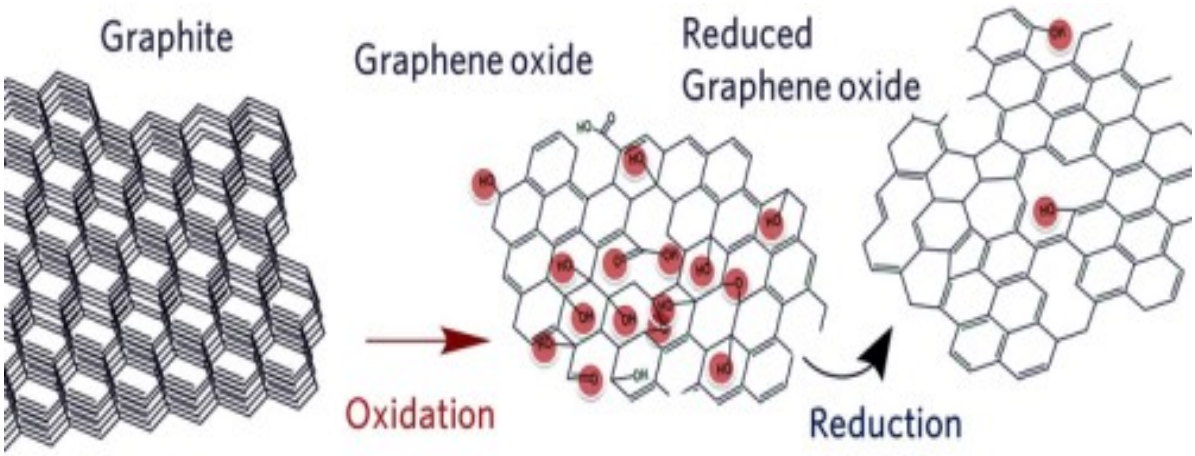

Figure 24: Schematic representation of the preparation of graphene. (University of Turkey Mathematics and Natural Science department)

4.2 Characterisation of graphite oxide and graphene

4.2.1 High Resolution Scanning electron microscopy (HR-SEM)

The morphology of graphene oxide and graphene was observed by scanning electron microscopy (HR-SEM) analysis and their images are shown in **Figure 25 (a)** and (**b)** respectively. **Figure 25 (a)** shows well-defined sheets of graphene oxide (GO) while **Figure 25 (b)** confirmed the reduced interlayer spacing of graphene also revealed by XRD diffraction, (as will be seen in later sections) resultant from the removal of oxygen-containing functional groups and molecules of water intercalated in the graphene oxide sheets upon reduction [239]. The energy dispersive x-ray spectrum (EDX) **Figure 26** shows the elemental composition of graphene oxide. Carbon showed a weight percentage of 51.46 % followed by oxygen with a weight percentage of 44.81 %. The presence of sulphur element with a weight percent of 3.74 % is attributed to sulphuric acid used during the washing of the materials.

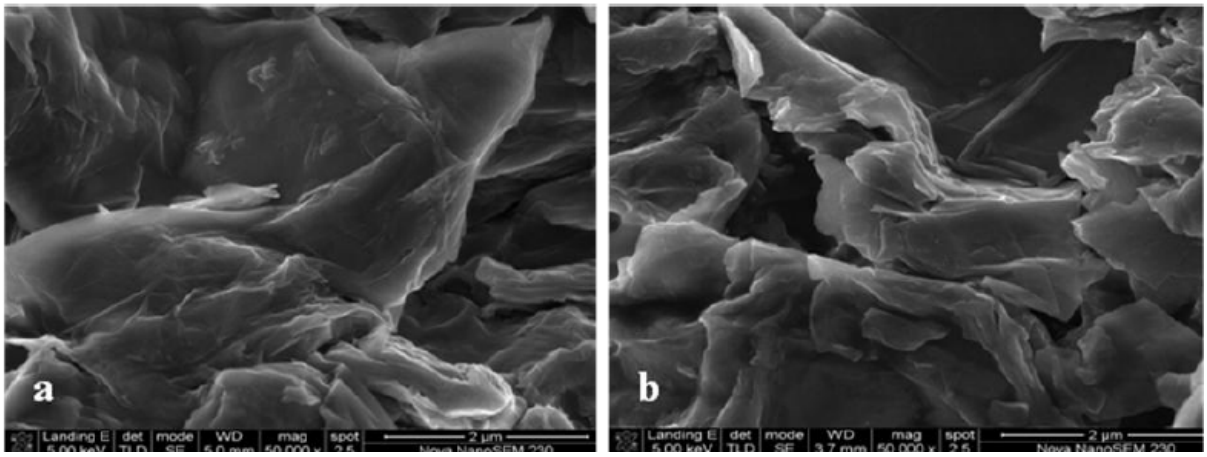

Figure 25: (a) HRSEM images of graphene oxide (b) HRSEM images of graphene

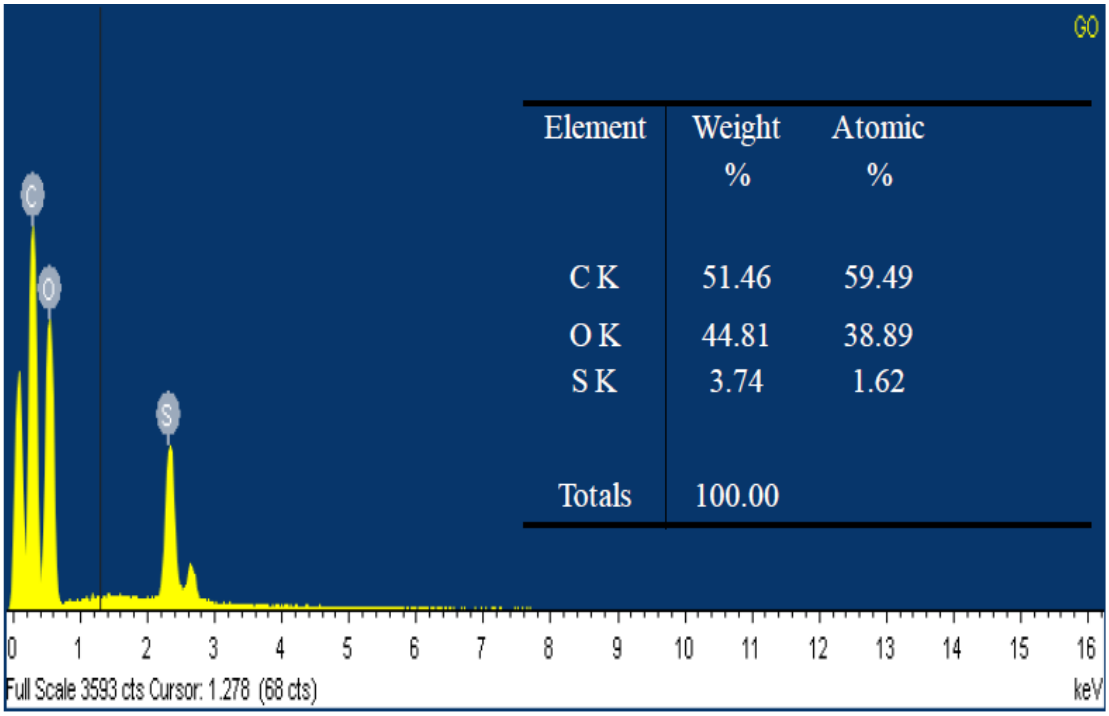

Figure 26: Energy dispersive X-ray spectrum of graphene oxide.

4.2.2 High resolution transmission electron microscopy (HR-TEM)

HR-TEM was also used to further characterize the exact structure of graphene oxide and graphene. The HR-TEM images can be observed in **Figure 27(a)** and **Figure 27(b)** respectively. The exfoliated graphene oxide (GO) resembled a surface of wrinkled silky sheets entangled with each other. The structure of graphene is different from graphene oxide where it is seen to exhibit thin silk like transparent sheets. **Figure 27(b)** clearly illustrates the individual layers of sheets expected of graphene. The elemental composition **Figure 28** of graphene oxide and graphene shows a higher carbon oxygen ratio for graphene than graphene oxide. The other elements are due to impurities and from the oxygen functional groups of the graphene oxide after reduction.

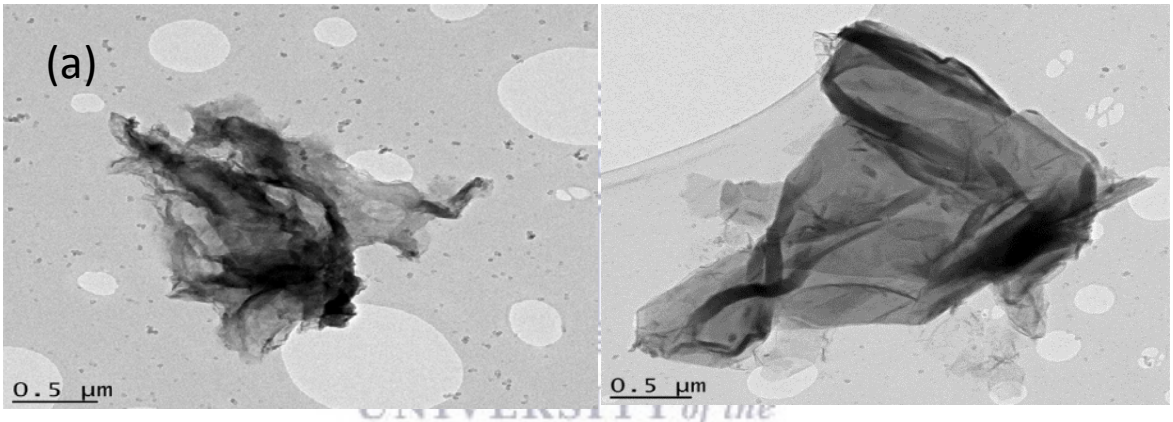

Figure 27: HR-TEM images of (a) graphene oxide and (b) graphene.

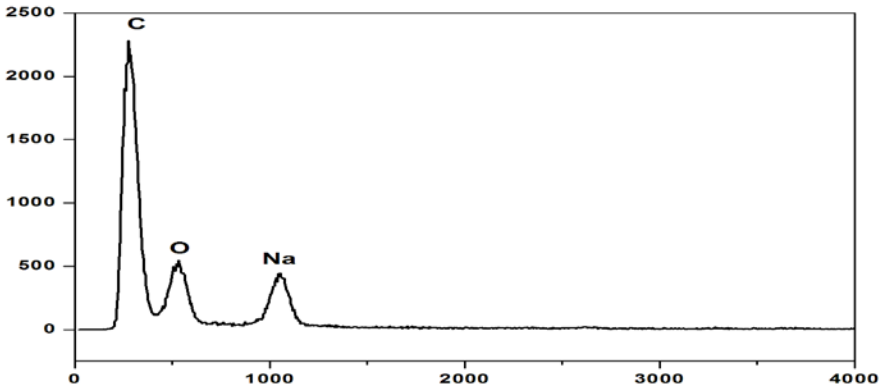

Figure 28: Energy dispersive X-ray spectrum of graphene.

4.2.3 Fourier Transform Infra-Red (FT-IR)

The Fourier Transform Infra-Red (FT-IR) spectra of graphite, graphene oxide (GO) and graphene are presented in **Figure 29**. The graphite showed no distinct peaks **Figure 29 (a)**. The graphene oxide (GO) spectrum **Figure 29 (b)** shows a peak representing OH stretching vibrations observed at 3442 cm^{-1} which was significantly reduced from its normal position due to deoxygenation. The C=O at 1631 cm^{-1} is this spectrum is due to the mechanism of exfoliation mainly because of expansion of CO_2 evolved into the interstices between graphene sheets during rapid heating, and the C-O stretching vibrations observed at 1058 cm^{-1} are due to the remaining carbonyl groups after the reduction process.

The peaks observed from 1212 to 1058 cm^{-1} are stretching vibrations resulting from graphene oxide indicating skeletal vibrations from unoxidized graphitic domain. The graphene spectra **Figure 29 (c)** indicates that the bulk of the oxygen-containing functional groups have been removed from graphene oxide. This establishes the reduction of graphene oxide which agrees with what Thema *et al* has reported [239].

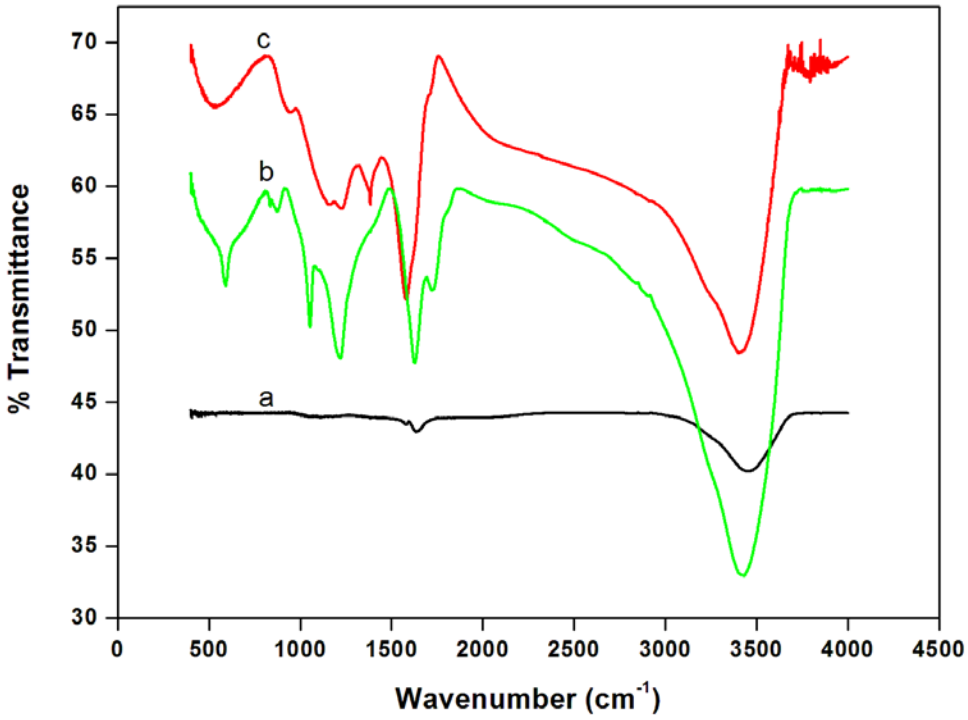

Figure 29: FTIR spectra of (a) graphite (b) graphene oxide and (c) graphene

4.2.4 X-ray diffraction (XRD)

X-ray diffraction (XRD) is the most widely used technique for general crystalline material characterisation. It is used to measure the average spacing's between layers or rows of atoms, determine the orientation of a single crystal or grain. The X-ray diffraction pattern (XRD) of graphite, graphene oxide and graphene is presented in **Figure 30**. The diffraction peak of graphite **Figure 30 (a)** was found at 26.86°, corresponding to a highly-organized layer structure with interlayer distance of 0.34 nm along the (002) orientation. The graphene oxide spectra **Figure 30(b)** shows the disappearance of the peak at 26.38° and the appearance of the peak at 10.38° which is an indication that the graphite has been completely oxidized after the chemical oxidation and exfoliation indicating an increase in d-spacing from 0.34 to 0.82 nm. This agrees with the spectra which Paulchamy *et al* found [240].

After chemical reduction, the hydrophilicity of water-dispersed GO sheet gradually decreased, resulting in an irreversible agglomeration of reduced graphene oxide (RGO, graphene) sheet. The broad peak at 25.88° indicates a random pucking of graphene sheets in the reduced graphene oxide. This peak corresponds to the 002 plane of graphite with interlayer spacing of 0.34 nm which is due to the removal of oxygen atoms that got into the graphite during the intercalation process. This confirms the reduction process of graphene oxide to graphene [239].

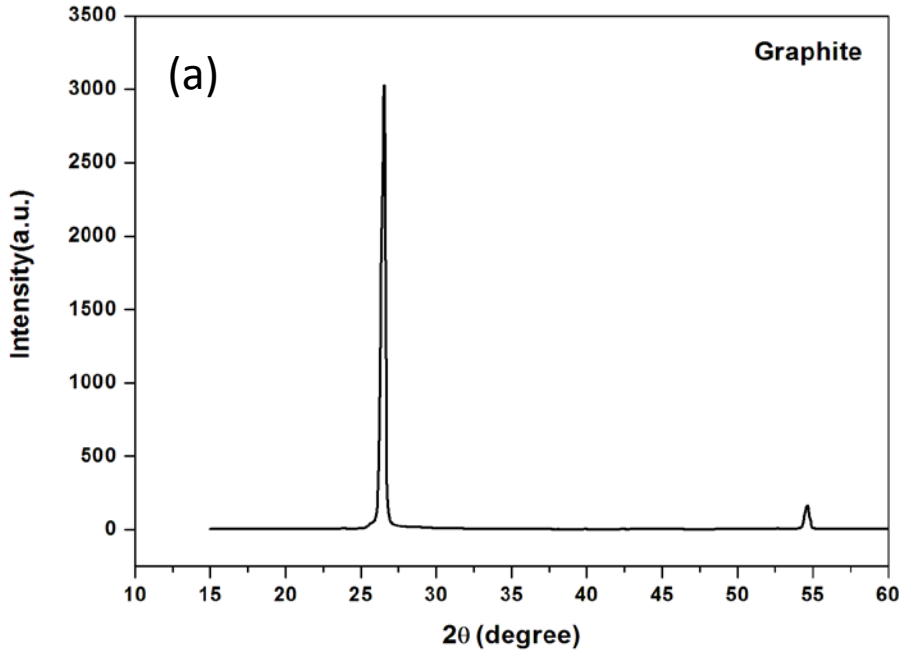

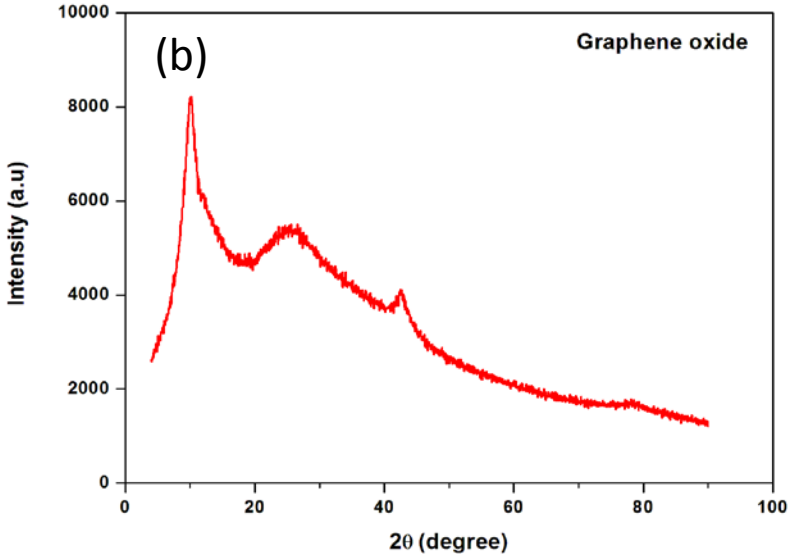

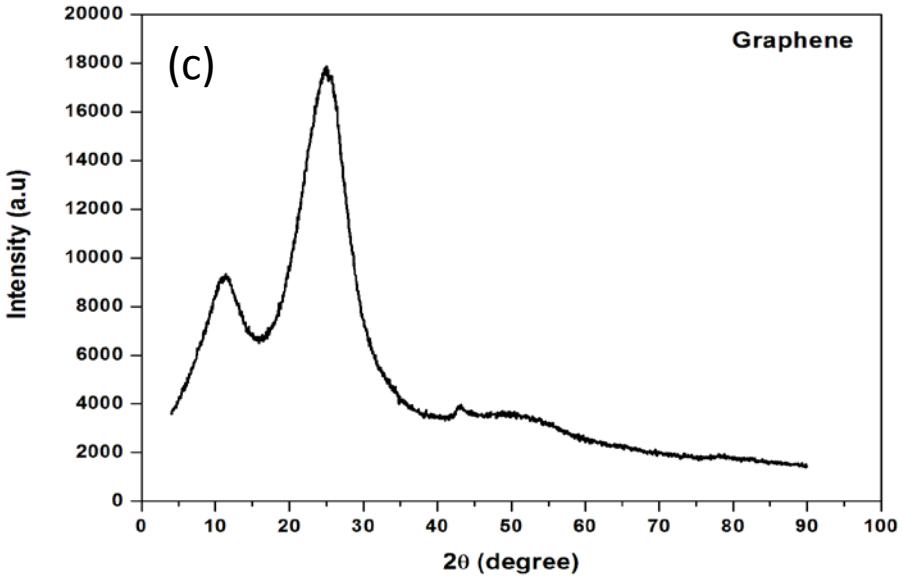

Figure 30: XRD pattern of (a) graphite (b) graphene oxide and (c) graphene

4.2.5 UV-Vis spectroscopy

Figure 31 shows the ultraviolet-visible spectra of graphene oxide and graphene. The spectrum of graphene oxide has an absorption peak at 227 nm which is shifted to 265 nm in graphene. This shift is due to the reduction of graphene oxide to graphene which occurs with the removal of the functional groups from graphene oxide. The absorption peak at 227 nm is due to the π-π^* transition of the aromatic C-C ring. The ultraviolet spectra of graphene show the shift at 265 nm which is due to the π-π^* transition of C-O bonds caused by exfoliation and intercalation in graphene. These spectra agree with those obtained by Thema *et al* [239].

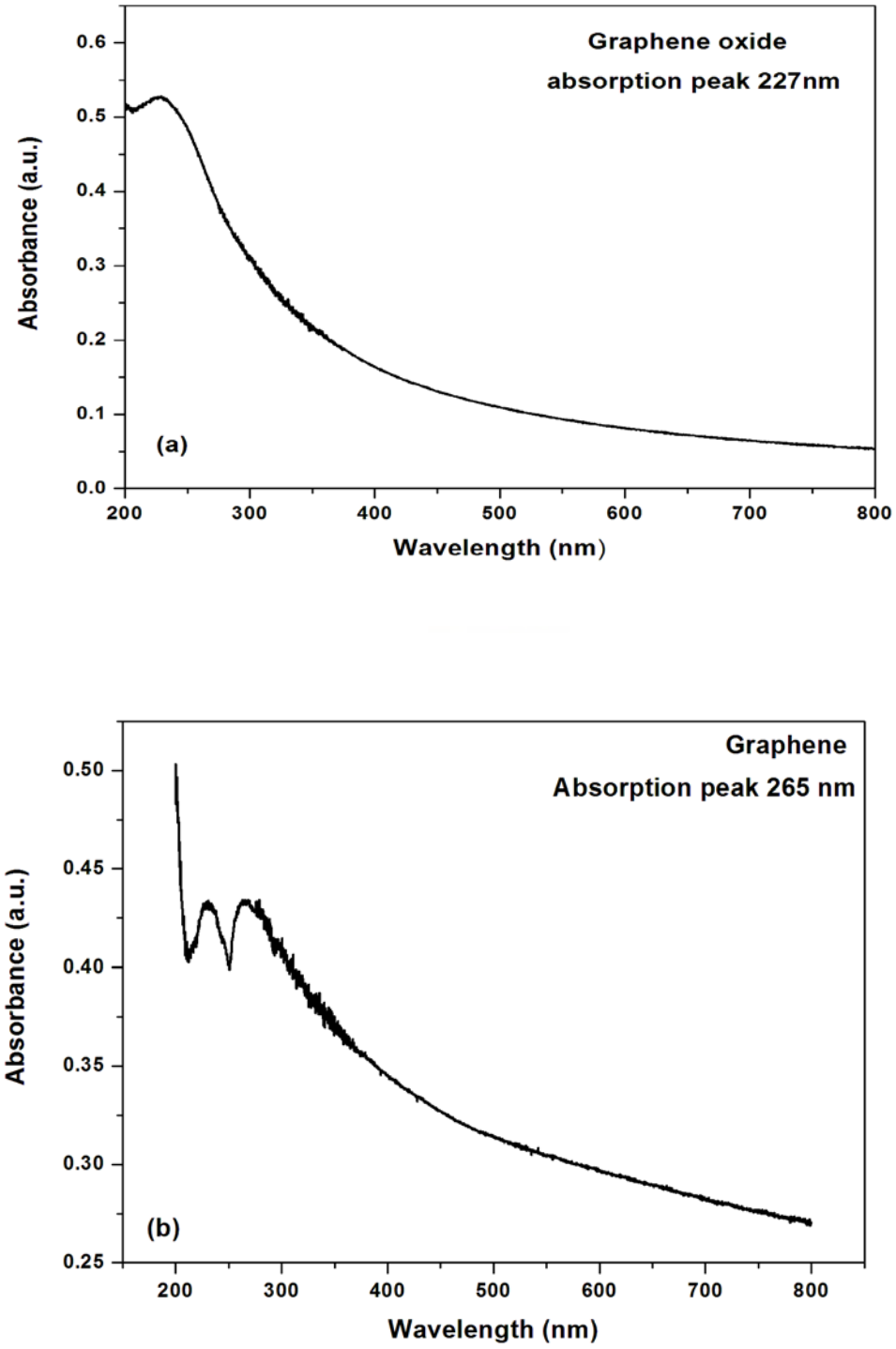

Figure 31: UV- visible spectra of (a) graphene oxide and (b) graphene

4.2.6 Atomic force microscopy (AFM)

The level of exfoliation was evaluated by Atomic force microscopy (AFM) **Figure 32** respectively. The GO sheets are expected to be thicker due to the presence of covalently bonded oxygen and the displacement of sp^3 hybridized carbon atoms slightly above and below the original graphene plane. The height difference between rows is ~1nm in GO and 1.2 nm in graphene indicating a single graphene oxide sheet due to the intercalating of oxygen into the graphite matrix. The atomic force microscopy showed that graphene oxide and graphene were obtained in the synthesis [240].

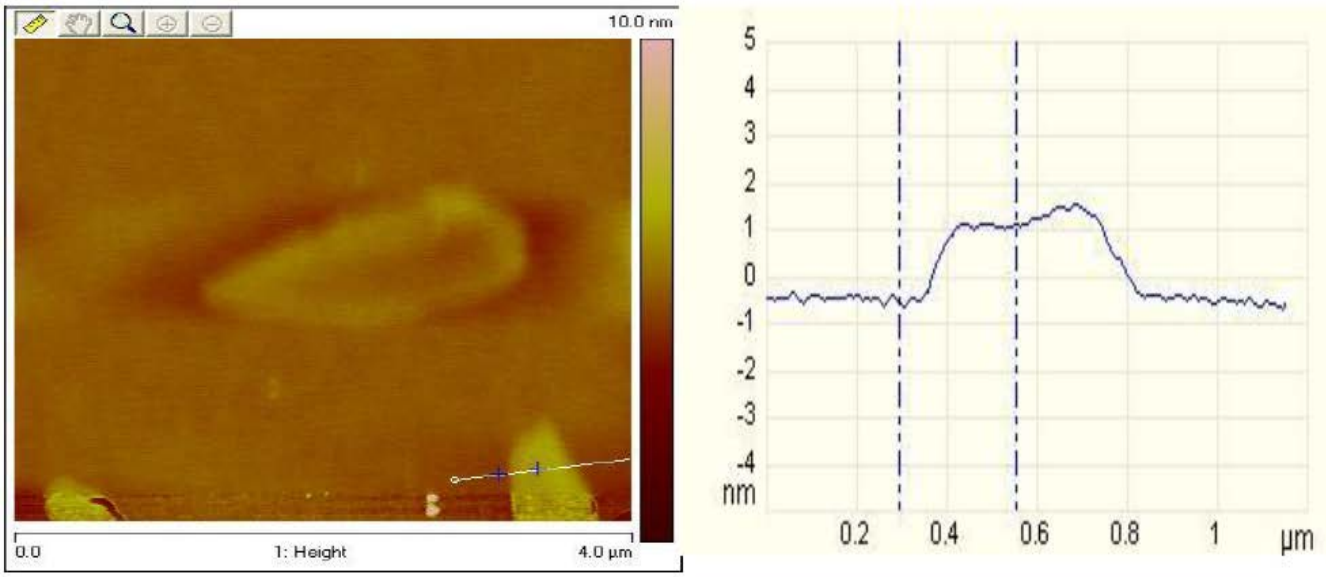

Figure 32: AFM images of graphene sheets with height profile.

4.2.7 Raman spectroscopy

The Raman spectra of graphene oxide and graphene are presented by **Figure 33**. Raman spectroscopy is a non-destructive technique that is widely used to obtain structural information about carbon- based materials [241]. The main features in Raman spectra of graphitic carbon-based materials are the G and D peaks and their overtones.

The first-order G and D peaks both arising from the vibrations of sp^2 carbons, appear at around 1580 and 1350 cm^{-1}, respectively. The G peak corresponds to the optical E_{2g} phonons at the brillouin zone centre resulting from the bond stretching of sp^2 carbon pairs in both, rings and chains. The D peaks represent the breathing mode of aromatic rings arising due to the defect in the sample [241]. The D-peak intensity is therefore often used as a measure for degree of disorder [242]. The shift and shape of the overtone of the D peak, known as 2D peak around 2680 cm^{-1}, can be correlated to the number of graphene layers [243-244]. The 2D peak is attributed to double resonance transitions resulting in the production of two phonons with opposite momentum. Further unlike the D peak, which is Raman active only in the presence of defects, the 2D peak is active even in the absence of any defects [245]. **Figure 33**(a) shows the Raman spectra of graphene oxide, while **Figure 33**(b) shows the Raman spectra of graphene. Comparing the spectra of graphene oxide and graphene we find the D and G bands of graphene appearing at 1345 cm^{-1} and 1583 cm^{-1} respectively. These bands are then shifted to 1340 and 1604 cm^{-1}, respectively in the graphene oxide spectra. Simultaneously, relative intensities of D/G were increased after hydrothermal reaction, which corresponds to work done by Stankovich *et al* [246]. This further confirms that graphene oxide was reduced to graphene. The absence of the 2D band around 2861 cm^{-1} after oxidation indicates that all graphite layers have been oxidized [239].

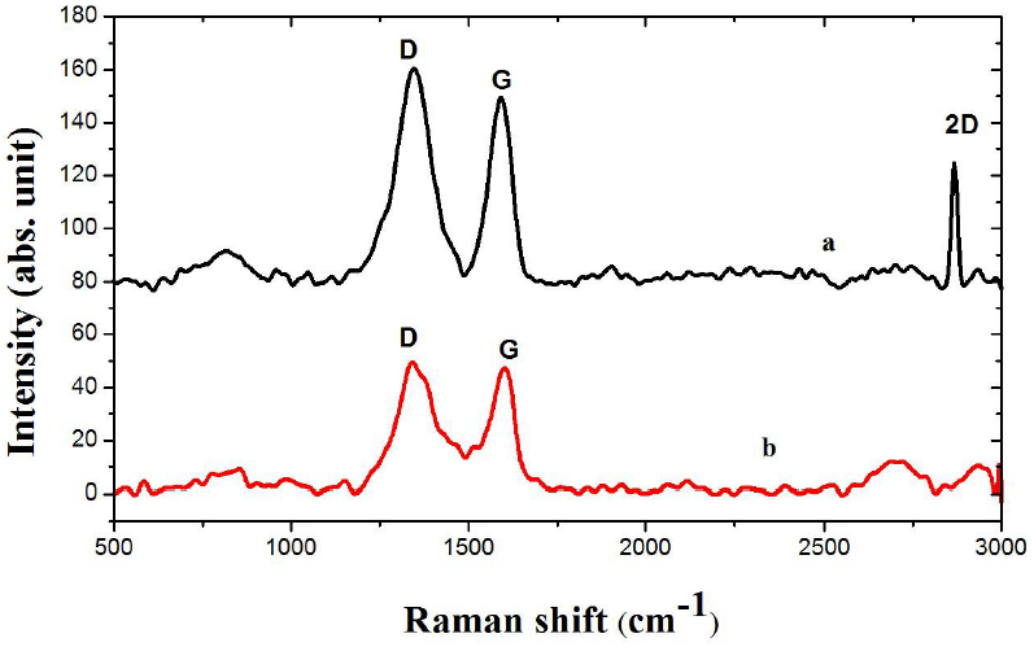

Figure 33: Raman spectra of (a) graphene oxide and (b) graphene

CHAPTER FIVE

RESULTS AND DISCUSSION-PART 2

This chapter presents all the results obtained from the chemical polymerization of graphene-poly (2,5-dimethoxyaniline) (PDMA-GA) composites and how they have been used to modify electrodes making them conductive and suitable for many applications. Also, included in this chapter is the morphological and structural characterisation of these composites. Electrochemical characterisations of these PDMA-GA modified electrodes by means of cyclic voltammetry (CV), square wave voltammetry (SWV) as well as their catalytic effect towards estradiol are discussed.

5.1 Introduction

Polyaniline (PANi) has many potential applications in various fields including anti corrosion, sensors, electrochromic devices and electronic devices. One major obstacle of PANi is its poor process ability resulting in poor solubility in common solvents and causing it to decompose before it melts [247]. To improve the process ability and solubility of PANi some people have reported on the complexation of polyanilines with sulfonic acids. [247-249]. Additionally, the synthesis of nanoparticles by the dispersion of PANi in polymeric stabilizers has also leaded to the improvement of the process ability of PANi [247]. Another way of improving the process ability of PANi is to use polyaniline derivatives, e.g. poly (2,5-dimethoxyaniline), poly (2-methoxyaniline), poly (methylaniline) etc. [248-250]. The substituent on the polymer chain decreases the stiffness of the polymers and this leads to an increase in the solubility of the polymer. [250-251]. The monosubstituted polyanilines which have been investigated have shown to exhibit low conductivity however, disubstituted polyaniline like Poly (2,5-dimethoxyaniline) have been reported to have conductivity similar to that of PANI yet with the advantage that they are soluble in most organic solvents [252-253]. Electrochemistry has been a successful tool in confirming the conductive nature of PDMA as shall be discussed in this chapter.

5.2 Characterization of the chemically prepared nanocomposites

5.2.1 Scanning electron microscopy (HR-SEM)

The surface morphology of Poly (2,5 - Dimethoxy aniline) PDMA and graphenated poly (2,5-dimethoxy aniline) PDMA-GA were studied using high resolution scanning electron microscopy (HR-SEM). The HR-SEM images of the prepared nanocomposites are presented in **Figure 34 (a) and (b)** respectively. The PDMA present flower like microfiber structures unlike the known hexagonal structure usually associated with PDMA. The reason for the absence of the hexagonal structure is because only one oxidant was used as opposed to using two oxidants which causes the resultant hexagonal structure. The PDMA-GA structure is less dense due to the presence of graphene and this finding is in good agreement with those reported by Mavundla *et al* [236].

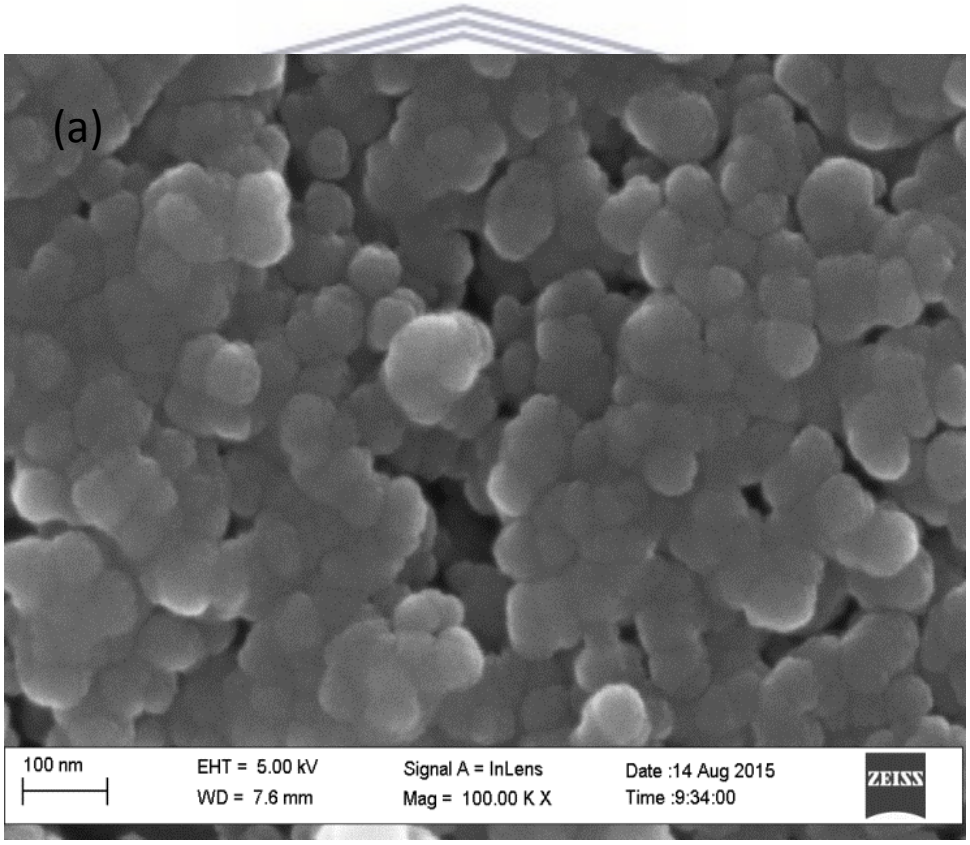

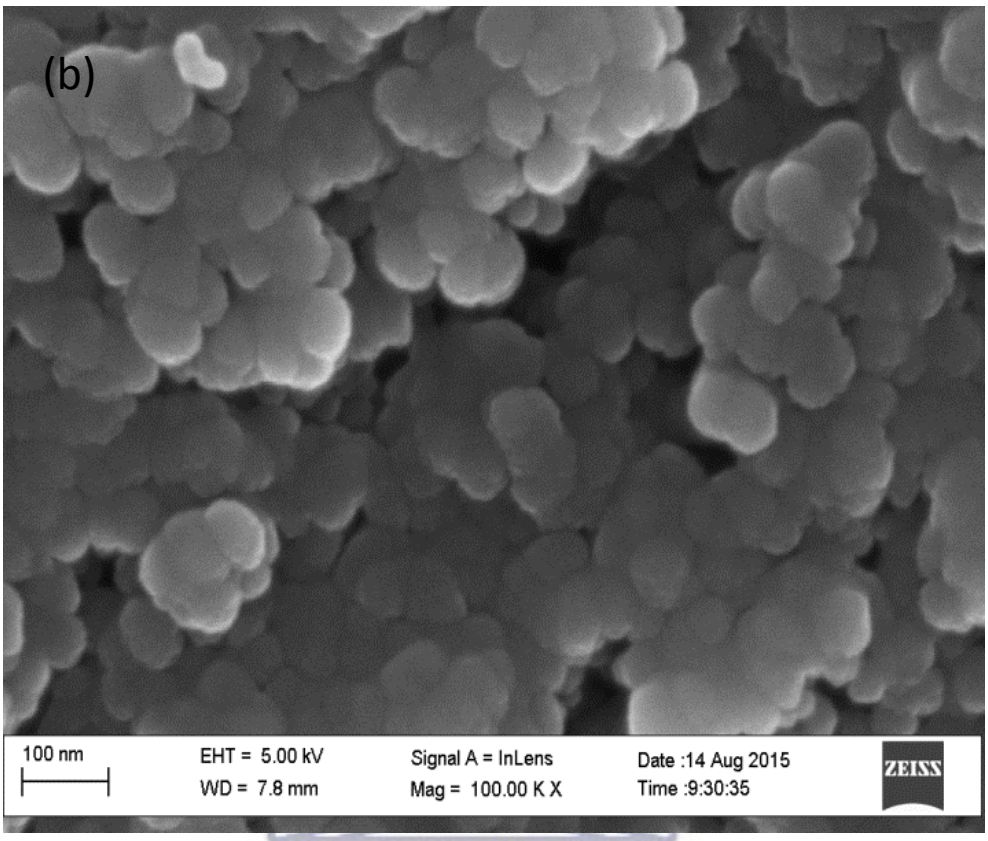

Figure 34: HR-SEM images of of (a) PDMA, (b) PDMA-GA

5.2.2 High resolution transmittance electron microscopy (HR-TEM)

HR-TEM images of the PDMA and PDMA-GA nanocomposites are represented in Figure **35 (a)** and **Figure 35 (b)** respectively. Large thin layers of entangled sheets like silky veils which are flat and transparent can be observed in **Figure 35 (b)**. This image clearly gives evidence of poly (2,5-Dimethoxy aniline) PDMA intercalating in between the surfaces of the graphene sheets, which is attributed to the dispersive interaction of the two materials. The type of polymerisation synthesis method has greatly contributed to the formation of the nanocomposite formed which was seen to, exhibit a higher conductivity than poly (2,5-Dimethoxy aniline) PDMA.

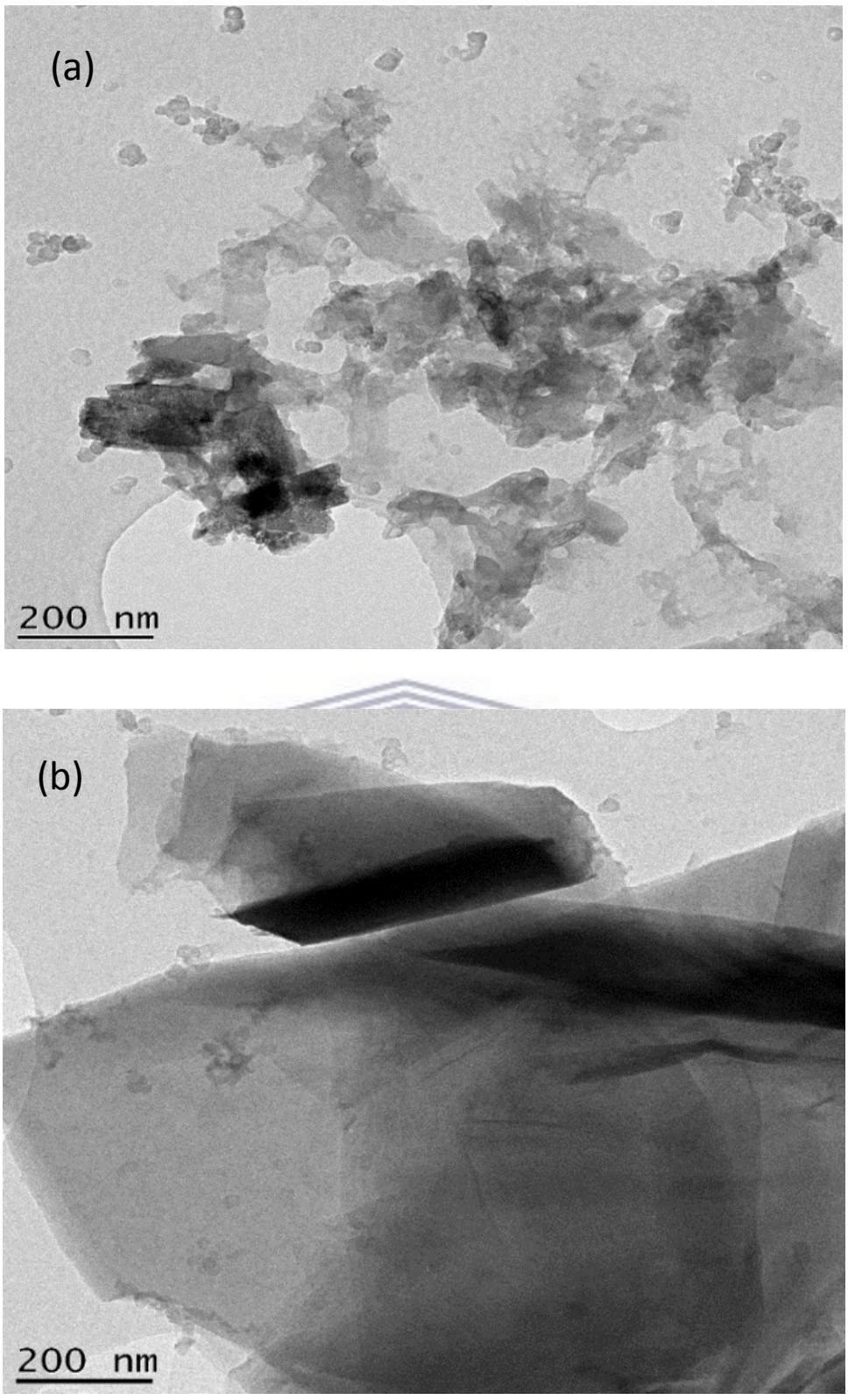

Figure 35: HR-TEM images of (a) PDMA, (b) GA –PDMA

5.2.3 Fourier transmission infrared (FT-IR)

Figure 36 gives an illustration of the FT-IR spectra of (a) GO (b) GA (c) PDMA and (d) PDMA-GA. The absorption peaks of the graphene oxide **Figure 36 (a)** can be seen by the functional groups corresponding to: C=O (1732 cm^{-1}), aromatic C=O (1626 cm^{-1}), epoxy C-O (1217 cm^{-1}), alkoxy C-O (1045 cm^{-1}), hydroxyl O-H (3443 cm^{-1}). These peaks are in close proximity to those reported in literature [243 464]. There is a large decrease in peak height observed after the reduction of graphene oxide to graphene which is evident in **Figure 36 (b)** due to the removal of oxygen containing groups. In the FTIR spectrum of PDMA **Figure 36 (c)** the absorption peaks observed at 1585, 1495 and 1405 cm^{-1} which are due to the stretching vibrations of quinodic (Q) and benzoic (B) groups possessed by PDMA. Additionally, the peaks observed at 1225 cm^{-1} and 1119 cm^{-1} are due to C-N stretching vibration of QBQ, QBB and BQQ, and N=Q=N stretching vibration. PDMA-GA spectrum **Figure 36 (c)** reveals an absence of the absorption bands observed in PDMA which is an indication of the intercalation of PDMA on the surface of graphene. These results are in good agreement with those obtained by Masikini *et al* [254] thus confirming the successful synthesis of this nanocomposite. **Figure 37** represents the FT-IR spectra of PDMA, PDMA-GO and PDMA-GA for comparison.

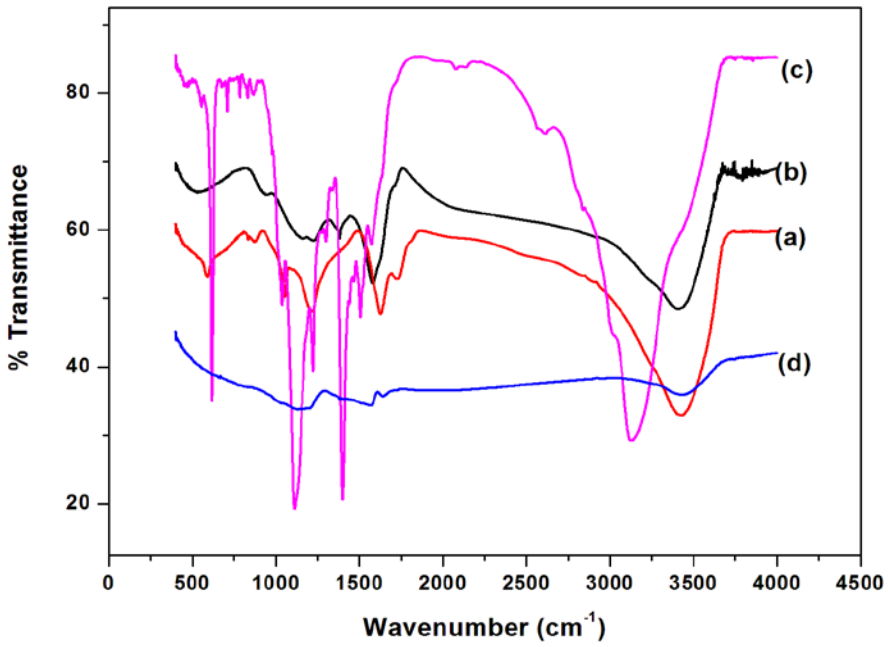

Figure 36: FTIR spectra of (a) GO (b) GA (c) PDMA (d) PDMA-GA.

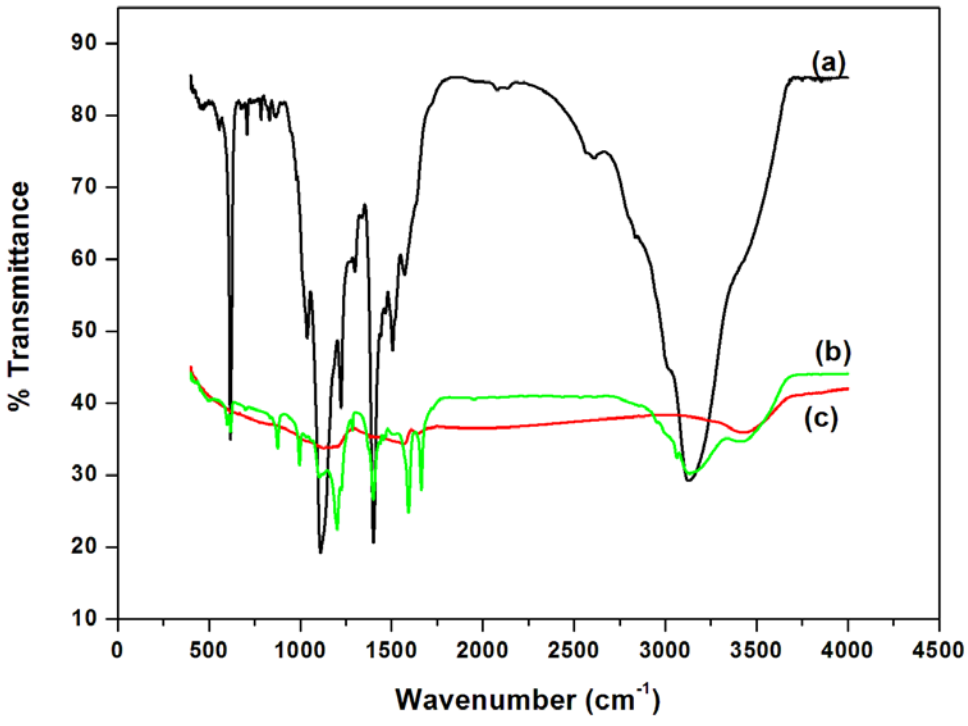

Figure 37: FTIR spectra of (a) PDMA (b) PDMA-GO and (c) PDMA-GA.

5.2.4 X-ray diffraction (XRD)

The XRD patterns of PDMA and PDMA-GA composites are presented in **Figure 38 (a) and (b)** respectively. Graphene exhibited diffraction peaks at 25.88° (002) and 42.86° (100) with some crystalline features of graphite-like structures similar to those reported in chapter 4 **Figure 30**. These diffraction peaks can be ascribed to the stacked sheets in graphene. [255-256]. The PDMA spectra exhibited a peak at 28.55° and another low intensity peak at 16.74°. As expected the PDMA-GA nanocomposite revealed broadened peaks at 25.75° that are similar in comparison to both graphene and PDMA, showing the interaction and merged peaks of both PDMA and graphene in the composite. This is in good agreement with the morphological data received from HR-SEM and HR-TEM studies of the nanocomposites.

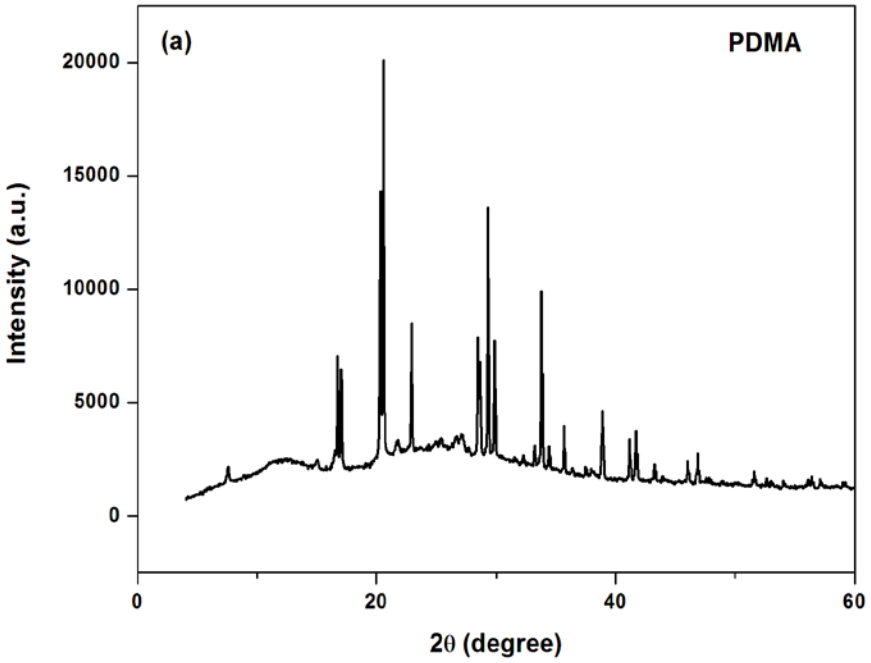

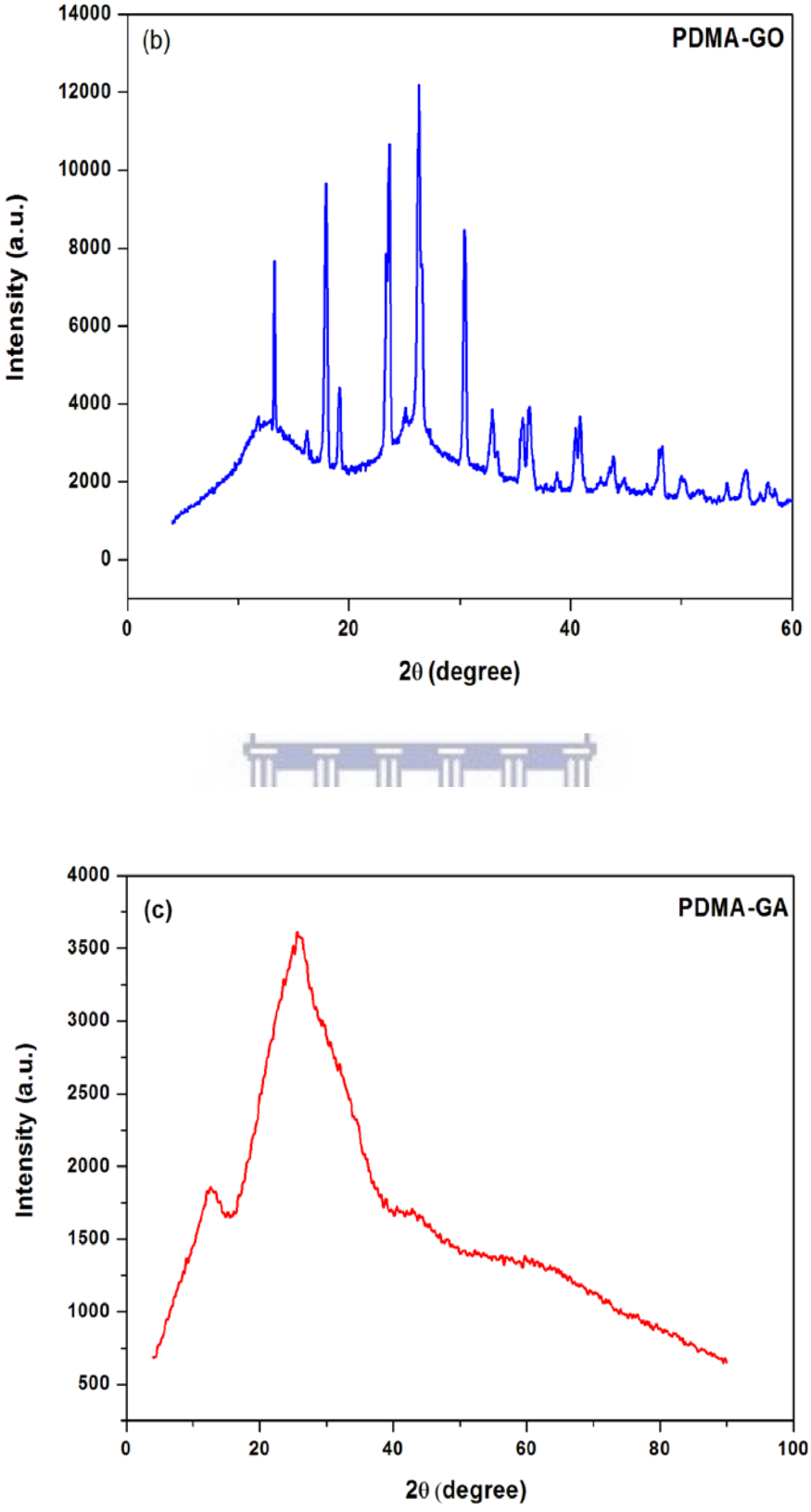

Figure 38: XRD patterns of (a) PDMA (b) PDMA-GO and (c) PDMA-GA.

5.2.5 UV-Vis spectroscopy

The UV-vis spectra of PDMA, PDMA- GO and PDMA-GA are presented in **Figure 39 (a), (b) and (c)** respectively**.** The UV-vis spectra of PDMA **Figure 39 (a)** show a peak around 308 nm and another broad peak starting from 450-650 nm. The band at 308 nm is due to the π-π^* transition of the benzoic rings and the broad peak from 450-650 nm is due to charge transfer excitons of the quinoid structure [226 447]. In the PDMA-GO **Figure 39 (b)** the peak at 320 nm shifted to 280 nm however it is reduced in **Figure 39 (c)**. This reduction in peak height can be attributed to the fact that the removal of the functional groups from the GO, has restored back the electronic configuration within the graphene sheets after the reduction reaction. [246].

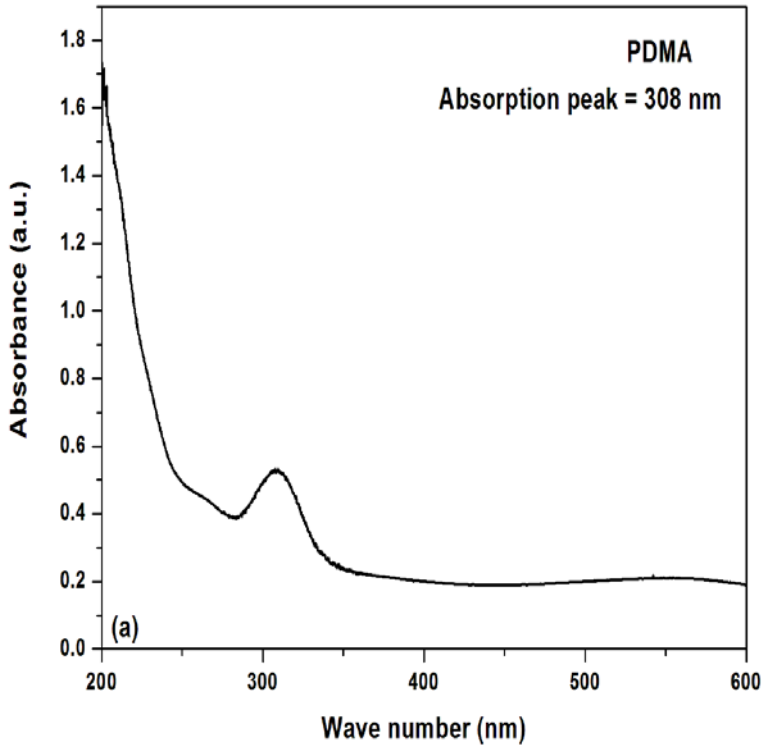

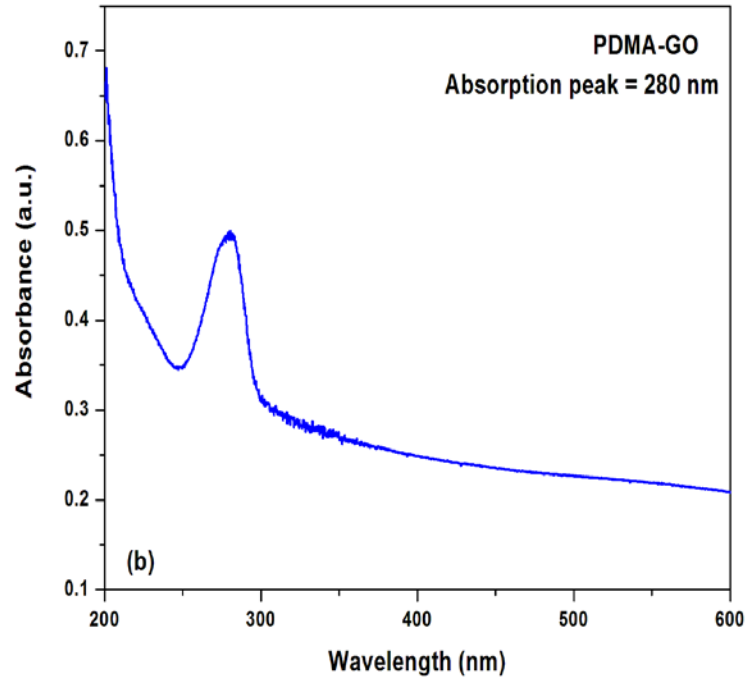

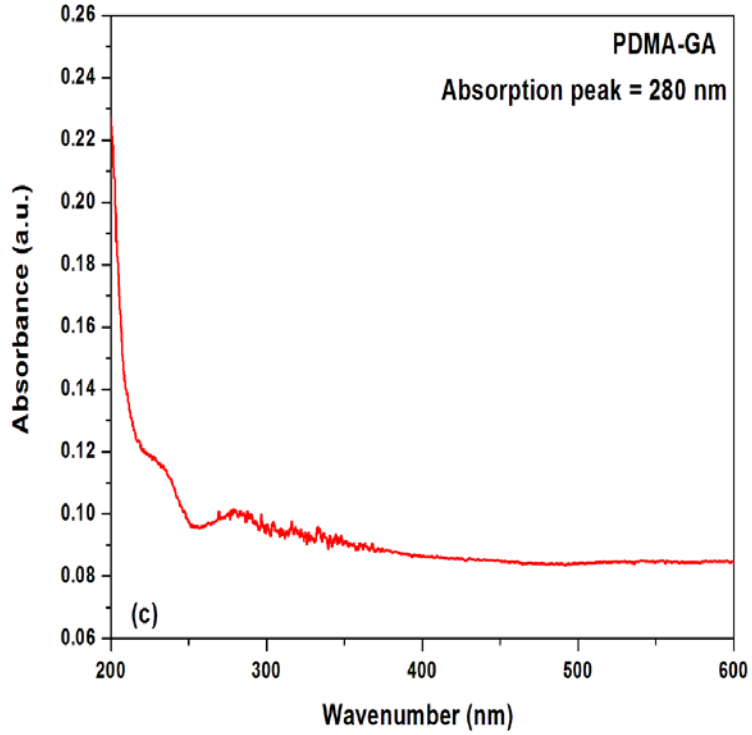

Figure 39: UV-vis of (a) PDMA, (b) PDMA-GO 5 and (c) PDMA-GA

5.2.6 Electrochemical impedance spectroscopy (EIS) of modified electrodes

The surface of the modified electrodes was studied using electrochemical impedance spectroscopy (EIS), due to it being an effective method to probe the surface of modified electrodes [257-259]. The measurements were performed in a cell containing 10 ml of 0.1 M phosphate buffer with a frequency range of 100 kHz to 0.1 Hz of which the amplitude of the alternating voltage was 10 mV as shown in **Figure 40**. The y-axis represents the negative number of the imaginary part of the measurement impedance while the x-axis represents the real part of the measured impedance. The diagram (Nyquist plots-real part of the impedance $Z^{'}$ vs imaginary $Z^{''}$) represents the charge transfer kinetics of the modified electrodes in which R, is the ohmic (internal or solution) resistance [258]. CPE is the capacitance phase element for the semiconductor‖ electrolyte interface, W (Warburg impedance) represents the mass transfer element while the R_{ct} is the charge- transfer resistance across the interface [260]. For a reaction that is reversible, the Nyquist plot usually exhibits two regions. One, a semicircle at a high frequency region which corresponds to an electron charge transfer process thus, the electron transfer resistance value can be measured directly and two a straight line of the plot at lower frequency region representing the diffusion-limited transport of the redox species from the electrolyte to the electrode interface. As shown in **Figure 40**, the Nyquist plot displayed significant differences in the diameter of the Nyquist semicircle upon the stepwise modification of the electrodes showing the capability of electron transfer of the different electrodes. The charge transfer resistance (R_{ct}) value for bare GCE was 17300 Ω, however, upon modification with polyaniline-graphene (PDMA-GA), a decrease in R_{ct} value to 12674 Ω was exhibited. This is a clear indication of the high conductivity nature of this nanocomposite and one with a more facile electron transfer capability compared to PDMA whose R_{ct} value was determined to be 2500 Ω. The charge transfer resistance (R_{ct}) values calculated after fitting the EIS data to the Randle's equivalent circuit diagram **Figure 15 (b)** in **Figure 40** can be observed in **Table 3**. Indicating that graphenated PDMA is suitable as conducting platform for electrocatalysis.

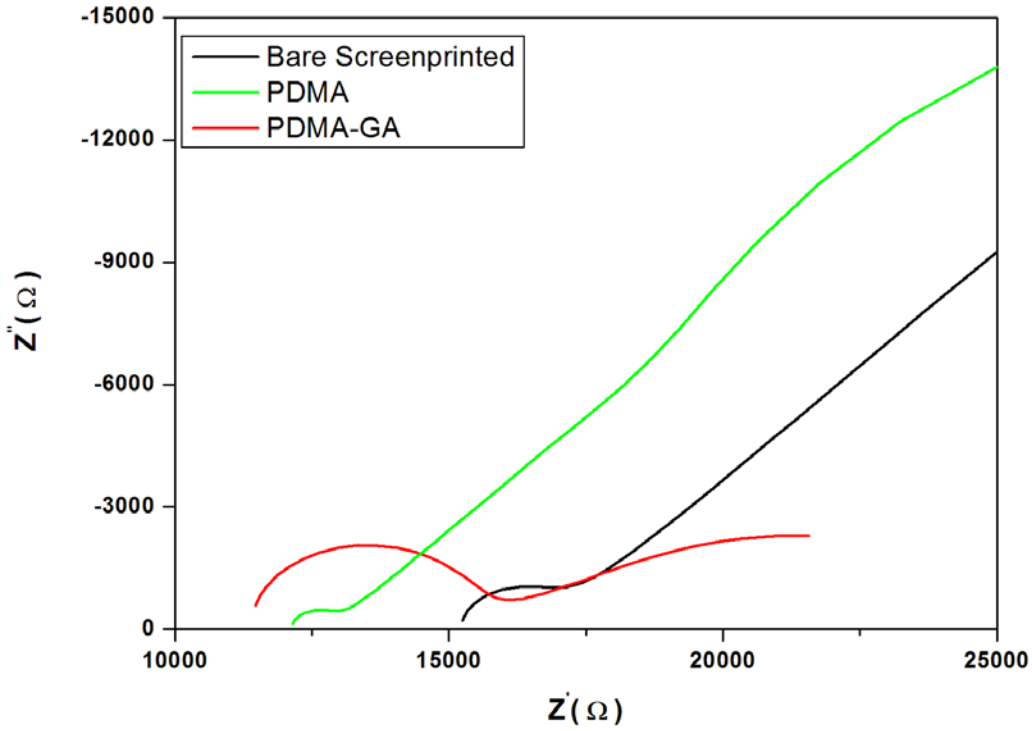

Figure 40: Nyquist plots of the EIS measurements of (a) Bare screen printed (b) PDMA and (c) PDMA-GA in 0.1 M Phosphate buffer.

Table 3: Impedance data obtained from the Randle equivalent circuit fitting from Figure 61

Electrode	R_s(Ω)	R_{ct}(Ω)	CPE(nF)	Z_w(k Ω $s^{½}$)
Bare SCRPNT	15.22	17300	311.5	30.82
PDMA	120.12	2500	288.46	20.88
PDMA-GA	11.38	12674	891.5	12.69

5.3 Electrochemical characterization of the modified nanocomposites.

5.3.1 Effect of Scan rate

The relationship of peak current and scan rate was studied using cyclic voltammetry. The results show that oxidation peak current is proportional to the square root of the scan rate from 20 – 200 mVs^{-1}. This suggests that the electrochemical process is diffusion controlled. In this study the optimum scan rate chosen was 150 mVs^{-1}.

5.3.2 Optimisation of the PDMA-GA film

5.3.2.1 Effect of film thickness

The aim of the thesis was the improved detection of estradiol through the modification of the electrode. The relationship between peak current and the amount of film deposited on the electrode were investigated at the results is shown in **Figure 41**.

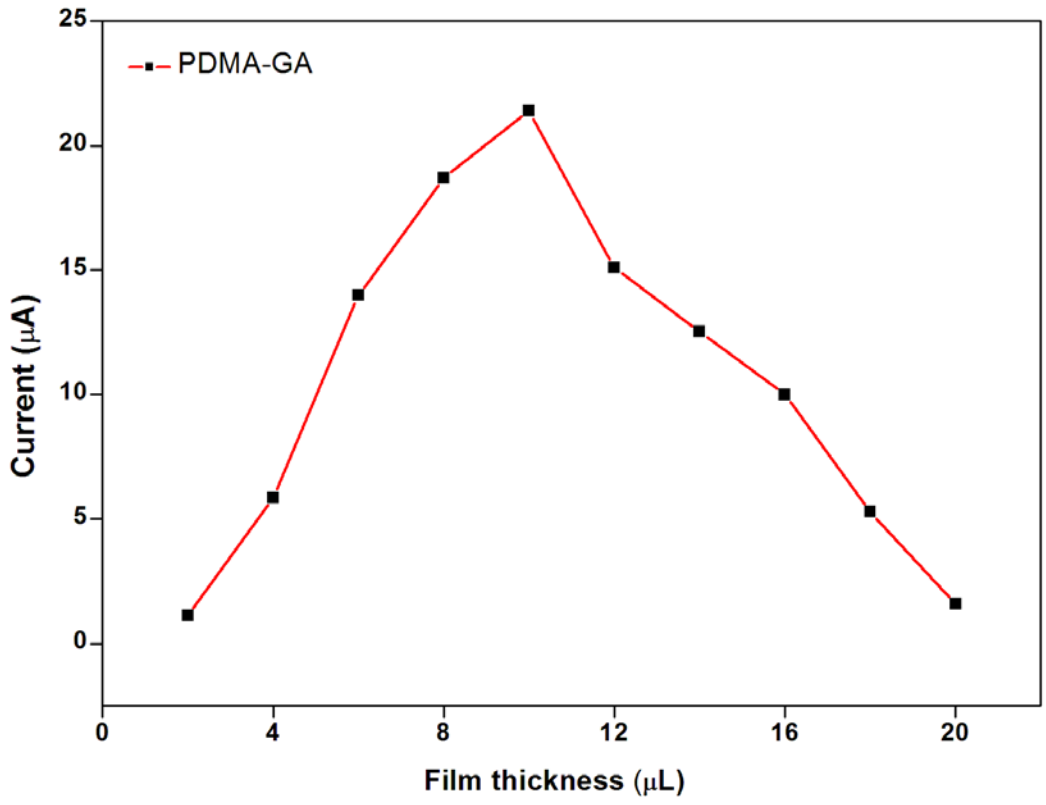

Figure 41: Influence of the film thickness on current

At the beginning the peak current increases with increase film-thickness. When it exceeds 10 µL, the peak current decreases. When the film thickness exceeds 10 µL the film becomes thick and blocks the electron transfer.

5.3.2 Effect of accumulation time

The effect of accumulation time on the peak current is presented in **Figure 42**. The peak also increases with an increase in accumulation time. Under the same experimental parameters, longer accumulation times will improve the peak current of estradiol. When the accumulation time is longer than 4 minutes, the peak current changes very slowly. This is consistent with adsorption processes.

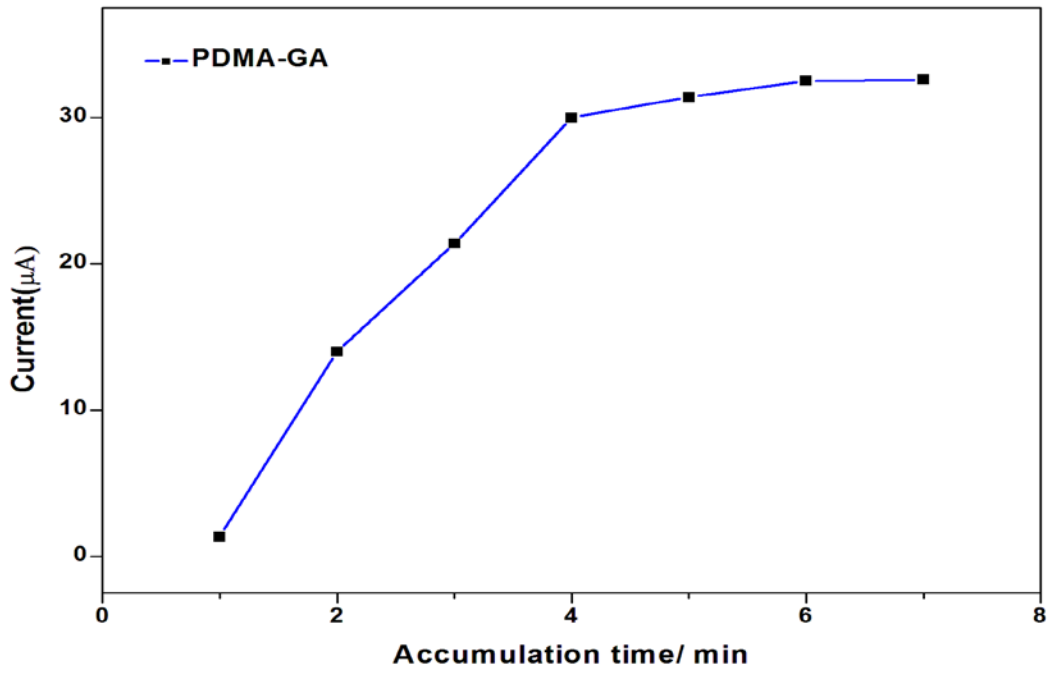

Figure 42: Effect of accumulation time on peak current

5.3.3 Cyclic voltammetry

Cyclic voltammetric responses of the different electrodes were prepared and their electro-chemical behaviour was observed in 0.1 M phosphate buffer (pH = 8.0) within a potential window of -1000 to + 1000 mV using screen printed electrodes. A different screen printed electrode was used for each voltammetric scan. The cyclic voltammograms showed different electrochemical surface activity for the different electrodes. Cyclic voltammograms of the different electrodes are presented in **Figure 43 (a - d)**. The bare screen printed electrode showed no electrochemical activity in the potential region of interest (-500mV - +500mV). On modification with graphene electrochemical activity was detected that correspond to the electrochemical behaviour of carbon containing compounds. This electrochemical activity is due to the transition between quinone/hydroquinone **Figure 43 (a)** [261]. The cyclic voltammograms presented in **Figure 43 (a - d)** showed a significant increase in current response from the bare screen printed electrode to the PDMA, PDMA-GO and the PDMA-GA respectively. These cyclic voltammograms also showed that the modification of the electrodes was successfully achieved.

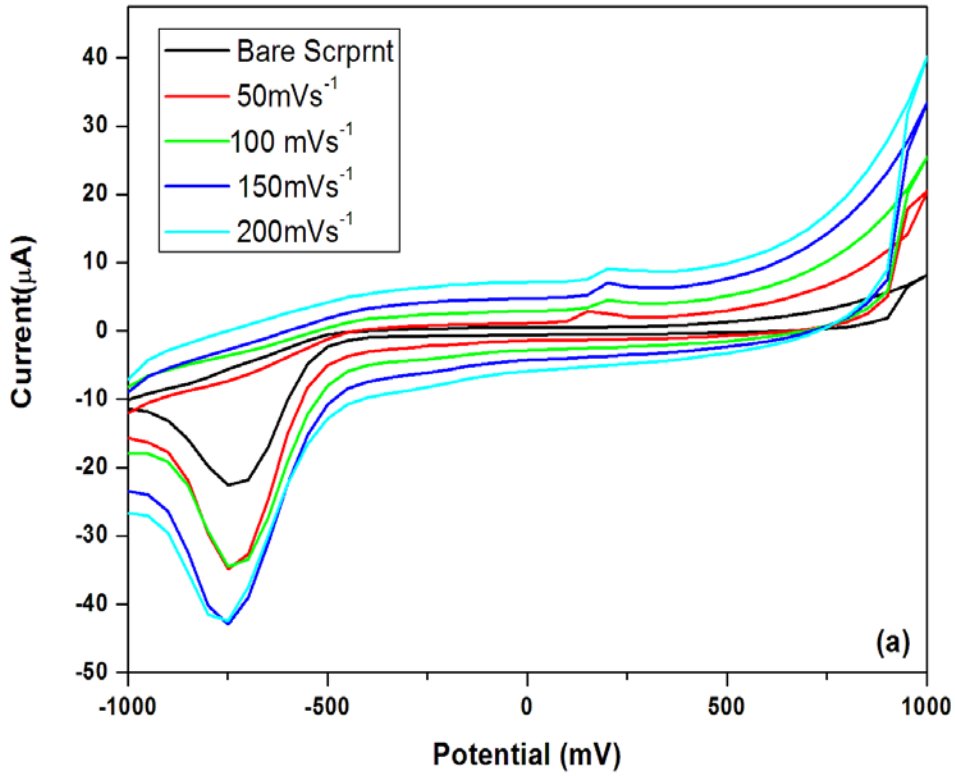

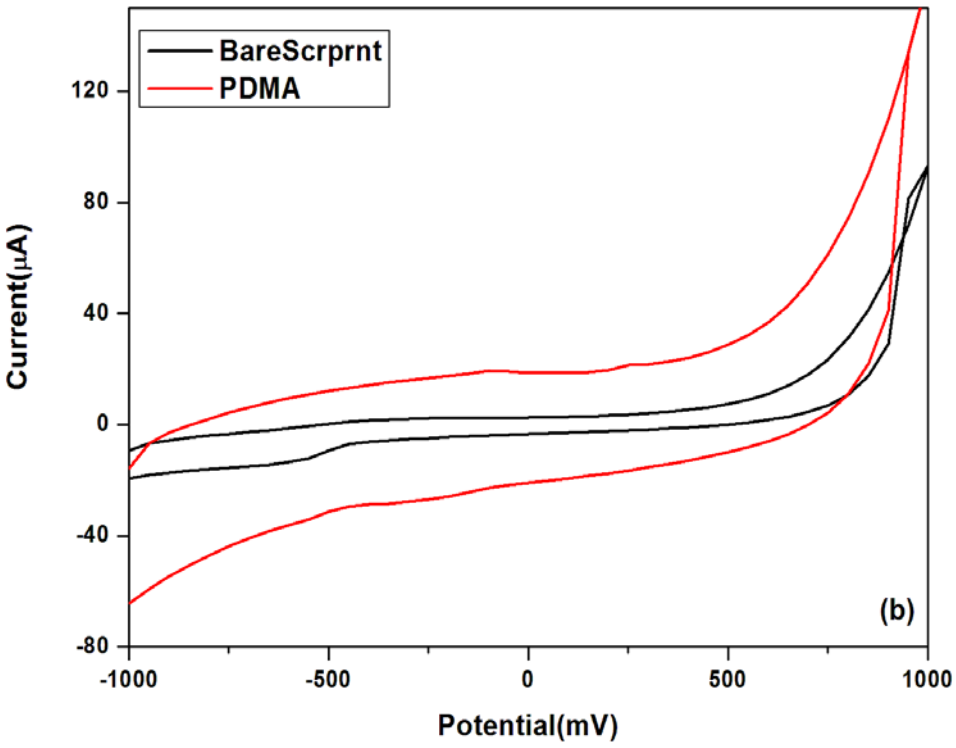

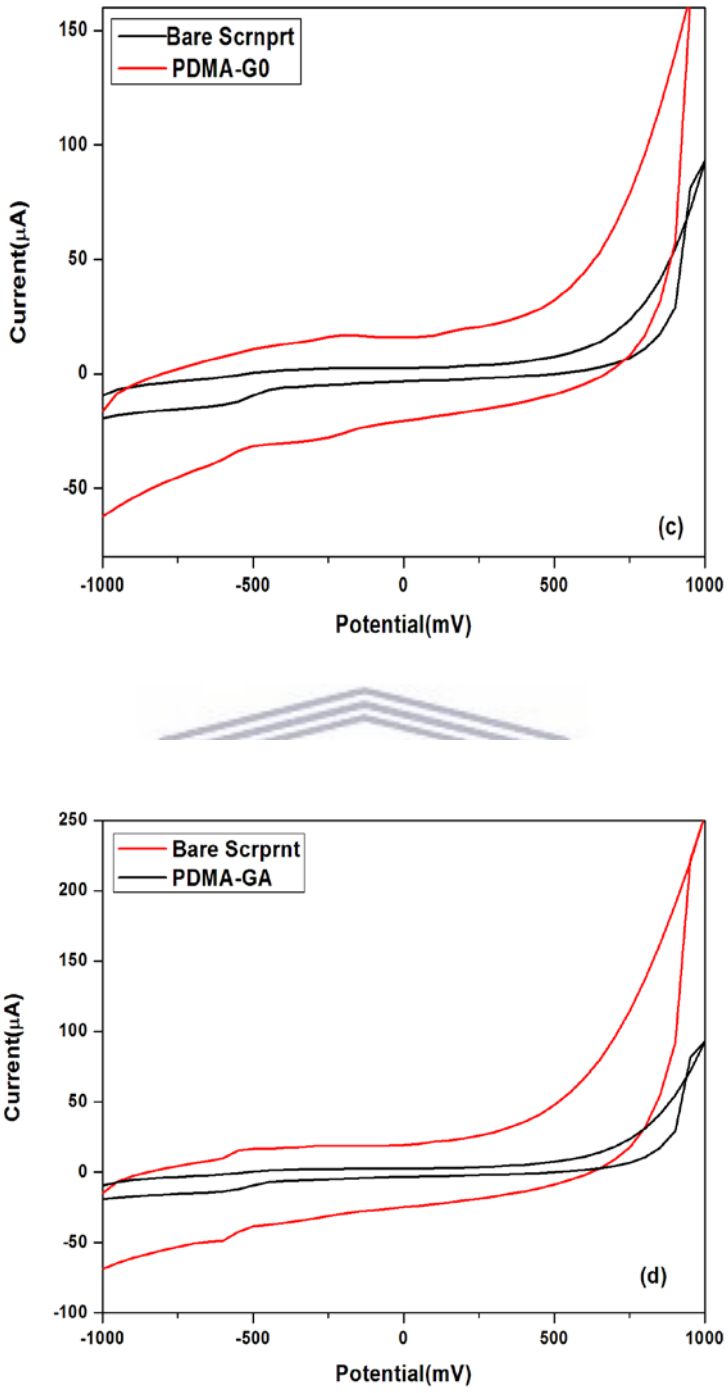

Figure 43: Cyclic voltammograms of (a) graphene modified screen printed electrode (b) PDMA (c) PDMA-GO and (d) PDMA-GA in Phosphate buffer (pH=8.0). Potential window: -1000 to 1000 mV.

5.3.4 Scan rate dependence of the modified electrode

The dependence of peak against scan rate was studied **Figure 44 (a) and (b)** respectively**.** The figure shows the plot of the anodic current versus scan rate for each of the redox peaks. **Figure 44 (b)** gave a linear equation of I_p = -1.33354 x 10^{-7} + 6.92966 x 10^{-9} x with a correlation coefficient r^2 = 0.99017. This electroactivity agrees with that of a thin film adsorbed electroactive species undergoing Nernstian reaction [262]. The surface concentration I^* (mol cm^{-2}) of the adsorbed electroactive species can be determined from the equation [173]. Consequently, the slope of the linear I vs υ of the first redox peak has been shown to be a one electron process [247].

$$\frac{I_{pa}}{\upsilon} = \frac{n^2F^2AI^*}{4RT} \qquad 17$$

From equation 1, n is the number of electrons transferred (n = 1), F is the faraday constant (96.584 C mol^{-1}), $I^*_{PDMA\text{-}GA}$ represent the surface concentration of the PDMA-GA composite film (mol cm^{-2}), A is the surface area of the electrode (0,071 cm^2), υ is the scan rate (mV s^{-1}), R is the gas constant (8,314 J mol^{-1} K^{-1}) and T is the absolute temperature of the system (298 K). The surface concentration of PDMA-GA film $I^*_{PDMA\text{-}GA}$ for the one electron transfer evaluated from the slope of the plot (I_{pa} vs υ) is 7.3619 x 10^{-9} mol cm^{-3}.

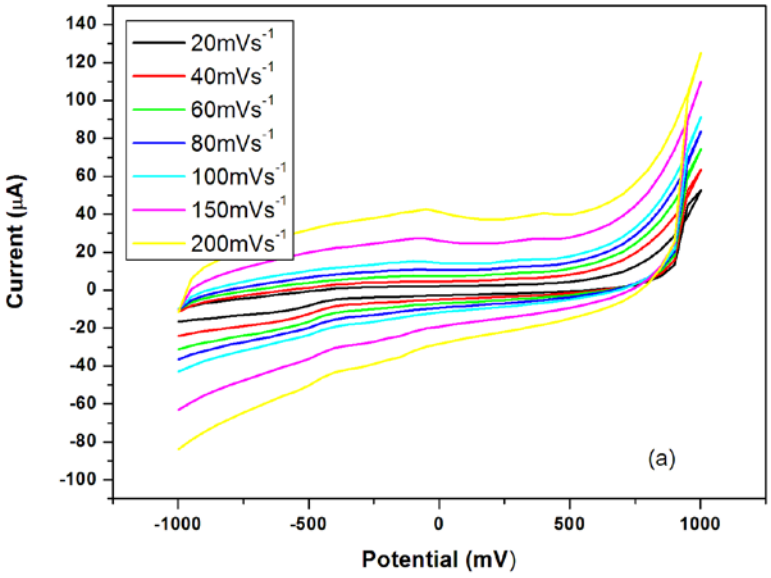

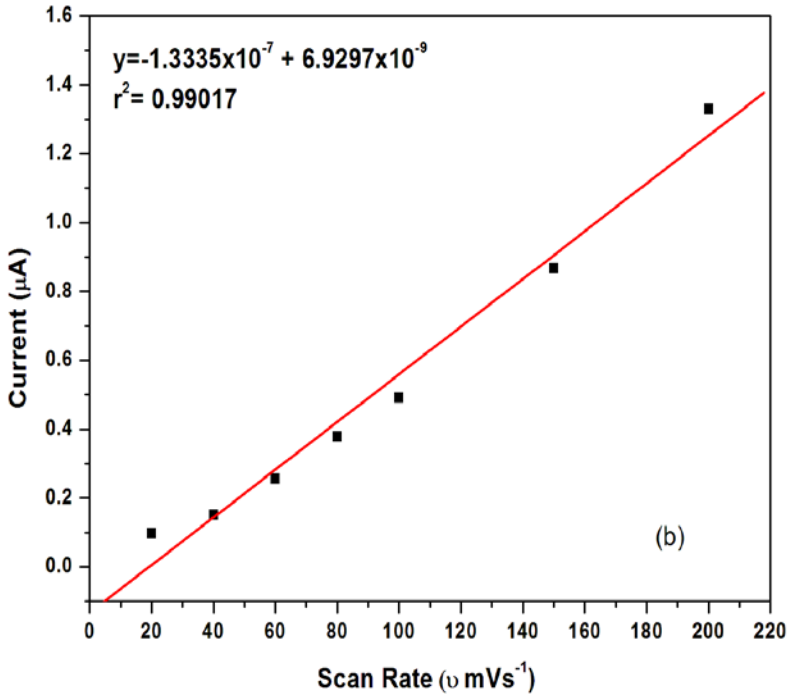

Figure 44: (a) voltammogram of PDMA-GA at different scan rates (b) Plot of Scan rate versus current.

5.3.5 Summary of electrochemical characterisation

We have successfully demonstrated the synthesis and characterisation of the novel PDMA, PDMA-GO and PDMA-GA composites, for further application in electrochemical sensors for estradiol detection. These nanocomposites have been extensively characterised by electron microscopy, spectroscopic and electrochemical techniques. The results of these studies have shown that PDMA, PDMA-GO and PDMA-GA have nanocomposite structures which are ideally suited for sensor applications. The utilisation of nanomaterials in sensors has greatly enhanced the detection of endocrine disruptors and the amplification of the signal associated with its detection. These two properties play a major role in trace level detection of environmental estrogens.

5.4 Response of modified electrode to estradiol

The electrocatalytic responses of the modified electrodes to different concentrations of estradiol were studied in phosphate buffer containing 10 % ethanol. A potential window of -1000 to + 1000 mV and scan rate of 150 mVs^{-1} were used as the working conditions. The SPCE was activated by cycling the potential from -1000 mV to +1000mV at a scan rate of 50 mVs^{-1} for 25 cycles, and then pre-treated using the same specifications as for the inactivated SPCE. This process resulted in the removal of any organic compounds and other contaminants that may be present in the carbon ink from the printing process. The oxidation of estradiol to the phenoxonium ion on the electrode surface is presented in **Scheme 1**. This phenoxonium ion formed a dimer or quinone, which causes fouling of the glassy carbon electrode surface, resulting in transient loss of detection signal of estradiol as previously stated. After numerous and unsuccessful attempts (washing the electrodes repeatedly, using nafion and surfactants) to overcome this problem, it was decided to abandon the glassy carbon electrode and replace it with screen printed carbon electrodes. Thus, each voltammetric measurement was carried out with a new screen printed electrode.

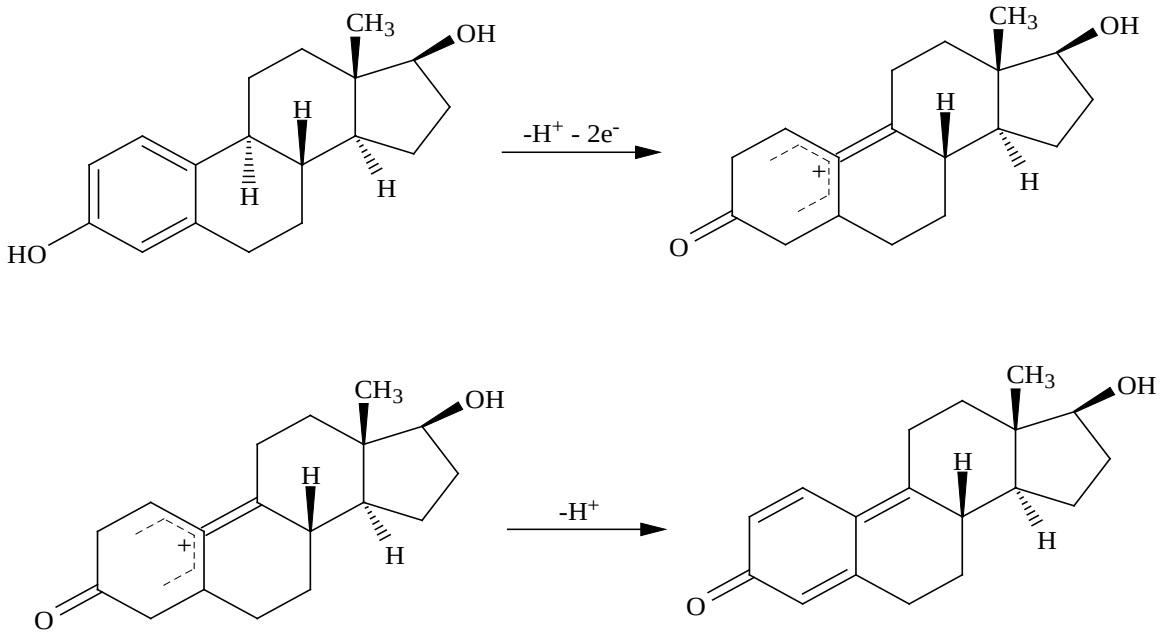

Scheme 1 Mechanism for the oxidation of estradiol.

5.4.1 Electrochemical application of the modified electrodes for estradiol detection

5.4.1.1 Electrochemical behaviour of the modified electrodes

The electrochemical behaviour of the bare carbon screen printed electrode and the modified carbon screen printed electrodes were investigated in 0.1 M phosphate buffer at a scan rate of 150 mVs^{-1}. **Figure 45** showed the cyclic voltammograms of the bare Screen printed carbon electrode (SPCE) and PDMA-GA screen printed carbon electrode in 0.1 M phosphate buffer and ethanol (90:10 v/v). The choice of the ethanol/buffer solution as previously mentioned is because ethanol is the only solvent that dissolves estradiol hence this mixture will be used mostly as the control. A scan rate of 150 mVs^{-1} and a potential window of -1000 to + 1000 mV were used for the voltammetry studies where the behaviour of the bare carbon screen printed electrode and the PDMA-GA electrode in ethanol/ phosphate buffer before the exposure to estradiol were evaluated.

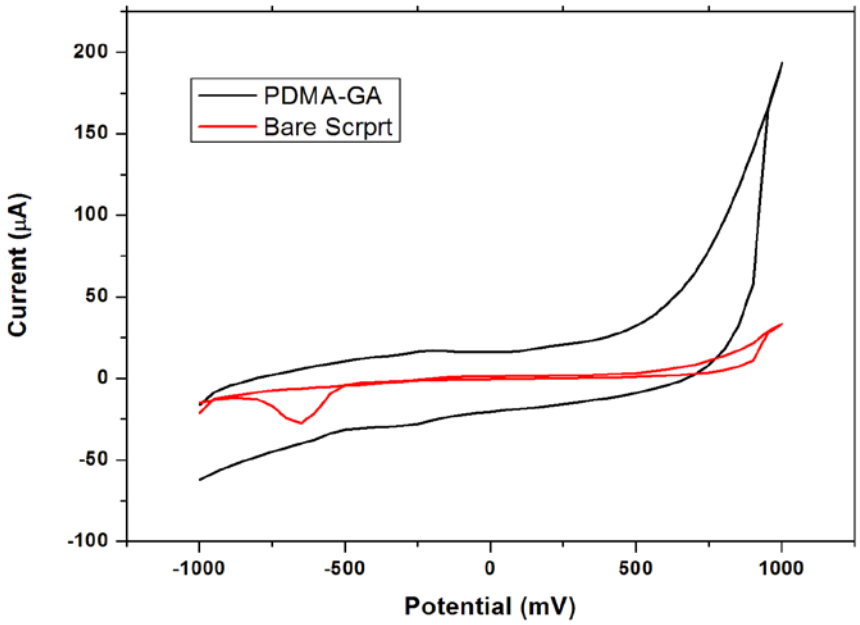

Figure 45: Cyclic voltammograms of bare Screen printed electrodes and PDMA- GA in ethanol/buffer (10/90 v/v) at scan rate 150 mVs^{-1}.

Figure 46 shows the electrochemical behaviour of the different modified electrodes namely, bare screen printed (SPCE), SPCE/PDMA, SPCE/PDMA-GO and SPCE/PDMA-GA in phosphate buffer (pH= 8) and a scan rate of 150 mVs^{-1} and a potential window of -1000 to +1000 mV where the electro-oxidation of 100 μM (1.0×10^{-4} M) estradiol dissolved in the ethanol and phosphate buffer (10/90 v/v) was evaluated. An anodic peak current can be observed at a potential around 600 mV upon the addition of 100μM (1.0×10^{-4} M) of estradiol indicating that the successful oxidation of estradiol has occurred. The PDMA-GA modified SPCE exhibited a higher catalytic activity property through the enhancement of the anodic peak during the oxidation of estradiol, compared to the response of the SPCE/PDMA and SPCE/PDMA-GO electrodes respectively towards estradiol. It should be noted that no visible electrochemical peaks were observed for the bare screen printed electrode indicated in **Figure 46.** However, two peaks one cathodic and one anodic, near 50 mV were observed attributed to the presence of ethanol.

Further experiments were performed in the absence of estradiol and in the presence of ethanol, and the same peaks were observed and fortunately these peaks did not interfere with further studies. This observation agreed with those confirmed by Janegitz *et al* [66].

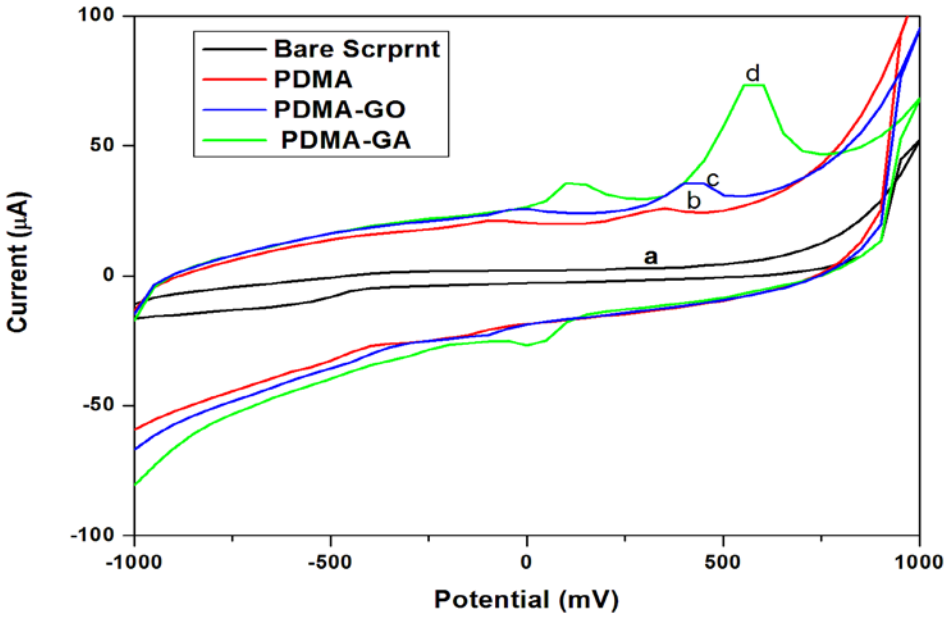

Figure 46: Cyclic voltammograms of (a) bare Screen printed electrode (SPCE) (b)SPCE/ PDMA (c) SPCE/PDMA-GO and (d) SPCE/PDMA-GA in the presence of 100 µM (1.0×10^{-4}) of estradiol at a scan rate of 150 mVs^{-1} and a potential window of -1000 to +1000 mV.

5.4.1.2 Effect of scan rate

The dependence of the peak current on the scan rate was also investigated in buffer containing 10% ethanol. Scan rate defines the speed of the potential sweep during the collection of data. Scan rate is one of the most important parameters that affect the redox properties of the sensor platforms in cyclic voltammetry. Since the concept of an inert electrode is idealistic, the surface of the electrode exerts an influence on the electrode reaction (even minutely) and can form bonds with species in solution [263].

For the understanding of the mechanism of the effect of graphene on the electrochemical properties of PDMA, the various scan rates 20 to 200 mVs^{-1} using the technique cyclic voltammetry. This will allow us to calculate electrochemical parameters such as film thickness, surface concentration and the diffusion coefficient. The working potential window was -1000 to +1000 mV and the concentration of the estradiol was 80 μM (8.0×10^{-5}M). An increase in the oxidation peak was observed with an increase in the scan rate. **Figure 47 (a)** shows the cyclic voltammograms of SPCE/PDMA-GA electrode at different scan rates in the presence of a constant concentration of estradiol. The plot of the anodic peak current versus the square root of the scan rate over the range of 20-200 mVs^{-1} is presented in **Figure 47 (b)** together with the corresponding linear fitting. The relationship between scan rate (υ) and peak current is often a diagnostic tool used for identifying the nature of the electrode process. The relationship in our study **Figure 47** gave a linear regression of I_p (μA) = 3.84×10^{-6} x -1.89×10^{-5} and has a correlation coefficient, r^2 = 0.9916. This result suggested diffusion controlled electrochemistry [264] which indicated that the process was limited by the rate of diffusion of estradiol from the solution to the surface of the electrode. It could also be observed that the peak potentials shifted with increase in scan rate denoting the irreversible behaviour of the system [265].

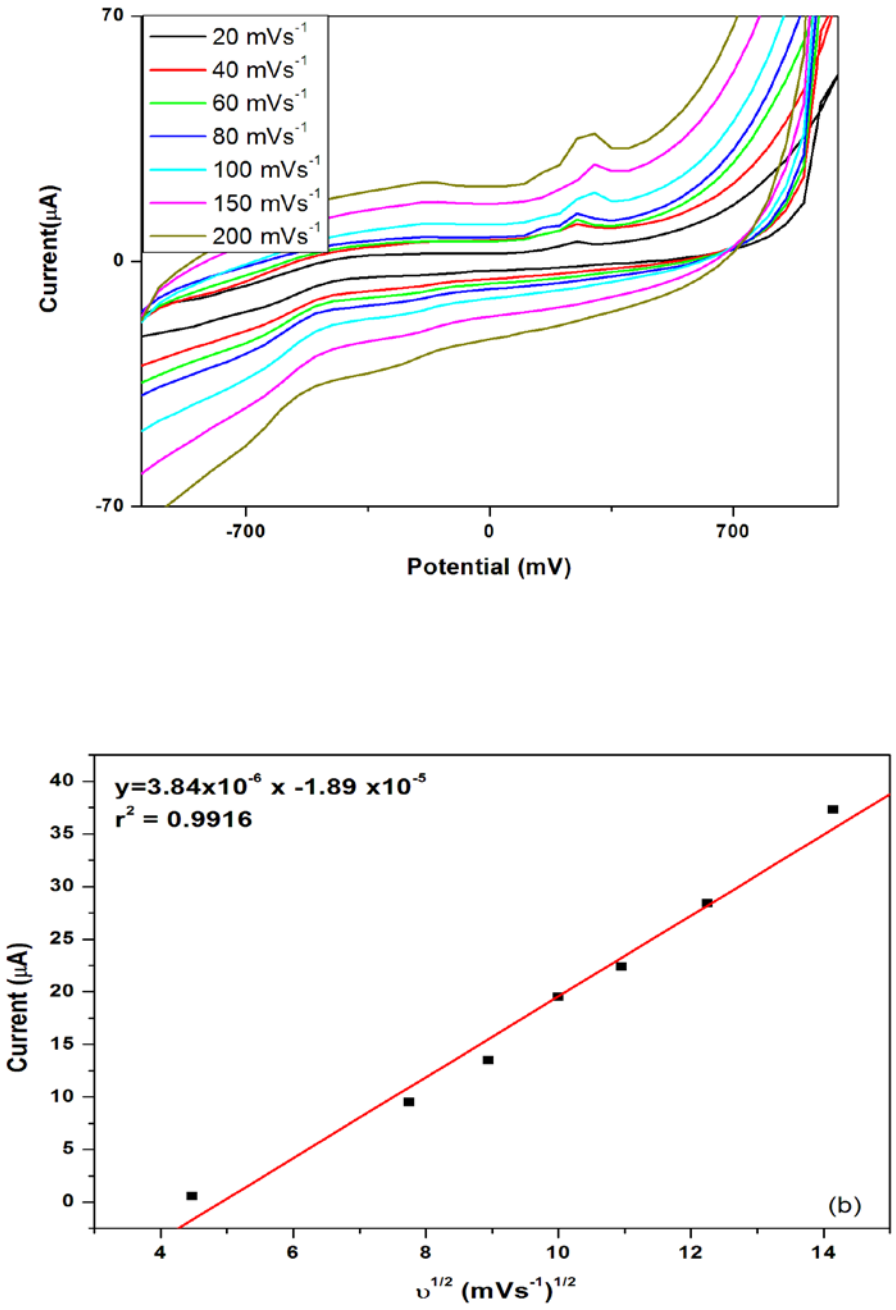

Figure 47: Cyclic voltammograms of (a) PDMA-GA in buffer/ethanol (90/10 v/v) in the presence of 1×10^{-4} M estradiol and (b) a plot of scan rate versus anodic peak currents.

The electron transport diffusion coefficient for D_e (in cm^2s^{-1}), for PDMA-GA was calculated (**Table 4**) from the Randle- Sevcik plot of peak current (I_p) versus the square root of scan rate ($\upsilon^{1/2}$). Using the Randel-Sevcik data and equation 1 (bard and Faulkner), the following equation was obtained for the determination of D_e:

$$I_p = 2.69 \times 10^5 . n^{\frac{3}{2}} . A . D_e^{\frac{1}{2}} . c . \upsilon^{\frac{1}{2}} \quad 18$$

Where F is the faraday constant (96.584 C mol^{-1}), $I^*_{PDMA\text{-}GA}$ represent the surface concentration of the PDMA-GA composite film (mol cm^{-2}), A is the surface area of the electrode (0,071 cm^2), υ is the scan rate (mV s^{-1}), R is the gas constant (8,314 J mol^{-1} K^{-1}) and T is the absolute temperature of the system (298 K), C is the concentration of the solution. The result from a plot of I_{pa} versus $\upsilon^{1/2}$ is then used and the slope is equal to:

$$Slope = 2.69 \times 10^5 . n^{\frac{3}{2}} . A . D_e^{\frac{1}{2}} . C \quad 19$$

The thickness of the nanoparticle film obtained by drop coating on the carbon screen printed electrode was also determined (**Table 4**). The calculation of this parameter was obtained using the equation which Iwuoha *et al* [266] used. The plot of plot of peak current (I_p) versus the square root of scan rate ($\upsilon^{1/2}$), gives the slope as indicated below.

$$\frac{I_{pa}}{\upsilon^{\frac{1}{2}}} = \frac{0.4463.(nF)^{\frac{3}{2}}.A.D_e.I^*}{L.(RT)^{\frac{1}{2}}} = slope \quad 20$$

Where F is the faraday constant (96.584 C mol^{-1}), $I^*_{PDMA\text{-}GA}$ represent the surface concentration of the PDMA-GA composite film (mol cm^{-2}), A is the surface area of the electrode (0,071 cm^2), υ is the scan rate (mV s^{-1}), R is the gas constant (8,314 J mol^{-1} K^{-1}) and T is the absolute temperature of the system (298 K), D_e is the transport diffusion coefficient.

Table 4: Electrochemical parameters

Electrode	Surface Concentration (I^* mol cm^{-3})	Diffusion coefficient (D_e)	Thickness of film (L cm)
PDMA-GA	7.3619×10^{-9}	4.024×10^{-12}	1.48×10^{-10}

5.4.1.3 Analytical application of the modified electrode

The electrocatalytic oxidation of estradiol was studied using PDMA, PDMA-GO and PDMA-GA electrodes. The cyclic voltammetric responses of the modified SPCE electrodes and the electrocatalytic properties of estradiol in 0.1 M phosphate buffer containing (10 % ethanol) between a potential window of -1000 to +1000 mV and scan rate of 150 mVs^{-1} is presented in **Figure 48, 50 and 52** respectively. In all three cyclic voltammogramms showed a similar behaviour towards the oxidation of estradiol. At low concentrations, we observed an irreversible anodic peak at 302 mV shifting positively to a maximum at 600 mV with the addition of estradiol (5 -220 µM). A comparison of the peak current for the three different electrodes (i.e. PDMA, PDMA-GO and PDMA-GA) is given in **Table 5**. The oxidation peak observed at approximately 600 mV for each electrode shows an increase from PDMA to PDMA- GA.

Calibration plots were obtained under the optimised conditions with additions of estradiol (5 – 220 µM) as represented in **Figures 49, 51 and 53** respectively. Calibration plots showed good linear correlation for the concentration ranges between 5 – 220 µM as obtained for the three prepared sensors (PDMA, PDMA-GO and PDMA-GA). The results obtained from the calibration curves are represented in **Table 5**.

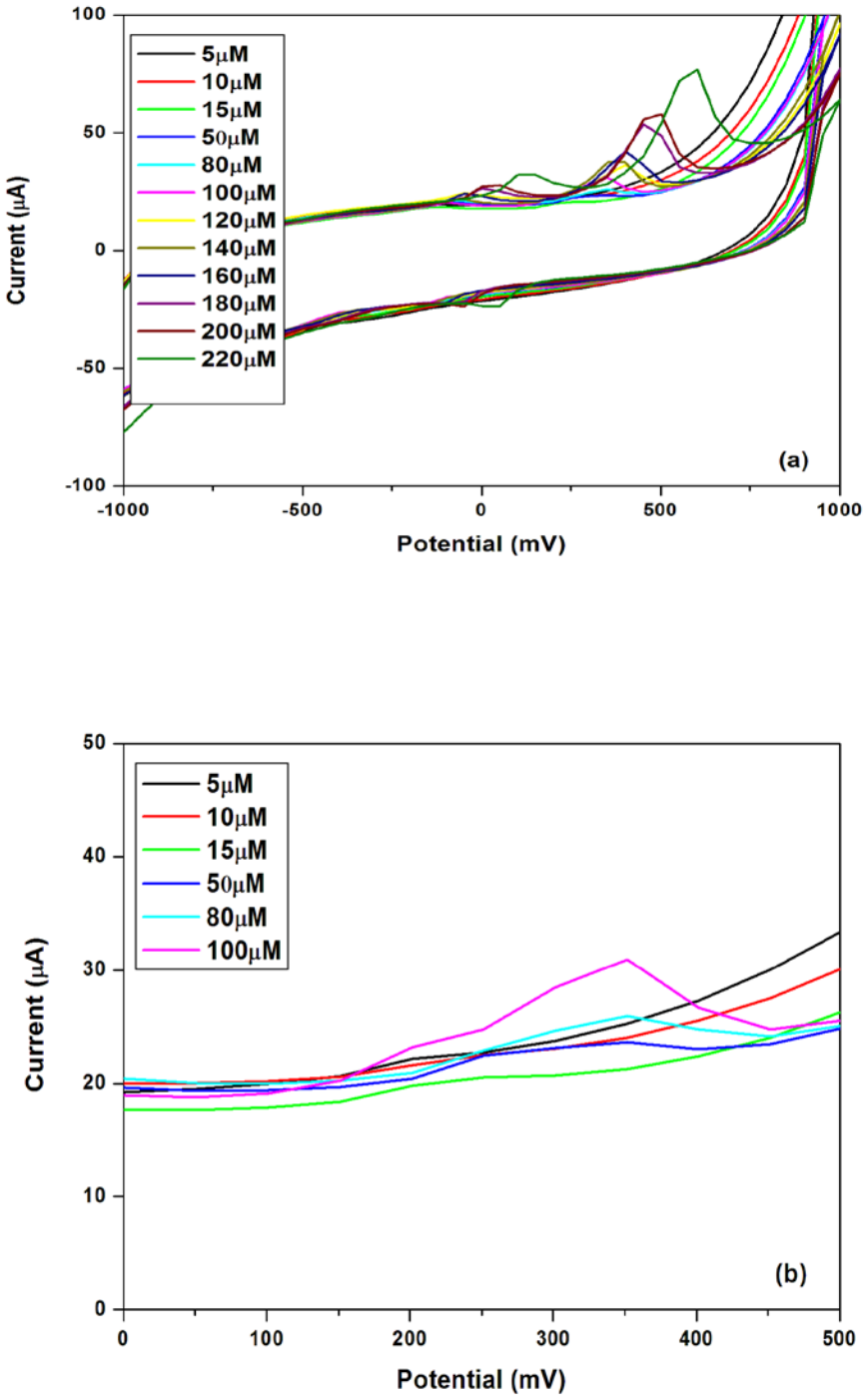

Figure 48: Cyclic voltammograms of (a) modified PDMA upon the addition of different concentrations (5 – 220 µM) of estradiol (b) at low concentrations of estradiol.

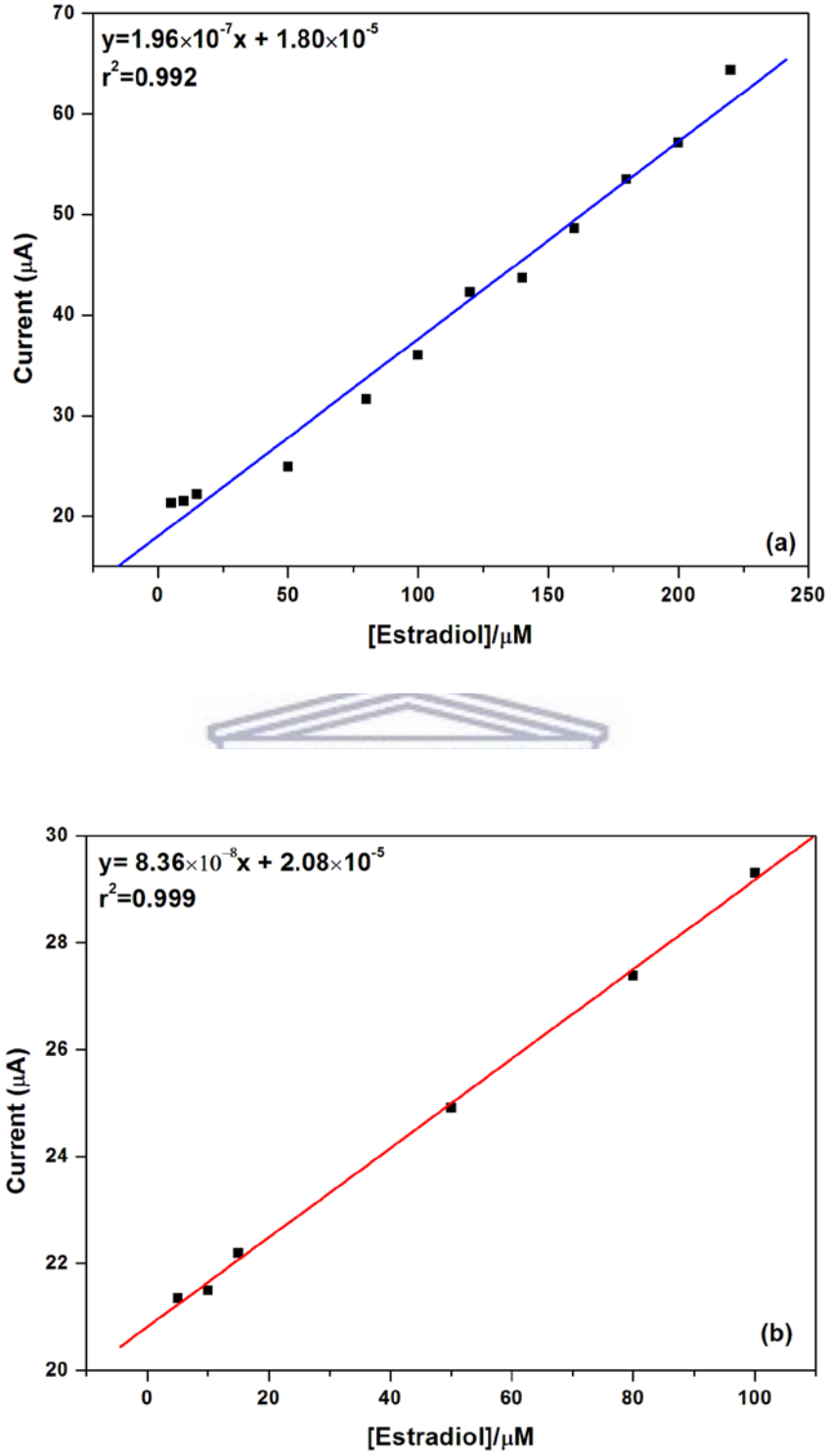

Figure 49: Calibration curves for (a) PDMA sensor upon the addition of different concentrations (5 – 220 µM) of estradiol (b) at lower concentrations of estradiol.

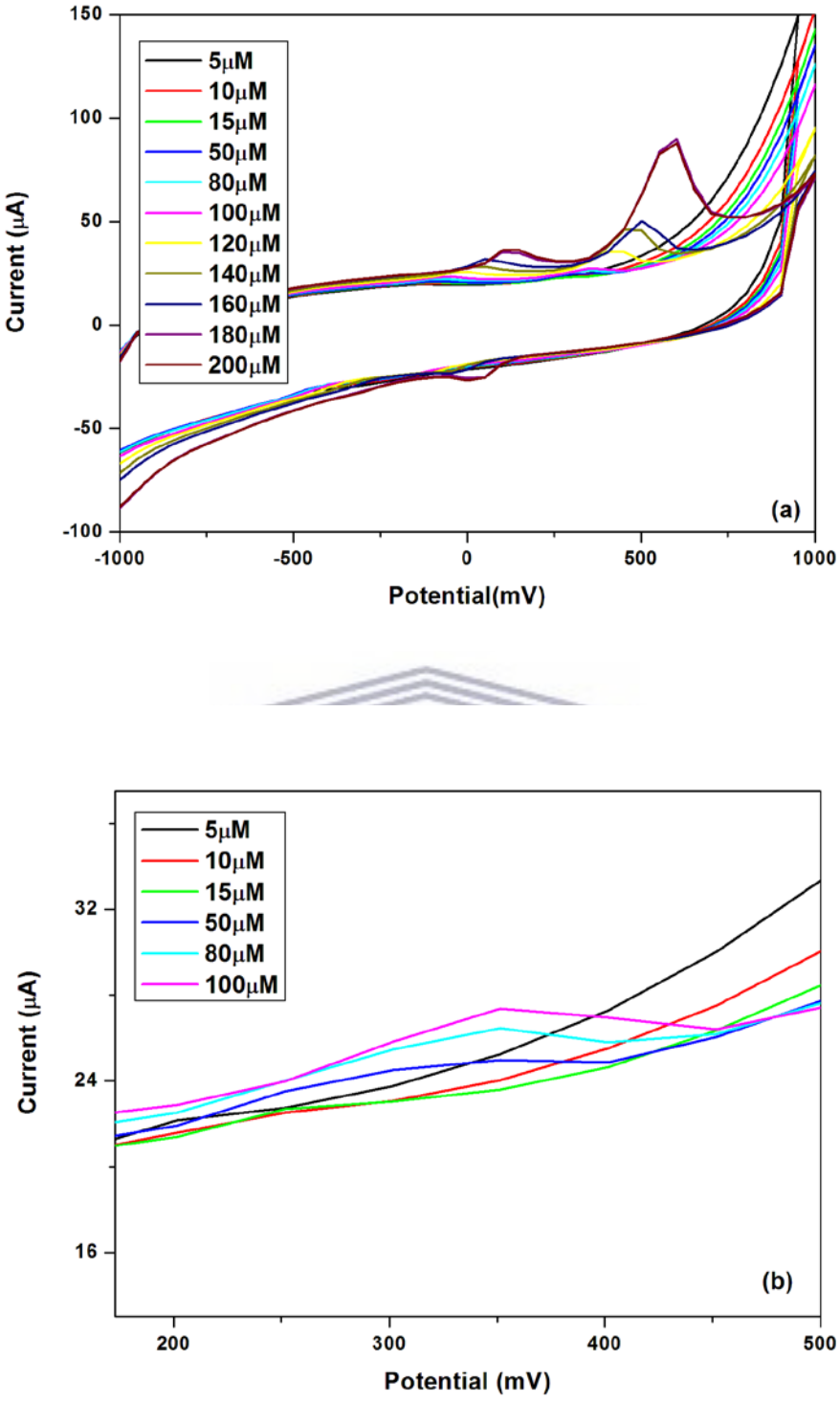

Figure 50: Cyclic voltammograms of (a) modified PDMA-GO upon the addition of different concentrations (5 – 220 µM) of estradiol (b) at low concentration of estradiol

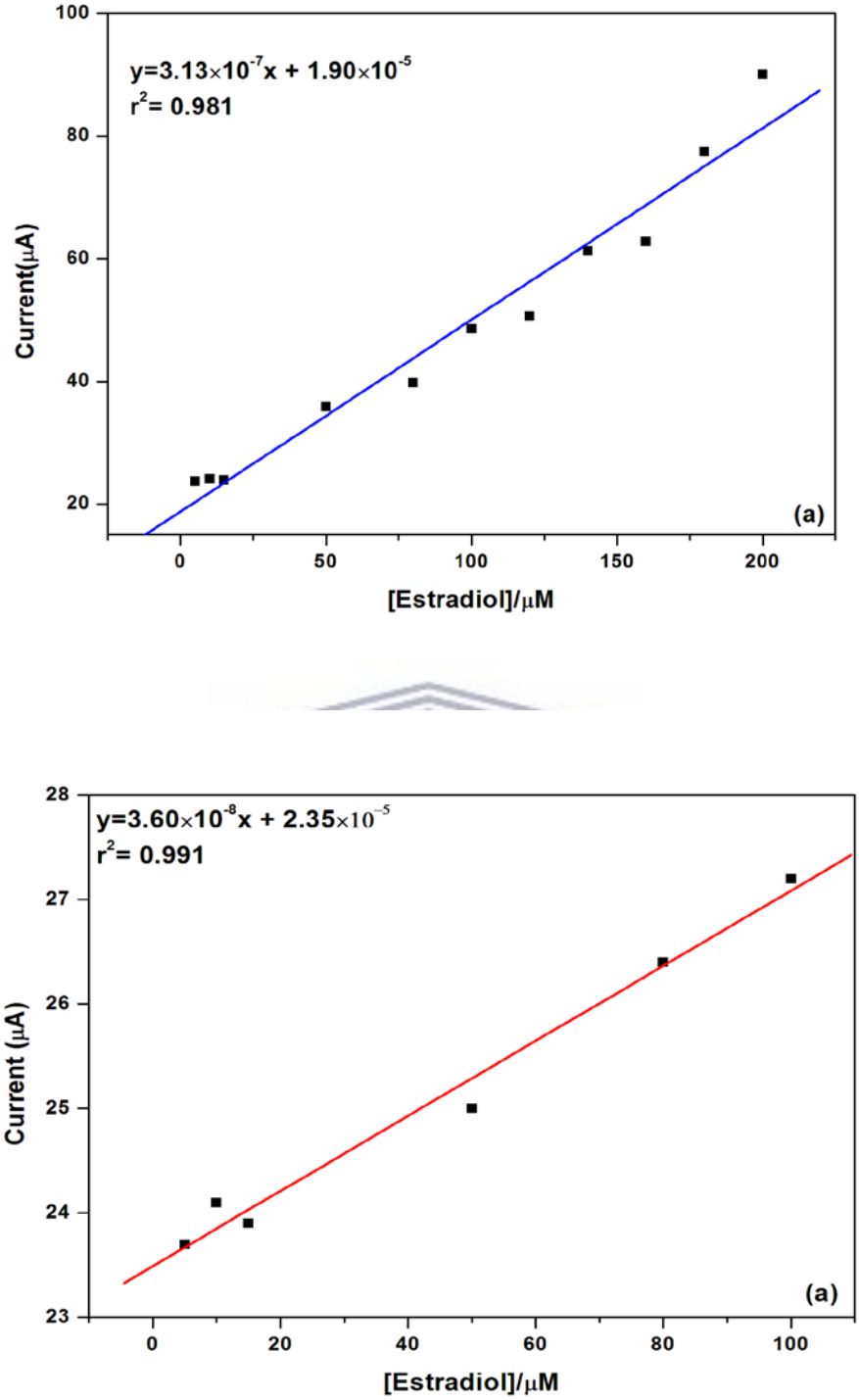

Figure 51: Calibration curves for (a) PDMA-GO sensor upon the addition of different concentrations (5 – 220 µM) of estradiol (b) at lower concentrations of estradiol

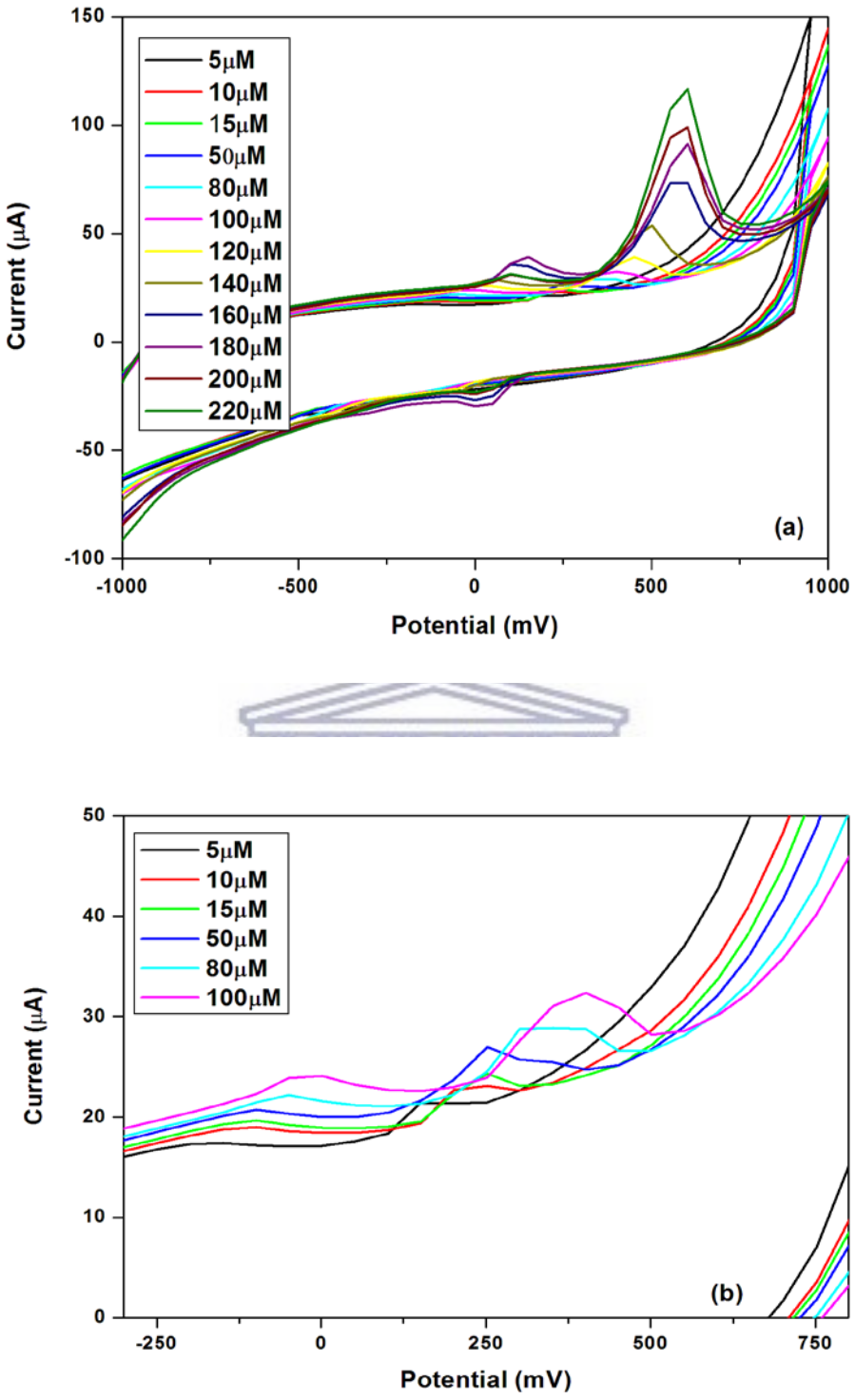

Figure 52: Cyclic voltammograms of (a) modified PDMA-GA upon the addition of different concentrations (5 – 220 μM) of estradiol (b) at low concentration.

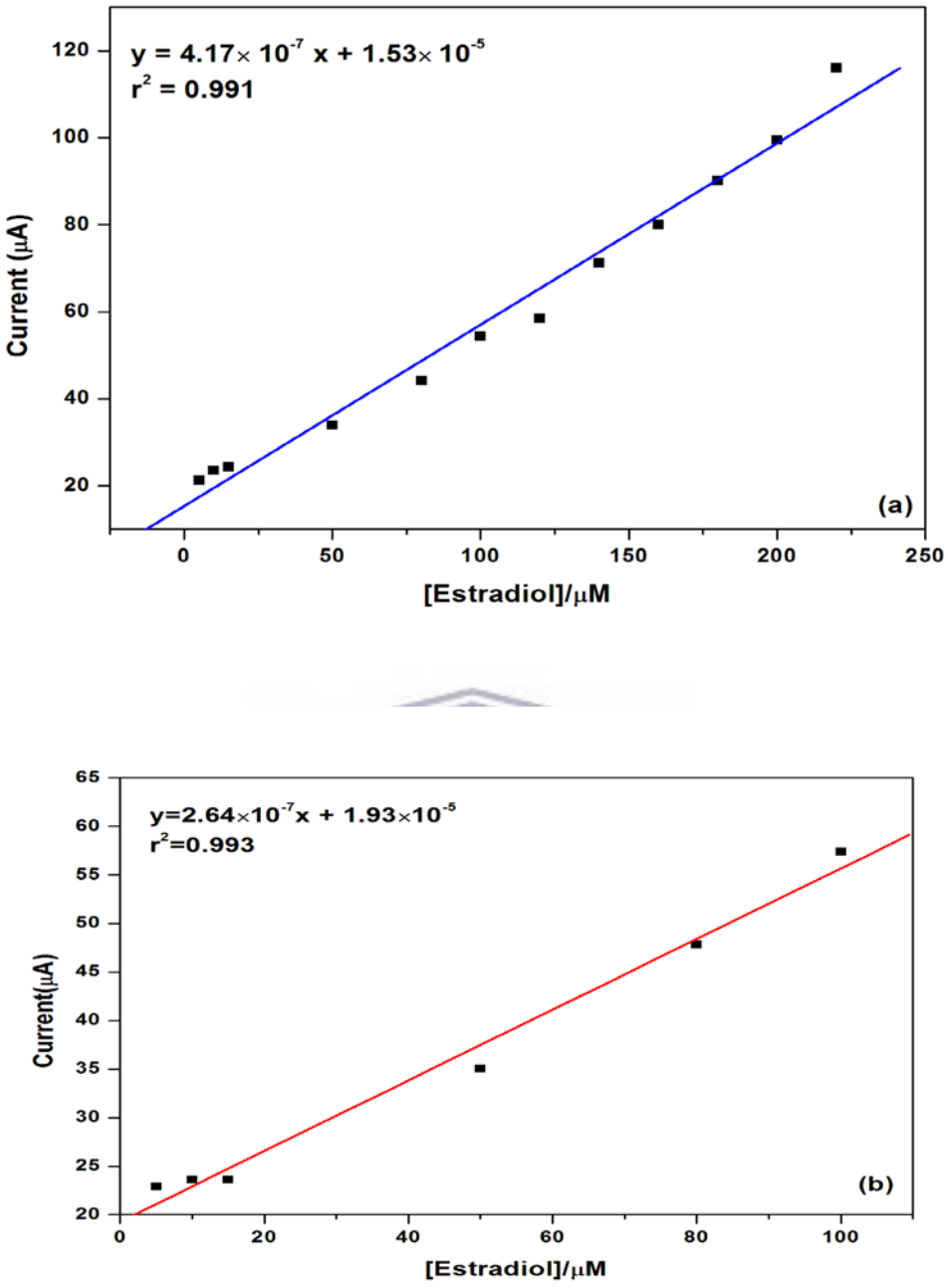

Figure 53: Calibration curves for (a) PDMA-GA sensor upon the addition of different concentrations (5 – 220 µM) of estradiol (b) at lower concentrations of estradiol.

Table 5: Summary of the comparative current responses and potentials for the oxidation of estradiol at the PDMA, PDMA-GO and PDMA-GA.

Electrode	I_{pa} (µA)	Potential (mV)
PDMA	76.81	603.38
PDMA-GO	88.69	603.38
PDMA-GA	116.08	603.38

Table 6: Calibration data for the determination of estradiol using PDMA,PDMA-GO and PDMA-GA at low concentrations (LC) and at high concentrations (HC).

Sensor	Regression	R^2
PDMA – (LC)	$y = 8.36 \times 10^{-8} x + 2.08 \times 10^{-6}$	0.999
PDMA- (HC)	$y = 1.96 \times 10^{-7} x + 1.80 \times 10^{-5}$	0.992
PDMA-GO (LC)	$y = 3.60 \times 10^{-6} x + 2.35 \times 10^{-5}$	0.991
PDMA-GO (HC)	$y = 3.13 \times 10^{-7} x + 1.90 \times 10^{-5}$	0.981
PDMA-GA(LC)	$y = 2.64 \times 10^{-7} x + 1.93 \times 10^{-5}$	0.993
PDMA-GA (HC)	$y = 4.17 \times 10^{-7} x + 1.53 \times 10^{-5}$	0.991

In summary, the evaluation of results for each of the modified screen printed carbon electrodes has shown an increase in current for concentrations of estradiol up to 220 µM for PDMA, PDMA-GO and PDMA-GA sensors respectively. **Table 6** summarises the current responses and potentials for each of the modified electrodes in 0.1 M phosphate buffer containing estradiol. From the results of the calibration curves **Table 6,** it was evident that the estradiol is being oxidised. Standard additions of estradiol showed that the peak current increased with an increase in concentration after each addition.

The square wave voltammetric results are represented in **Figures 54, 56** and **58** respectively where the calibration curves for the respective modified electrodes are represented in **Figures 55, 57 and 59**. The results obtained from the square wave voltammograms confirmed that what was obtained from the cyclic voltammetric measurements was indeed a true reflection of the successful operation of the sensors. The square wave voltammograms show an increase in peak current with increase in estradiol concentration for all the modified electrodes. Notably enough, the PDMA-GA modified SPCE showed the best response to estradiol oxidation which was similar to results obtained from cyclic voltammetry.

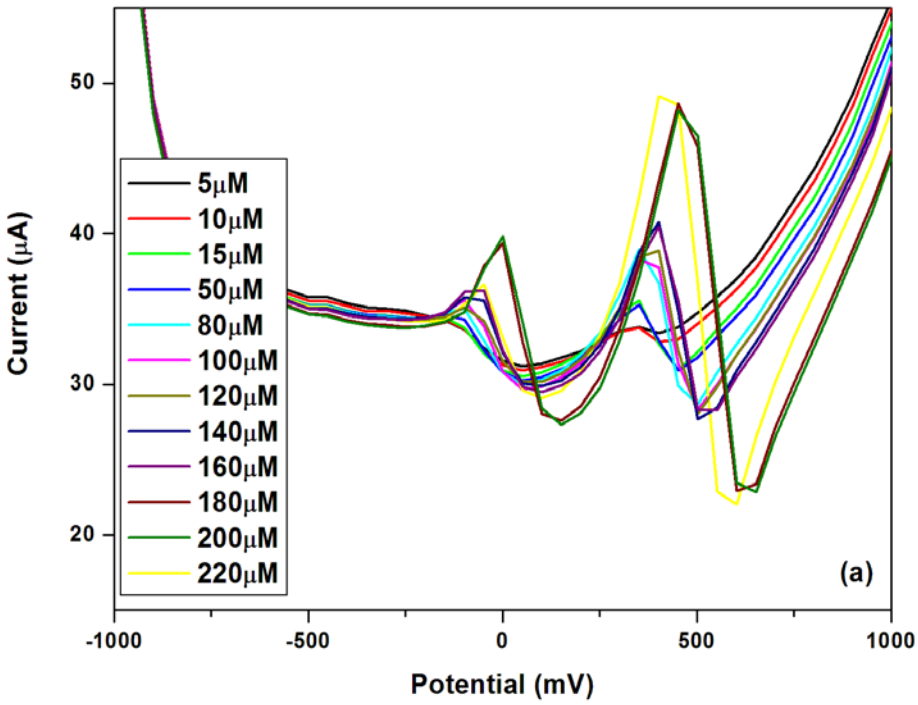

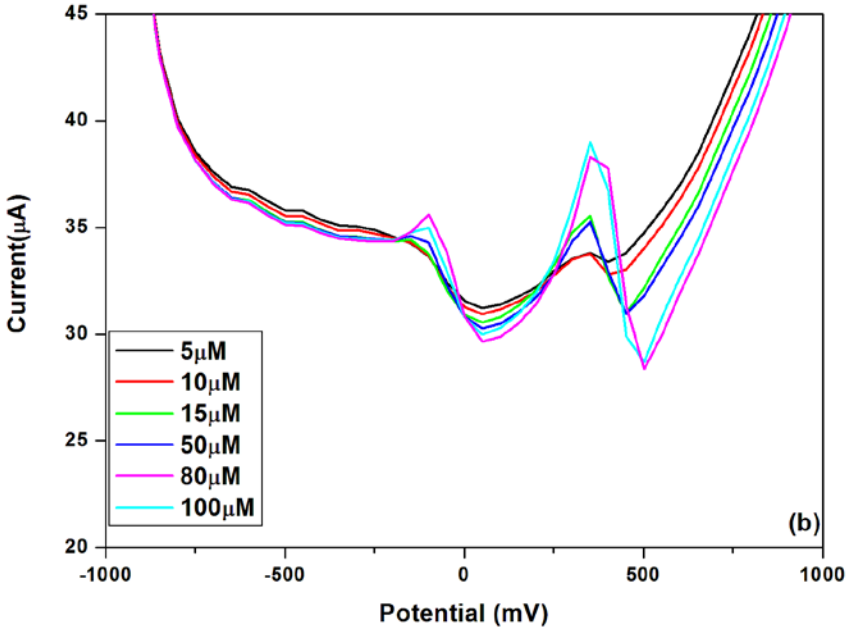

Figure 54 Square Wave Voltammograms of (a) modified PDMA upon addition of different concentrations of estradiol (5 – 220 μM) (b) at low concentrations of estradiol

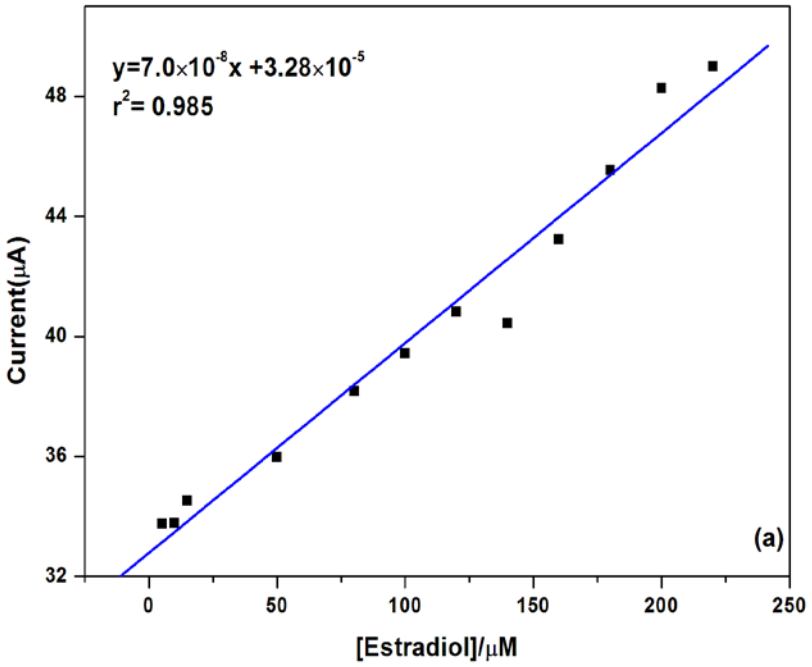

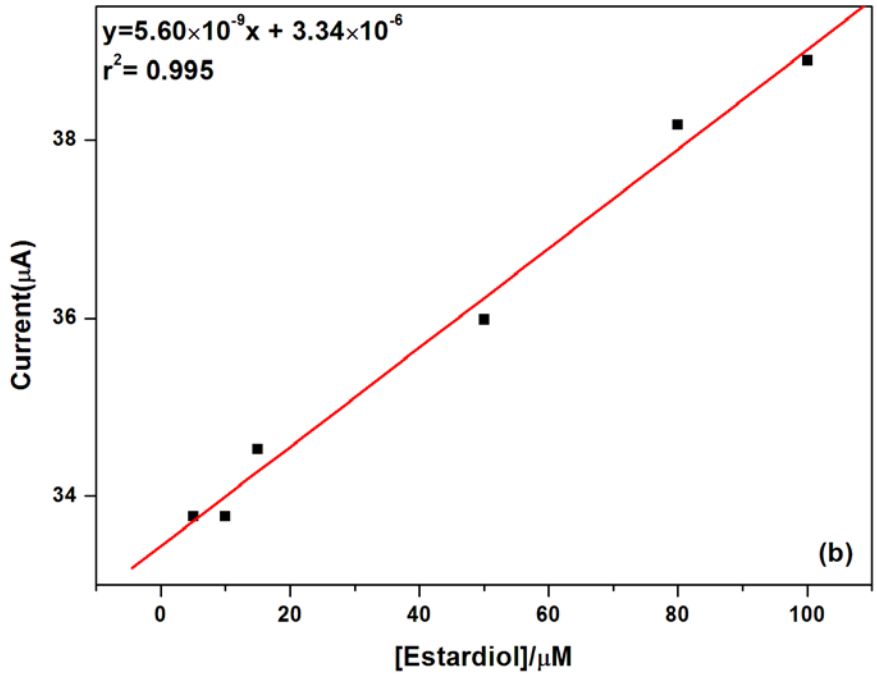

Figure 55: Plot of calibration curves of anodic peak current versus concentration (a) modified PDMA upon addition of different concentrations (5 – 220 µM) of estradiol (b) at lower concentrations of estradiol.

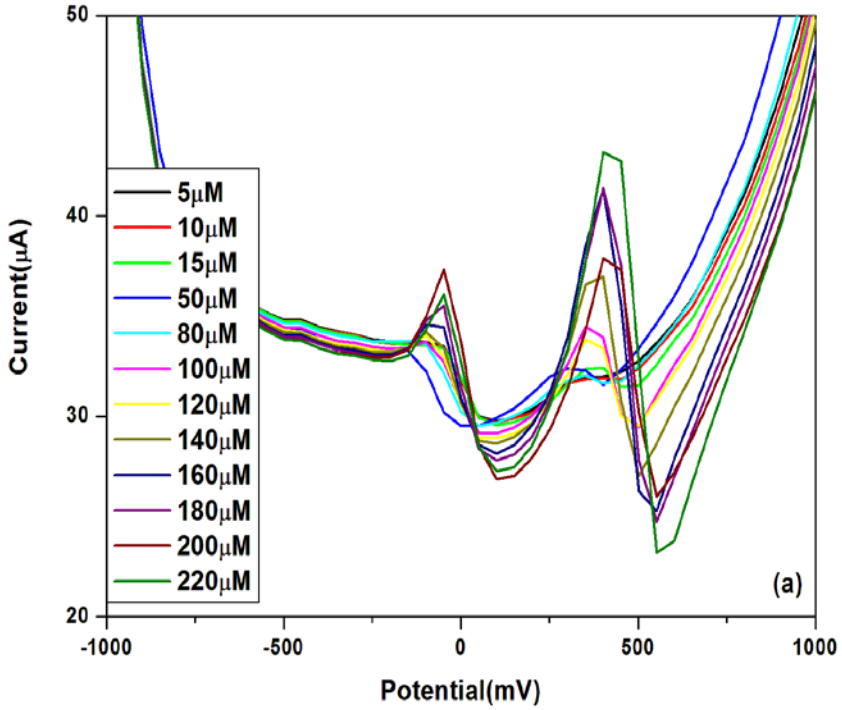

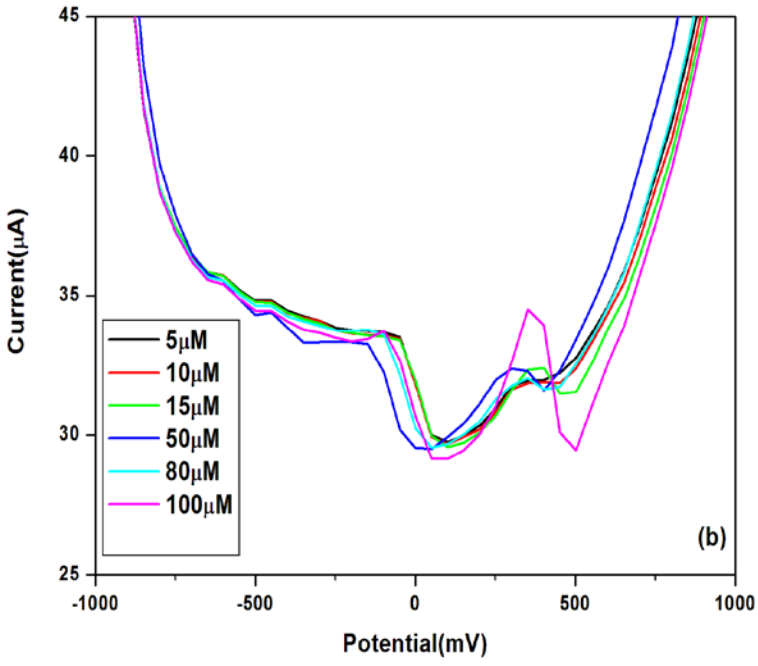

Figure 56: Square Wave Voltammograms of (a) modified PDMA-GO upon addition of different concentrations of estradiol (5 – 220 µM) (b) at low concentrations of estradiol

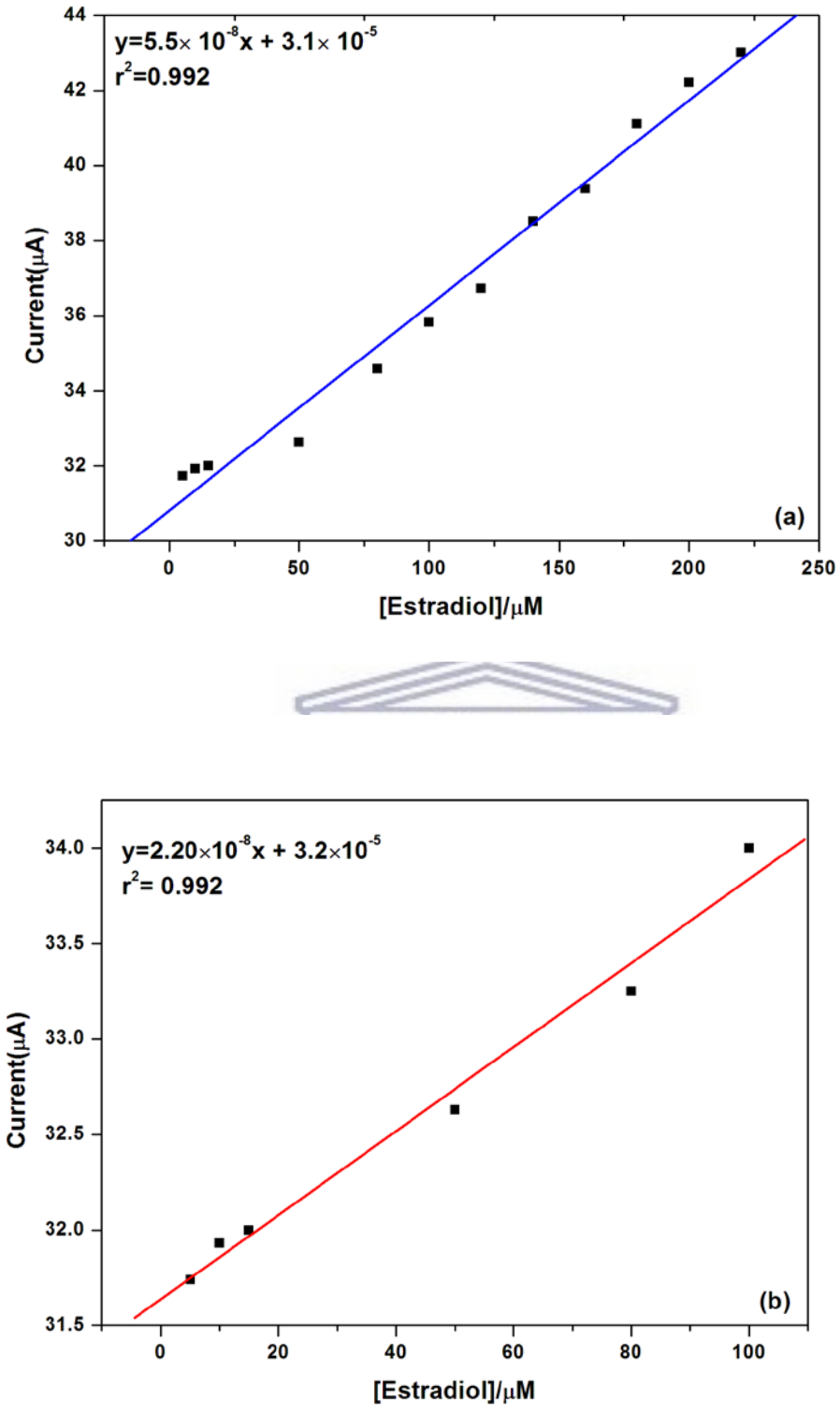

Figure 57: Plot of calibration curves of anodic peak current versus concentration (a) modified PDMA-GO upon addition of different concentrations (5 – 220 µM) of estradiol (b) at lower concentrations of estradiol.

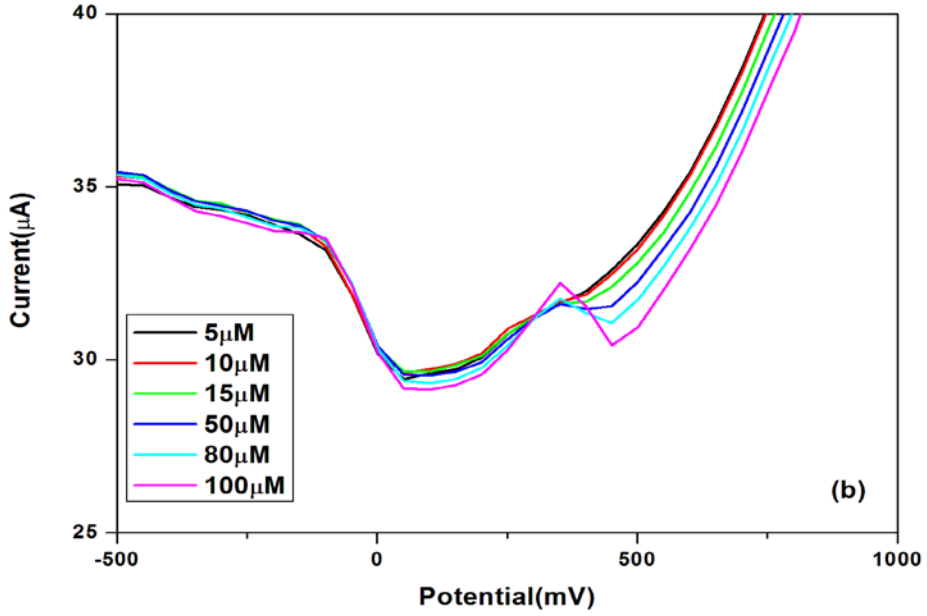

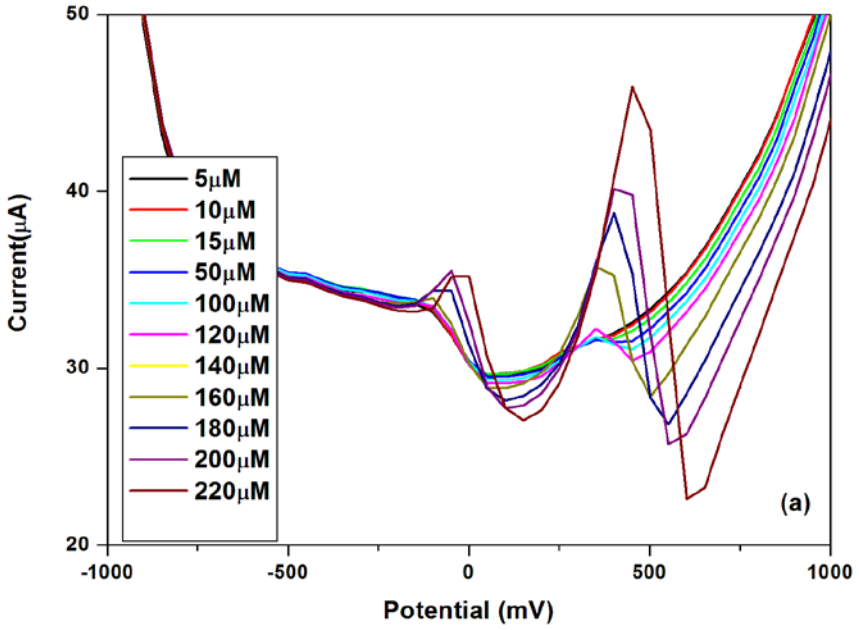

Figure 58: Square Wave Voltammograms of (a) modified PDMA-GA upon addition of different concentrations of estradiol (5 – 220 µM) (b) at low concentrations of estradiol.

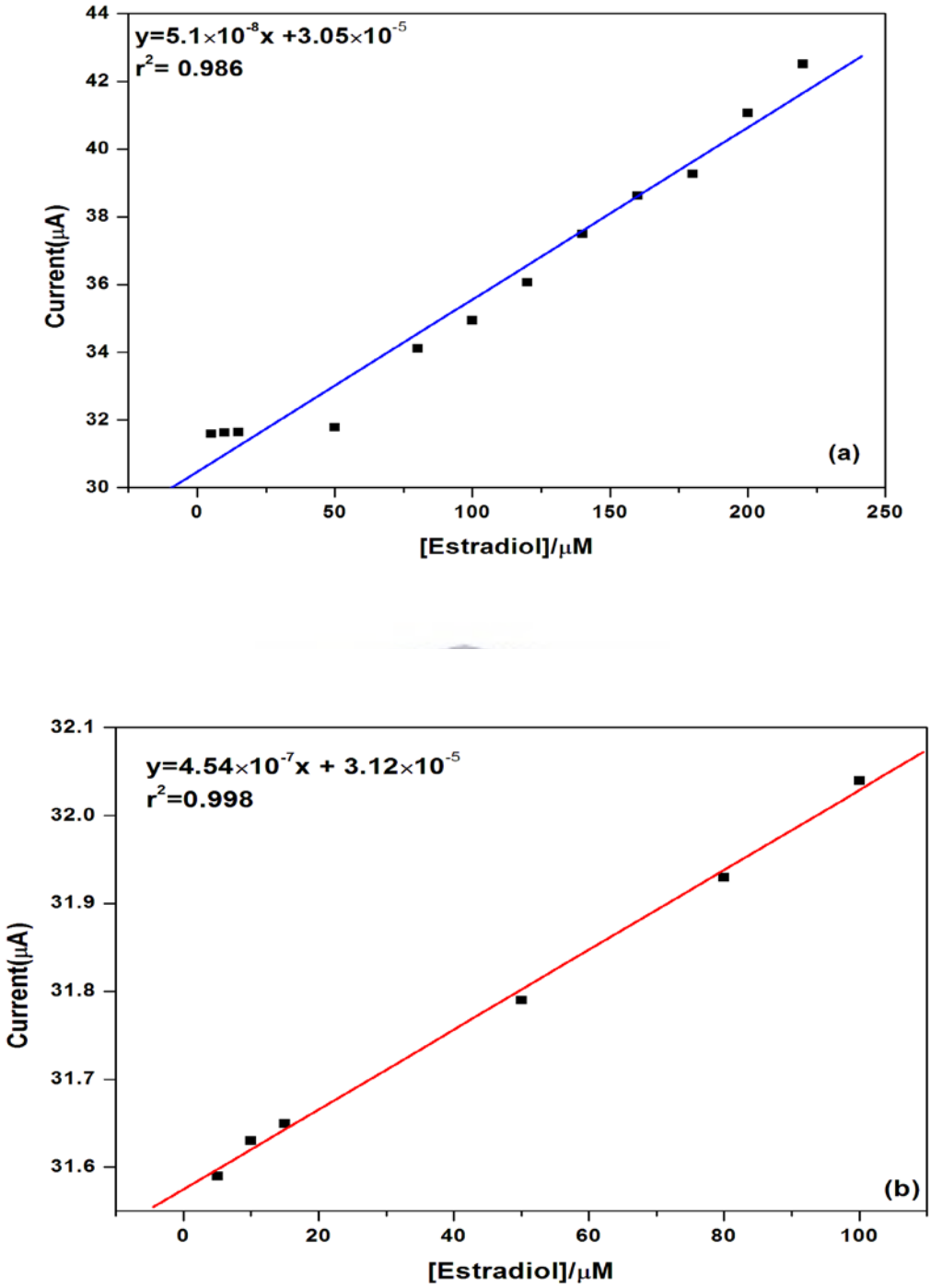

Figure 59: Plot of calibration curves of anodic peak current versus concentration (a) modified PDMA-GA upon addition of different concentrations (5 – 220 µM) of estradiol (b) at lower concentrations of estradiol.

5.5 Comparison of calculated results for different sensor platforms

A comparison of the different sensors prepared was examined via evaluation of linearity (LR), limit of detection (LOD), repeatability and reproducibility. The reproducibility, accuracy and sensitivity of the PDMA, PDMA-GO and PDMA-GA sensors was examined by a comparison of the correlation coefficient, linearity and standard deviation as tabulated in **Table 7.** The limit of detection was determined as the minimum detectable concentration, which is the lowest concentration that can be distinguished at a stated level of probability, from a sample not containing the analyte (estradiol) or any one of the analyte solutions as the lowest working concentration. The detection limit (LOD) was determined using the formula:

$$LOD = \frac{3 \times SD}{m} \qquad 21$$

Where SD is the standard deviation, and m is the slope of the linearity [266].

Table 7: Analytical parameters obtained for the modified sensors (PDMA, PDMA-GO and PDMA-GA)

Sensor	R^2	Linear range (LR)	Limit of Detection LOD	Sensitivity
PDMA	0.995	5×10^{-6} - 2×10^{-4}	3.71×10^{-4}	7.86×10^{-8}
PDMA-GO	0.992	5×10^{-6} - 2×10^{-4}	5.74×10^{-5}	3.1×10^{-7}
PDMA-GA	0.998	5×10^{-6} - 2×10^{-4}	1.19×10^{-7}	6.40×10^{-5}

The carbon electrode used in this study was based on the performance of the glassy carbon electrode and the screen-printed electrode in the detection of estradiol. The sensitivities of each sensor were calculated from the slope of the calibration curve divided by the area of the carbon screen printed electrode (0.071 cm^2). The sensitivity of PDMA, PDMA- GO and PDMA-GA sensors was found to be $7.86\times10^{-8,}$ 3.1×10^{-7} and 6.40×10^{-5} respectively.

The smaller values obtained for the PDMA and PDMA-GA sensors is an indication of the poor sensitivity when compared to PDMA-GA. These results proved that the PDMA-GA sensor was very sensitive when compared to the PDMA and PDMA-GO sensors and thus has the potential to be used in real samples.

5.6 Reproducibility, Stability and Interference Studies

Stability and reproducibility studies were carried out to test the performance of the modified SPCE/PDMA-GA electrode. Cyclic voltammetric analysis repeatedly for 5 successive measurements (n = 5) in 0.1 M Phosphate buffer containing ethanol towards the oxidation of estradiol (1.0×10^{-4} M) gave a 1.5 % reduction relative to standard deviation indicating good reproducibility for the sensor. After monitoring the sensor for three weeks at an interval of three days to check for storage ability in which it was stored in the refrigerator at 5°C, 88.86 % of its initial current response was recovered. In this study the influences of other organic compounds on the peak current of estradiol were investigated and the results are presented in **Table 8**. Ascorbic acid, caffeine, vitamin B and phenol almost do not interfere with the determination of estradiol, however the influence of estrone and estradiol are serious. These compounds are hydrophobic and contain a hydroxy group, which may cause the oxidation of the benzene ring. This in turn will cause an increase to the oxidation peak current of estradiol.

The characteristics of the proposed electrode were compared with those reported in the literature to estradiol detection as shown in T**able 9.** It can be noted that the PDMA-GA sensor presented a similar linear range and comparable limit of detection as compared to the other electrochemical sensors developed to determine estradiol a clear indication of its potential use in real samples.

Table 8: Influences of other compounds on the peak current of 1×10^{-4} M estradiol. Scan rate 150 mVs^{-1}

Interferent	Concentration (M)	Signal Change (%)
Ascorbic acid	1×10^{-3}	0.93
Caffeine	1×10^{-3}	2.31
Vitamin B	1×10^{-3}	0.46
Phenol	1×10^{-3}	1.97
Estrone	1×10^{-3}	5.34
Estriol	1×10^{-3}	6.65

Table 9: Comparison of some reported electrodes for estradiol determination

Electrode	Linear Range (M)	Limit of Detection (M)	Reference
CTAB- Nafion	$2.5\times10^{-8} - 1.5\times 10^{-6}$	1.0×10^{-9}	152
Pt/MWNTs/GCE	$5.0\times10^{-7} - 1.5\times 10^{-5}$	1.8×10^{-7}	267
CNT/Ni(cyclam)-GCE	$5.0\times10^{-7} - 4.0\times 10^{-5}$	6.0×10^{-8}	154
MWNT-[bmin]PF6/GCE	$1.0\times10^{-8} - 1.0\times 10^{-6}$	5.0×10^{-9}	268
Poly(L-serine)/GCE	$1.0\times10^{-7} - 3.0\times 10^{-5}$	2.0×10^{-8}	269
(FeTPyPz)/CP	$4.5\times10^{-5} - 4.5\times 10^{-4}$	1.3×10^{-5}	270
RGO-DHP/GCE	$4.0\times10^{-7} - 4.5\times 10^{-4}$	7.7×10^{-8}	153
PDMA-GA	$2.5\times10^{-8} - 1.5\times 10^{-6}$	1.19×10^{-7}	This work

CHAPTER SIX

RESULTS AND DISCUSSION-PART 3

6.1 Conclusion

The aim of the research study towards the development of electrochemical sensors for the detection and quantification of estradiol has been achieved. The novel sensor has been based on conducting poly (2,5- dimethoxy polyaniline) doped with graphene nanocomposite which was synthesised chemically. The motivation and objective previously stated in chapter one were fully realised.

Chapter four of the thesis discussed the chemical preparation and characterisation of graphene oxide and graphene which was confirmed by various characterisation techniques. A thin sheet of graphene (thickness of 1.35 nm) was prepared and identified by AFM, and used in sample preparations.

Chapter five discusses the preparation, characterisation and catalytic properties of poly (2,5-dimethoxy polyaniline) (PDMA), poly (2,5-dimethoxy polyaniline) graphene oxide and poly (2,5-dimethoxy polyaniline) graphene modified screen printed electrodes, prepared chemically using in a situ polymerisation method. The modified screen printed electrodes revealed their catalytic properties for the first time, towards the oxidation of estradiol, in phosphate buffer mixed with ethanol used as the working electrolyte. A dynamic linear range of the anodic peak and estradiol concentration was over the range of 2.5×10^{-5} to 1.0×10^{-3} and a detection limit of 4.39×10^{-7} M was obtained.

The successful constructed platform has displayed a well and excellent reproducibility in the cyclic voltammetric measurements and a great sensitivity towards estradiol, providing low detection limits with excellent correlation to reported literature. The reason for this is the

combination of PDMA with graphene which has provided highly catalytical properties to the nanocomposite, improving the sensitivity and the determination of estradiol.

This work has provided a platform for developing a highly sensitive and selective electrochemical sensor for estradiol and has opened a promising route to an environmentally friendly method for the detection of environmental estrogens.

6.2 Future work and Recommendations

The following further investigations are envisaged as future work to research activities.

The proposed method of chemical preparation has proven to be efficient. However electrochemical deposition of the nanocomposite needs to be pursued.

The developed sensor based on graphene and poly (2,5-dimethoxy polyaniline) represents only a sample of the group of semiconductors. Further studies need to be done on other derivatives of polyaniline.

To produce more specific and sensitive sensor devices, sensor devices using gold, platinum and pencil electrodes should be explored. Additionally, more electrocatalytic research work on other environmental estrogens should be investigated.

REFERENCES

1. Rodriguez-Mozaz, S.; Marco, M.; Lopez de Alda, M.; Barceló, D. Biosensors for environmental monitoring of endocrine disruptors: a review article. *Bioanal Chem* **2004,** 378, 588–598.
2. Dempsey, E.; Diamonds, D.; Collier, A. Development of a biosensor for endocrine disrupting compounds based on tyrosinase entrapped within a poly (thionine) film *Biosensors Bioelectronics* **2004**, 20 (2), 367–377
3. Bevan, C.L.; Porter, D.M.; Prasad, A.; Howard, M.J.; Henderson, L.P. Environmental Estrogens Alter Early Development in Xenopuslaevis. *Environmental Health perspectives* **2003,** 11(4),488-496.
4. Amaral Mendes, J.J. The endocrine disrupter: a major medical challenge. *Food and Chemical Toxicology* **2002,** 40,781-788.
5. National Inst. of Environ. Health Sci. Endocrine Disruptorshttp://www.nieh.nih.gov/, Feb. **2007**
6. Colborn, T.; VomSaal, F, S.; Soto, A. Developmental Effects of Endocrine-Disrupting Chemicals in Wildlife and Humans. *Environmental Health Perspectives* **1993,** 5, 378-378.
7. Kase1, R.; Hansen, P.; Fischer, B.; Manz1, W.; Heininger, P.; Reifferscheid, G. Integral Assessment of Estrogenic Potentials of Sediment-Associated Samples. *Environmental Science Pollution Res* **2008,** 15 (1),75-83.
8. Ce´spedes, R.; Lacorte, S.; Raldu´, D.; Ginebreda, A.; Barcelo, D.; Pin, B. Distribution of endocrine disruptors in the Llobregat River basin (Catalonia, NE Spain). *Chemosphere* **2005** 61,1710–1719.

9. European Commission: European workshop on impact of endocrine disrupters on human health and the environment. Environmental and Climate Research Programme, DGXII, Report EUR 17549, **1997**.

10. Campbell, C. G.; Borglin, S. E.; Green, F. B.; Grayson, A.; Wozei, E.; Stringfellow, W. T. Biologically directed environmental monitoring, fate, and transport of estrogenic disrupting compounds in water: A review. *Chemosphere* **2006,** 65, 1265–1280.

11. Isidori, M.; Lavorgna, M.; Nardelli, A.; Parrella, A. Toxicity on crustaceans and endocrine disrupting activity on Saccharomyces cerevisiae of eight alkylphenols. *Chemosphere* **2006,** 64, 135–143.

12. Cajthaml, T.; Kresinova, Z.; Svobodova, K.; Monder, M. Biodegradation of endocrine-disrupting compounds and suppression of estrogenic activity by ligninolytic fungi. *Chemosphere* **2009,** 75, 745-750.

13. Pothitou, P.; Voutsa, D. Endocrine disrupting compounds in municipal and industrial wastewater treatment plants in Northern Greece. *Chemosphere* **2008,** 73,1716–1723.

14. Hintemann, T.; Schneider, C.; Scholer, H.F.; Schneider, R.J. Field study using two immunoassays for the determination of estradiol and ethinylestradiol in the aquatic environment. *Water Research* **2006**, 40, 2287-2294.

15. Tanaka, T.; Takeda, H.; Ueki, F.; Obata, K; Tajima, H.; Takeyama, H.; Goda, Y.; Fujimoto, S.; Matsunaga, T. Rapid and sensitive detection of 17β-Estradiolin environmental water using automated immunoassay system with bacterial magnetic particles. *Journal of Biotechnology* **2004,** 153-159.

16. Wen, Y.; Zhou, B.S.; Xu, Y.; Jin, S.W.; Feng, Y.Q. Analysis of estrogens in environmental waters using polymer monolith in polyether ether ketone tube solid- phase micro extraction combined with high performance liquid chromatography, *Journal of Chromatography A* **2006,** 1133, 21-28.

17. IARC (International Agency for Research on Cancer) Chemicals and Industrial Processes Associated with Cancer in Humans, Lyon, France. **1979,** 21, 279.

18. Verbeke, R.; Pottie, G.; Stevens, J. Quality of the meat after the application of anabolic agents in young calves. *Environmental Quality and Safety Supplement* **1976**, 5, 123-130.

19. Chang, H.S.; Choo, K.H.; Lee, B.; Choi. S.J. The methods of identification, analysis and removal of endocrine disrupting compounds (EDCs) in water. *Journal of Hazardous Materials* **2009,** 1-12

20. Ying, G.-G.; Kookana, R.S.; Chen, Z. On-line solid-phase extraction and fluorescence detection of selected endocrine disrupting chemicals in water by high-performance liquid chromatography. *Journal of Environmental Science and Health* **2002**, B37, 225–234.

21. Hattori, K.; Takeuchi, T.; Ogata, M.; Takanohashi, A.; Mikuni, K.; Nakanishi, K.; Imata, H. Detection of environmental chemicals by SPR assay using ranchedcyclodextrin as sensor ligand. *Journal of Inclusion Phenomena and Macrocyclic Chemistry* **2007,** 57, 339–342.

22. Draisci, R.; Palleschi, L.; Ferretti, E.; Marchiafava, C.; Lucentini, L.; Cammarata, P. Quantification of 17-estradiol residues in bovine serum by liquid chromatography–tandem mass spectrometry with atmospheric pressure chemical ionization. *Analyst* **1998**, 123, 2605–2609.

23. Fedeniuk, R.W.; Boison, J.O.; MacNeil, J.D. Validation of a gas chromatography–mass spectrometry method for the determination of pg/mL levels of 17-estradiol and 17-trenbolone in bovine serum. *Journal of Chromatography* **2004,** B 802, 307–315.

24. Draisci, R.; Volpe, G.; Compagnone, D.; Purificato, I.; delli Quadri, F. Development of an electrochemical ELISA for the screening of 17-estradiol and application to bovine serum. *Analyst* **2000,** 125, 1419–1423.

25. Wang, J. Electrochemical biosensors: Towards point-of-care cancer diagnostics. *Biosensors and Bioelectronics* **2006,** 21, 1887–1892.

26. Zhao, G.; Yang, X. A label-free electrochemical RNA aptamer for selective detection of theophylline. *Electrochemistry Communications* **2010**, 12,300–302.

27. Drummond, T.G.; Hill, M.G.; Barton, J.K. Electrochemical DNA sensors. *Nature Biotechnology* **2003**, 21, 1192-1199.

28. Li, N.; Lee, Y.; Ong, L.H. A polyaniline and nafion composite film as a rechargeable battery. *J Applied Electrochem* **1992**, 22, 512-516.

29. Trinidad, F.; Montemayer, M.C.; Fatas, E. Performance study of Zn/ZnC12, NH4C1/polyaniline/carbon battery. *J. Electrochem. Soc.* **1991,** 138, 3186-3189.

30. Teasdale, P.R.; Wallace, G.G. Molecular recognition using conducting polymers: basis of an electrochemical sensing technology. *Analyst* **1993**, 118, 329-324.

31. Bartlett, P.N.; Chung, S.K.L. Conducting polymer gas sensors --Part III. *Sensors and Actuators* 1989, 20, 287-292.

32. Dhawan, S.K.; Trivedi, D.C. EMI shielding with organic conductive polymers. *J. Electromagnetic Compatability* **1991,** 4, 1-4.

33. Trivedi, D.C.; Dhawan, S.K. Grafting of electronically conducting polyaniline on insulating surfaces. *J. Mater. Chem* **1992,** 2, 1091.

34. Paul, E.W.; Ricco, A.J.; Wrighton, M.S. Resistance of polyaniline films as a function of electrochemical potential and the fabrication of polyaniline based microelectronic devices. *J. Phys.Chem* **1985,** 89, 1441-1447.

35. Dhawan, S.K.; Trivedi, D.C. Electrochemical behaviour of polyaniline in aromatic sulphonic acids. *Poly. Inter.* **1991**, 25, 55.

36. Boyle, A.; Geniès, E.M.; Lapkowski, M. Application of electronic conducting polymers as sensors: polyaniline in the solid state for the detection of solvent vapours and polypyrolle for the detection of biological ions in solutions. *Synth. Met* **1989**, 28, 769.

37. Josowicz, M.; Applications of conducting polymers in potentiometric sensors Analyst. **1995,** 120, 1019.

38. Adeloju, S.B.; Wallace, G.G. Conducting polymers and the biological sciences: new tools for bio- molecular communications. *Analyst* **1996,** 121, 699.

39. Dhawan, S.K.; Trivedi, D.C. Investigations on the effect of 5- sulphosalicyclic acid on the properties of polyaniline. *Synth Met* **1993,** 120, 309.

40. Dhawan, S.K.; Kumar, D.; Ram, M.K.; Chandra, S.; Trivedi, D.C. Application of conducting polyaniline as sensor material for ammonia. *Sensors and Actuators* **1997,** B 40, 99-103.

41. Watanabe, A.; Mori, K.; Iwasaki, Y.; Nakamura, N.K. *Macromolecules* **1987**, 20, 1793.

42. MacDiarmid, A.G.; Chiang, J.C.; Epstein, A.J. *Faraday Discuss Chem. Soc.* **1989** 88, 317.

43. Geim, A.K.; Novoselov, K.S. *Nat Mater* **2007,** 6, 183

44. Novoselov, K.S.; Geim, A.K.; Morozov, S.V.; Jiang, D,; Zhang, Y.; Dubonos, S.V. ;Grigorieva, A.A. Firsov, *Science* (Washington, DC) 306 ,**2004**, 666.

45. Ohta, T.; Bostwick, A.; Seyller, T.; Horn, K.; Rotenberg, E. *Science* (Washington D.C) 313, **2006,** 951.

46. Pumera, M. *Chem Rec*. **2009,** 9, 211.

47. Liang, M.; Zhi, L. *J. Mater.Chem* **2009,** 19, 5871.

48. Yang, W.; Ratinac, K.R.; Ringer, S.P.; Thordason, P.; Gooding, J.J.; Braet, F.; Angew. *Chem.Int. Ed. Engl*. **2010**, 49, 2114.

49. Shao, Y.; Wang, J.; Wu, H.; Liu, J.; Aksay, I.A.; Lin, Y. *Electroanalysis* (NY) **2010,** 22, 1027

50. Pumera, M.; *Chem. Eur J.* **2009**, 15, 4970

51. Banks, C.E.; Crossley, A.; Salter, C.; Wilkins, S.J.; Compton, R.G.; *Angew. Chem. Int. Ed. Engl* **2006,** 45, 2533.

52. Pumera, M.; Iwai, H. *J. Phys. Chem* .**2009**, C 113, 4401.

53. ŠLjukic, B.; Banks, C.E.; Compton, R.G. *Nano Lett* **2006**, 6, 1556.

54. Pumera, M.; Iwai, H. *Chem. Asian J*. **2009,**554.

55. Dai, X.; Wildgoose, G.G.; Compton, R.G. *Analyst* (Cambridge, UK) **2006,** 131 ,901

56. Batchelor-McAuley, C.; Wildgoose, G.G.; Compton, R.G.; Shao, L. *M.L.H. Green, Sens, Actuators* **2008**, B 132, 356.

57. Pumera, M.; Iwai, H. Miyahara, Y. *Chem. Phys. Chem*. **2009**, 10, 1770.

58. Pubchem.ncbi.nlm.nih.gov/compound/estradiol.

59. Ying, G.G.; Kookana, R.S.; Chen, Z. On-line solid-phase extraction and fluorescence detection of selected endocrine disrupting chemicals in water by high-performance liquid chromatography, *Journal of Environmental Science and Health B37* **2002**, 225-234.

60. Hattori, K.; Takeuchi, T.; Ogata, M.; Takanohashi, A.; Mikuni, K.; Nakanishi, K.; Imata, H. Detection of environmental chemicals by SPR assay using branched cyclodextrin as sensor ligand, *Journal of Inclusion Phenomena and Macrocyclic Chemistry 57* **2007**, 339-342.

61. Draisci, R.; Palleschi, L.; Ferretti, E.; Marchiafava, C.; Lucentini, L.; Cammarata, P. Quantification of 17β – estradiol residues in bovine serum by liquid chromatography-tandem mass spectrometry with atmospheric pressure chemical ionization, *Analyst* 123 **1998**, 2605-2609.

62. Fredeniuk, R.W.; Boison, J.O.; MacNeil, J.D. Validation of a gas chromatography-mass spectrometry method for the determination of pg/mL levels of 17 β – estradiol and 17β-trenbolone in bovine serum, *Journal of Chromatography B 802* **2004**, 307-315.

63. Draisci, R.; Volpe, G.; Compagnone, D.; Purificato, I.; delli Quadri, F. Development of an electrochemical ELISA for the screening of 17β-estradiol and application to bovine serum, *Analyst* 125, **2000**, 1419-1423.

64. Lad, U.; Khokhar, S.; Kale, G.M. Electrochemical creatinine biosensors, *Analytical Chemistry* 80, **2008**, 7910-7917.

65. Hu, S; Wu, K, Yi, H, Cui, D: Voltammetric behaviour and determination of estrogens at Nafion-modified glassy carbon electrode in the presence of cetyltrimethyl- ammonium bromide, *Analytica Chimica Acta* 464 (**2002**) 209-216.

66. Janegitz, B.C.; dos Santos, A.F.; Faria, R.C.; Zucolotto, V.; Electrochemical determination of estradiol using a thin film containing reduced graphene oxide and dihexadecylphosphate. *Materials Science and Engineering* C37 (**2014**) 14-19

67. Liu, X; Wong, D.K.Y.; Electrocatalytic detection of estradiol at a carbon nanotube|Ni(Cyclam) composite electrode fabricated based on a two-factorial design. *Analytica Chimica Acta* 594 (**2007**) 184-191.

68. History of Natural and Synthetic Polymers. chemrat.com

69. Duke, C.B.; Schein, L.B. Organic solids: is energy- based theory enough. *Physics today*, **1980**, 33, 42-48.

70. Bloor D.; Movaghar B; Conducting polymers. IEEE proceedings **1983**, 130, 225- 232

71. Trojanowicz, M.; velKrawczyk, T.K. Electrochemical biosensors based on enzyme immobilized in electropolymerized films *Mikrochim.Acta* **1995**, 121, 167-181.

72. Situmorang, M.; Gooding, J.J.; Hibbert, D.B.; Barnett, D. Electrodeposited polytyramine as an immobilization matrix for enzyme biosensors. *Biosensors bioelectronics* **1998** 13, 953-962.

73. Schumann, W.; Conducting polymers and their application in amperometric biosensors. *Mikrochim. Acta* **1995**, 121, 1-29.

74. Wring, S.A.; Hart, J.P.; Chemically modified carbon-based electrodes and their application as electrochemical sensors for the analysis of biological important compounds. *Analyst* **1992**, 117, 1215-1229.

75. Guiseppe-Elie A.; Wallace, G.G.; Matsue, T. Chemical and biological sensors based on electrically conducting polymers. In: Skotheim T., Elsenbaumer R., Reynolds J.R.,'Handbook of conducting polymers, 2nd ed. Marcel Dekker, New York, pp693-991 Chapter 34.

76. Bidan G.; Electroconducting conjugated polymers, new sensitive matrices to build chemical or electrochemical sensors A review. *Sens. Actuat.* **1992**, B 6, 45-56

77. Greene, R. L.; Street, G.B.; Suter, L.J. Superconductivity in polysulfur nitride $(SN)_x$, *Phys. Rev. Lett* **1975,** 34, 577-579.

78. Minot, M.J.; Peristein, J.H.; Mixed valence square planar complexes: a new class of solids with high electrical conductivity in one dimension. *Phys. Rev. Lett*. **1971**, 26,371-373.

79. Shirakawa, H.; Louis, E.J.; MacDiarmid, A.G.; Chiang, C.K.; Heeger, A.J. Synthesis of electrically conducting polymers: halogen derivatives of polyacetylene,$(CH)_x$. *J. Chem. Soc. Chem. Cummun*. **1977**, 578.

80. Ivory, D.M.; Miller, G.G.; Sowa, J.M.; Shacklette, L.W.; Chance, R.R.; Baughman, R.H. Highly conducting charge transfer complexes of poly (p-phenylene). *J. Chem. Phys* **1979**, 71, 1506-1507.

81. Rabolt, J.F.; Clarke, T.C.; Kanazawa, K.K.; Reynolds, J.R.; Street, G.B. Organic metals: poly (p-phenylene sulphide) Hexafluoroarsenate. *J.Chem. Soc.Chem. Commun* **1980**, 347-348.

82. Kanazawa, K.K.; Diaz, A.F.; Geiss, R.H.; Gill, W.D.; Kwak, J.F.; Logan, J.A.; Rabolt, J.F.; Street, G.B. Organic metals: polypyrolle, a stable synthetic metallic polymer. *J. Chem. Soc. Chem. Commun*. **1979**, 854-855.

83. Tourillon, G.; Garnier, F.; Stability of conducting polythiophene and derivatives. *J. Electrochem. Soc*. **1983**, 130, 2042-2044.

84. Heeger A.J.; In: Skotheim, T.A.(Ed.), Handbook of Conducting Polymers, vol II , Marcel Dekker, New York, 729 and references therein. **1986**.

85. Kroschwitz, J.I. In: Kroschwitz, J.I. (Ed.) Electrical and Electronic Properties of Polymers. Wiley, New York. **1988**.

86. Gerard M.; Chaubey A.; Malhotra B.D.; Application of conducting polymers to biosensors. *Biosensors and Bioelectronics* **2002**, 17, 345-359.

87. Wang, J. Analytical electrochemistry Second Ed. John Wiley & Sons, Inc., New York, NY 10158-0012, **2006**, 31-32

88. Tan, S. N.; Ge, L.; Tan, H.Y.; Loke, W.K.; Gao, J.; Wang, W. Paper-based enzyme immobilization for flow injection electrochemical biosensor integrated with a reagent loaded cartridge towards portable modular device. *Analytical Chemistry* **2012**, 84, 10071-10076.

89. Geoghenan, M.; Hadziioannou, G. Polymer Electronics, Oxford University Press, 22 **2013**

90. Saini, P.; Choudhary, V. Structural details, electrical properties, and electromagnetic interference shielding response of processable copolymers of aniline. *Journal of Materials science* **2013**, 48, 797-804.

91. Van Krevelen, D.W.; Te Nijenhuis, K. Properties of polymers: their correlation with chemical structure; their numerical estimation and prediction from additive group contributions, Access Online via Elsevier, **2009**.

92. Moliton, A.; Hiorns, R.C. Review of electronic and optical properties of semiconducting π-conjugated polymers: applications in optoelectronics. *Polymer International* **2004**, 53, 1397-1412.

93. Jaiswal, M.; Menon, R. Polymer electronic materials: a review of charge transport. *Polymer International* **2006**, 55, 1371-1384.

94. Tovide, O.O. Graphenated polyaniline nanocomposites for the determination of polyaromatic hydrocarbons in water. **2013**.

95. Noufi, R.; Frank, A.J.; Nozik, A.J. Stabilization of n-type silicon photoelectrodes to surface oxidation in aqueous electrolyte solution and mediation of oxidation reaction by surface attached organic conducting polymers. *J. Am. Chem. Soc.* **1981**, 103, 1849-1850.

96. Noufi, R.; Tench, D.; Warren, L.F.; Protection of n- Ga As photoanodes with photoelectrochemically generated polypyrolle films. *J. Electrochem. Soc* **1980**, 127, 2310-2311.

97. Bull, R.A.; Fan, F.R.; Bard, A.J. Polymer films on electrodes. *J. Electrochem. Soc* **1983**, 130, 1636-1638.

98. Audebert, P.; Bidan, G. Polyhalopyrolles: Electrochemical synthesis and some characteristics. *J. Electroanal. Chem* **1985**, 190,129-139

99. Saraswathi, R.; Gerard, M.; Malhotra, B.D. Characteristics of aqueous polycarbazole batteries. *J. Appl. Polym. Sci.* **1999**, 74, 145-150.

100. Kawai, T.; Kuwabara, T.; Wang, S.; Yoshino, K.; Secondary battery characteristics of poly(3-alkylthophene) . *Jap. J. Appl. Phys*. **1990**, 29,602-605.

101. Santhanam, K.S.V.; Gupta, N.; Conducting-polymer electrodes in batteries. TRIP 1, **1993**, 284-289.

102. Gazard, M., In: Skotheim, T.A. (Ed.), Handbook of Conducting Polymers, vol. 1. Marcel Dekker, USA. **1986**, 673.

103. Zinger, B.; Miller, L.L.; Timed release of chemicals from polypyrolle films. *J. Am. Chem. Soc*. **1984**, 106, 6861-6863.

104. Friend, R.H. (Ed.). Conductive Polymer II, Rapra Review Report, 6 (3), 23. **1993**.

105. Iwuoha, E.I.; Villaverde, D.S.; Garcia, N.P.; Smyth, M.R.; Pingarron, J.M. Biosens. Bioelectron. **1997**, 12. 749.

106. Han, M.G.; Cho, S.K.; Oh, S.G.; Im, S.S. *Synth. Met* **2002**, 126, 53.

107. Zhang, Z.; Wei, Z.; Zhang, L.; Wan, M. *Acta Materialia* **2005**, 53, 1373.

108. Luo, X.; Killard, A.J.; Morrin, A.; Smyth, M.R. *Anal Chim. Acta* **2006**, 575, 39.

109. Xue, W.; Fang, K.; Qiu, H.; Li, J.; Mao, W.; *Synth. Met* **2006**, 156, 506.

110. Huang, L.M.; Wen, T.C.; Gopalan, A. *Synth. Met*. **2002**, 130, 155.

111. Wei, Y.; Focke, W.W.; Wnek, G.E.; Ray, A.; Macdiarmid, A.G.; *J. Phys. Chem*. **1989**, 93, 495.

112. Gök, A.; Sari, B.; Talu, M. *Synth. Met*. **2004**, 142, 41.

113. Leclerc, M.; Guay, J.; Dao, L.H. *Macromolecules* **1989**, 22, 641.

114. Zheng, W.Y.; Levon, K.; Laasko, J.; Osterholm, J.E. *Macromolecules* **1994**, 27, 54.

115. Pandey, S.S.; Annapoomi, S.; Malhotra, B.D. *Macromolecules* **1993**, 26, 3190.

116. Kim, B.J.; Oh, S.G.; Han, M.G.; Im, S.S. *Langmuir* **2000**, 16, 5841.

117. Guramoto, N.: Genies, E.M. *Synth. Met*. **1995**, 68, 191.

118. Lu, X.; Yu, Y.; Chen, L.; Mao, H.; Zhang, W.; Wei, Y. *Chem. Lett*. **2004**, 33, 512.

119. Kun, H.; Xiao-Hong, M.; Meixiang, W. *J.Appl. Polym. Sci*.**2006**, 100, 3050.

120. Wei, Z.; Wan, M. *Adv. Mater* **2002**, 14, 1314.

121. Jing, L.; Kun, F.; Hong, Q.; Shouping, Li.; Weimin, M. *Synth. Met*. **2004**, 142, 107.

122. Kathleen, G.; Killard, A.J.; Hanson, C.J.; Cafolla, A.A.; Smyth, M.R. *Talanta* **2006**, 68, 1591.

123. Njuguna, J.; Pielichowski, K.; *J. Mater Sci*. **2004**, 39, 4081.

124. Malinaus, A. *Polymer* **2001**, 42, 3957.

125. Lund, H.; Hammerich, O.; Organic Electrochemistry, Marcel Dekker Inc.: New York, **1991**.

126. Benjan, D.; Duca, A.; Croatia *Chemica Acta* **1998**, 71, 745.

127. Chiang, J.C.; Macdiarmid, A.G.; *Synthetic Metals*. **1986**, 13, 193.

128. Macdiarmid, A.G.; Chiang, J.C.; Richter, A.F.; Epstein, A.J.; Synth. Met. **1987**, 18, 285.

129. Heinze, J.; Frontana-Uribe, B.; Ludwigs, S.; Electrochemistry of conducting polymer-persistent models and new concepts. *Chemical reviews* **2010**, 110, 8, 4724-4771, ISSN0009-2665.

130. Palys, B.; Kudelski, A.; Syankiewicz, A.; Jackowska, K.; Influence of anions on formation and electroactivity of poly (2,5-dimethoxy aniline). *Synthetic Metals*, **2000**, 108, 111-119.

131. Alvial, G.; Matencio, T.; Neves, B.R.A.; Silva, G.C.; Blends of poly (2,5-dimethoxy aniline) and fluoropolymers as protective coatings. *Electrochimica Acta*, **2004**, 49, 3507-3516.

132. Huang, L.M.; Wen, T.C.; Gopalan, A.; Ren, F.; Synthesis and characterisation of soluble conducting poly(aniline-co-2,5-dimethoxyaniline). *Material Letters*, **2003**, 57, 1765-1774.

133. Chen, S.S.; Wen, T.C.; Gopalan, A.; Electrosynthesis and characterisation of conducting copolymer having S-S links. *Synthetis Metals*, **2003**, 132, 133-143.

134. Patil, V.; Sainkar, S.R.; Patil, P.P.; Growth of poly (2,5-dimethoxy aniline) coatings on low carbon steel. *Synthetic metals*, **2004**, 140, 57-63.

135. Bavastrello, V.; Sutra, E.; Carrara, S.; Erokhin, V.; Nicolini, C.; poly- (2,5-dimethoxy aniline)-MWNTs nanocomposite a new material for conductometric acid vapour sensors. *Sensors and Actuators* B, **2004**, 98, 247-253.

136. Somerset, V.S.; Mercaptobenzothiazole-on-gold biosensors systems for organophosphate and carbamate pesticide compounds.**2007**

137. Fedorko, P.; Trznadel, M.; Pron, A.; Djurado, D.; Planés, J.; Travers, J. New analytical approach to the insulator-metal transistion in conductive polyaniline. *Synthetic metals*, **2010** Vol. 160, 15-16, 1668-1674, ISSN0379-6779.

138. Geniés, E.M.; Boyle, A.; Lapkowski, M.; Tsintavis, C. Polyaniline- A historical survey. *Synth. Met*. **1990,** 36, 2, 139-182, 0379-6779.

139. Pron, A.; Rannou, P. Processible conjugated polymers: from organic semiconductors to organic metals and superconductors. *Progress in polymer science* **2002**, 27, 1, 135-190, ISSN0079-6700.

140. Wallace, G.; Spinks, G.; Kane-Maguire, L.; Teasdale, P. Conductive Electroactive Polymers. **2009** CRC Press, Taylor & Francis Group, ISBN 978-1-4200-6709-5, Boca Raton.

141. Stejskal, J.; Sapurina, I.; Trchová, M. Polyaniline nanostructures and the role of aniline oligomers in their formation. *Progress in polymer science* **2010**, 35, 12, pp 1420-1481, ISSN0079-6700.

142. Tanaka, K.; Wang, S.; Yamabe, T. Will bipolarons be formed in heavily oxidized polyaniline? *Synthetic metals* **1990**, 36, 1, 129-135, ISSN0379-6779.

143. Patil, R.; Harima, Y.; Yamashita, K.; Komaguchi, K.; Itagati, Y.; Shiotani, M. Charge carriers in polyaniline film: a correlation between mobility and in-situ ESR measurements. *Journal of Electroanalytical Chemistry* **2002**, 518, 1, 13-19, ISSN 1572-6657.

144. Chiang, J.; MacDiarmid, A. Polyaniline: Protonic acid doping of the emeraldine form to the metallic regime. *Synthetic metals* **1986**, 13, 1-3, 193-205, ISSN0379-6779.

145. Tanaka, J., Mashita, N., Mizoguchi, K., Kume, K., (1989), "Molecular and electronic structures of doped polyaniline" *Synthetic metals*, Vol. 29, No. 1, (March **1989**), pp 175-184, ISSN0379-6779.

146. Inzelt, G. Conducting polymers- A New Era in Electrochemistry. *Springer-Verlag*, **2008**, ISBN 978-3-540-75929, Berlin, Heidelberg.

147. Monkman, A.; Adams, P. Optical and electronic properties of stretch-orientated solution-cast polyaniline films. *Synthetic metals* **1991**, 40, 1, 87-96, ISSN0379-6779.

148. Zhou, H.; Wen, J.; Ning, X.; Fu, C.; Chen, Kuang, Y. Electrosynthesis of polyaniline films on titanium by pulse potentiostatic method. *Synthetic metals*, **2007**, 157, 2-3,

98-103, ISSN0379-6779.

149. Probst, M.; Holze, R. Time-and temperature-dependent changes of the in situ conductivity of polyaniline and polyindole. *Electrochimica Acta* **1995**, 40, 2, 213-219, ISSN0013-4686.

150. Kankare, J. Electronically conducting ploymers: Basic methods of synthesis and characterization, In: Electrical and Optical polymer Systems: Fundamental methods and applications, Ed. By: Wise, D.; Wnek, G.;Trantolo, D.; Cooper, J.; Gresser, D. pp. 167-199, Marcel Dekker, ISBN 0824701186, New York. **1998.**

151. Mandic, Z.; Duic, Lj.; Kovacicek, F. The influence of counter-ions on nucleation and growth of electrochemically synthetized polyaniline film. *Electrochimica Acta*, **1997**. 42, 9, 1389-1402, ISSN0013-4686.

152. Zotti, G.; Cattarin, S.; Commis, N. Cyclic potential sweep polymerization of aniline: The role of anions in the polymerization mechanism. *Journal of Electroanalytical Chemistry and Interfacial electrochemistry* **1988**, 239, 1-2, 387-396, ISSN1572-6657.

153. Bade, K.; Tsakova, V.; Schultze J. Nucleation, growth and branching of polyaniline from microelectrode experiments. *Electrochimica Acta* **1992**, 37, 12, 2255-2261, ISSN0013-4686.

154. Córdova, R.; del Valle, M.; Arratia, A.; Gomez, H.; Schreiber, R. Effects of anions on the nucleation and growth mechanism of polyaniline. *Journal of Electroanalytical Chemistry and Interfacial electrochemistry* **1994**, 377, 1-2, 75-83, ISSN1572-6657.

155. Inzlet, G.; Pineri, M.; Schultze, J.; Vorotyntsev, M. Electron and proton conducting polymers: recent developments and prospects. *Electrochimica Acta* **2000**, 45, 15-16, 2403-2421 ISSN0013-4686.

156. Cruz, C.; Ticianelli, E.; Electrochemical and ellipsometric studies of polyaniline films grown under cyclic conditions. *Journal of Electroanalytical Chemistry*, **1997**.428, 1-2, 185-192, ISSN1572-6657.

157. Arsov L.J.; Plieth, W.; KoBmehl. Electrochemical and Raman spectroscopic studies of polyaniline; influence of the potential on the degradation of polyaniline. *Journal of Solid State Electrochemistry* **1998**, 2, 5, 355-361, ISSN1432-8488.

158. Lapkowski M. Electrochemical synthesis of linear polyaniline in aqueous solutions. *Synthetic Metals* **1990**, 35, 1-2,169-182 ISSN0379-6779.

159. Pruneanu, S.; Csahók, E.; Kertész, V.; Inzelt, G. Electrochemical quartz crystal microbalance study of the influence of the solution composition on the behaviour of polyaniline electrodes. *Electrochimica Acta*, **1998** .43, 16-17, 2305-2323, ISSN0013-4686.

160. Majidi, M.; Kane-Maguire, L.; Wallace, G. Enatioselective electropolymerization of aniline in the presence of (+) or (-) camphorsulfonate ion: a facile route to conducting polymers with preferred one-screw-sense helicity. *Polymer*, **1994**, 35, 14,3113-3115 ISSN0013-4686.

161. Huang, J.; Kaner, R.B. Nanofiber formation in the chemical polymerization of aniline: a mechanistic study. *Agnew. Chem. Int. Ed*. **2004**a, 43, 5817-5821, 1433-7851.

162. Huang, J.; Kaner, R.B. A general chemical route to polyaniline nanofibers. *J. Am. Chem. Soc*. **2004** b, 126, 3, 851-855, 0002-7863.

163. Zhang, Z.M.; Wei, Z.X.; Wan, M.X. Nanostructures of polyaniline doped with inorganic acids. *Macromolecules*, **2002** 35, 15, 5937-5942, 0024-9297.

164. Qui, H.J.; Wan, M.X.; Matthews, B.; Dai, L.M. Conducting polyaniline nanotubes by template-free polymerization. *Macromolecules*, **2001** 34, 4, 675-677, 0024-9297.

165. Wei, Z.X.; Wan, M.X. Hollow microspheres of polyaniline synthesized with an aniline emulsion template. *Adv.Mater*. **2002**, 14, 18, 1314-1317, 0935-9648.

166. Do Nascimento, G.M.; Silva, C.H.B.; Temperini, M.L.A. Electronic structure and doping behaviour of PANi-NSA nanofibers investigated by resonance Raman spectroscopy. *Macromol Rapid Commun*, **2006** 27, 4, 255-259, 1022-1336.

167. Gao, H.; Jiang, T.; Han, B.; Wang, Y.; Du, J.; Liu, Z.; Zhang, J. Aqueous/ionic liquid interfacial polymerization for preparing polyaniline nanoparticles. *Polymer*, **2004**, 54, 9, 3017-3019, 0032-3861.

168. Rodrigues, F.; Do Nascimento, G.M.; Santos, P.S. Dissolution and doping of polyaniline emeraldine base in imidazolium ionic liquids investigated by spectroscopic techniques. *Macromol. Rapid Commun* **2007**, 28, 5, 666-669, 1022-1336.

169. Davis Jr.; J.H., Gordon, C.M.; Hilgers, C.; Wasserscheld, P. Synthesis and purification of ionic liquids, In" Ionic Liquids in Synthesis Wassercheid, P.& Welton, T. (Eds.), 7-40, Wiley-VCH, 3-527-60070-1, New York. **2002.**

170. Wasserscheid, P.; Keim, W. Ionic liquids- New" solutions" for transition metal catalysis. *Angew. Chem. Int. Ed*. **2000**, 39, 21, 3773-3789, 1433-7851.

171. Dupont, J. On the solid, liquid and solution structural organization of imidiazolium ionic liquids. *J. Braz. Chem. Soc.* **2004**, 15, 3, 341-350, 0103-5053.

172. Earle, M.J.; Esperança, J.M.S.S.; Gilea, M.A.; Lopes, J.N.C.; Rebelo, L.P.N.; Magee, J.W.; Seddon, K.R.; Wildegren, J.A. The distillation and volatility of ionic liquids. *Nature*, **2006** 439, 7078, 831-834, 0028-0836.

173. Do Nascimento, G.M. Spectroscopy of Polyaniline Nanofibers. *Nanofibers* **2010**, 438 isbn 978-953-7619-86-2.

174. Shultz, J.S.; Taylor, R.F.; Introduction to chemical and biological sensors **1996.**

175. Nylander, C. Chemical and biological sensors. Journal of Phys E. Sci. Instrum, **1985**, 18.

176. Stetter, R.J.; Penrose W.R.; Yao S. Sensors chemical sensors, electrochemical sensors. *Journal of the electrochemical society* **2003**, 150**,** S11-S16.

177. Hulanicki, A.; Glab S.; Folke I. Chemical sensors definitions and classification. *Pure and applied chemistry* **1991**, 63, 9, 1247-1250.

178. Thévenot D.R.; Toth, K.; Durst R.A.; Wilson, G.S. Electrochemical biosensors: recommended definitions and classifications. *Biosensors and Bioelectronics* **2001**, 16, 121-131.

179. Shultz, J.S.; Taylor, R.F. Handbook of chemical and biological sensors. Taylor and Francis **1996**.

180. Klink, M.J. Development of Polyaniline Nanotube Electrocatalysts and Sensor Devices for Phenolic- Pollutants **2007**.

181. Skoog, D.A.; West, D.M.; Holler, F.J.; Crouch, S.R. Skoog and West's Fundamentals of Analytical Chemistry. 9th edition.

182. P. Zanello; Inorganic Electrochemistry, Theory, Practice and Applications, Cambridge, UK: The Royal Society of Chemistry, **2003.**

183. Bard, A.J.; Faulkner, L.R.; Electrochemical Methods, Wiley & Sons, New York, **2001**; Chapters 3, 5, 7, 10 and 13.

184. Schmickler, W.; Interfacial Electrochemistry. Oxford University Press, Oxford, **1996**.

185. Parsons, R. Chem Rev, **1990**, 90, 813.

186. Randles, J.E.B.; Trans Faraday Soc, **1984**, 44, 327.

187. Pankaj, S.; et al, Anal Chem, **1997**, 69, 1662

188. Macdonald, J.R.; Impedance Spectroscopy, Wiley/ Interscience, New York, 1987.

189. Keddam, M.; Mattos, O.R.; Takenouti, H.J.J. *Electrochem. Soc*, **1981**, 128,257,266

190. Schmidt, E.; et al. *Electrochim Acta*, **1986**, 31, 1041.

191. Cai, M; Park, S.M.; *J. Electrohem. Soc.* **1996**, 143, 2125.

192. Cha, D.K.; Park, S.M.; *J. Electrochem. Soc*. **1997**, 144, 2573.

193. Lay, P.; et al; *J.Appl Electrochem*. **1985**, 15, 755.

194. Karunathilaka, S.A.G.R. ; *J.Appl Electrochem*. **1983**, 13, 577.

195. Cha, D.K.; Park, S.M.; *J. Electroanal Chem. Soc*. **1998**, 459, 135.

196. Piao, T.; *J. Electrochem. Soc*. **1999**, 146, 2794.

197. Kim, Y-O.; Park, S.M.; *J. Electrochem. Soc.* **2001**, 148, A194.

198. Gabrielli, C.; Haas, O.; Takenouti, H. *J. Appl. Electrochem*, **1997**, 17, 82.

199. Johnson, B.; Park, S.M.; *J. Electrochem. Soc*. **1996**, 143, 1269.

200. Lee, J-Y; Park, S.M.; *J. Electrochem. Soc*. **2000**, 147, 4189.

201. Park, S-M; Yoo, S-J; Electrochemical Impedance Spectoscopy for Better Electrochemical Measurements, *J. Analytical Chemistry*, **2003**.

202. Margarita P., Quinteiro R., "Fourier Transform Infrared (FT-IR) Technology for the Identification of Organisms", *Clinical Microbiology Newsletter,* (22), No. 8 (**2000**).

203. Greensteet, J.E., Norris, K.P., "The existence of differences between the infrared absorption spectra of bacteria", *Spectrochim. Acta***,** 9: 177-182 (**1957**).

204. Goulden, J.D.S., Sharpe, M.E., "The infrared absorption spectra of lactobacilli", *J. Glen.Microbiol***.,** 19: 76-86 (**1958**)

205. Jackson, M., Mantsch, H., "Biomedical infrared spectroscopy:, In: Mantsch and D. Chapman (eds), *Infrared spectroscopy of biomolecules***,** Wiley-Liss, NY (**1996**).

206. Riddle, J.W. et al., "Bacterial identification by infrared spectrophotometry", *J.Bacteriol***,** 72: 593-603 (**1956**)

207. Maquelin K., Kirschner, C., :Identification of medically relevant microorganisms by vibrational spectroscopy", *Journal of Microbiological Methods***,** 51: 255-271 (**2002**),

208. Naumann, D., Fijala, V., Labischinski, H., :The rapid differentiation and identification of pathogenic bacteria using Fourier Transform Infrared spectroscopic and multivariate statistical analysis", *J.Mol,Struct***.,** 174: 165-170 (**1988**)

209. Gomez, M.A., Perez, M.A.B., Gil, F.J.M., "Identification of species of Brucella using Fourier transform infrared spectroscopy", *Journal of Microbiological Methods***,** 55: 121-131 (**2003**)

210. Lipkus, A.H., Chittur, K.K., Vesper, S.J., "Evolution of infrared spectroscopy as a bacterial identification method", J. Ind.Microbiol., 6:71-75 (**1990**).

211. Curk, M.C., Peledan F., Hubert, J.C.; "Fourier Transform infrared (FT-IR) spectroscopy for identifying Lactobacillus species", *FEMS Microbiol, Lett*., 123: 241-248 (**1994**).

212. Siebert, F., "Infrared spectroscopy applied to biochemical and biological problelms", In: Sauer, K (Ed), Biochemical Spectroscopy, *Methods in Enzymology*, 246: 501-526 (**1995**).

213. Jackson, M.; Sowa, M.G., "Infrared spectroscopy: a new frontier in medicine". *Biophys. Chem*., 68: 109-125 (**1997**).

214. Diem, M., Boydston-White, "Infrared spectroscopy of cells and tissues: shining light onto a novel subject", *Appl. Sepctrosc*., 53: 148-161 (**1999**).

215. Wenning, M., Seiler, H., Scherer, S., "Fourier-transform infrared microspectroscopy, a novel and rapid tool for identification of yeast", *Applied and Environmental Microbiology*, 68(10): 4717-4721 (**2002**).

216. Sacksteder, C., Barry, B.A., "Fourier Transform Infrared Spectroscopy: A Molecular Approach to an Organismal Question", *Journal of Phycology*, 37: 197-199 (**2001**).

217. Naumann, D., Infrared and NIR Raman spectroscopy in medical microbiology", In: Manch, H.H., Jackson, M. (Eds), Infrared Spectroscopy: New Tool in Medicine, *SPIE Proceeding Series (3257***)**, SPIE, Bellingham, WA, 245-257 (**1998**).

218. Naumann, D., et al., "The characterization of microorganisms by Fourier-transform infrared spectroscopy (FT-IR)", In W.H. Nelson (ed), Modern techniques for rapid microbiological analysis, VCH, NY (**1991**).

219. Duygu, D.C.; Baykal, T.; Aciköz, I; Yildiz, K; Fourier Transform Infrared (FT-IR) Spedtroscopy for Biological Studies, G.U. *Journal of Science*, **2009**, 22(3), 117-121.

220. Ahwalat, N.; Raman Spectroscopy: A Review, International journal of computer science and mobile computing, 3, 11, 680-685, **2014**.

221. Last, J.; Russel, P.; Nealy, F.P.; Murphy, C.J.; The Application of Atomic Force Microscopy to Vision Science, Investigative Opthalmology and Visual Science (IOVS), 51, 21, **2010.**

222. Barthelmy, D.; X-ray Diffraction, FEI, **2014.**

223. Science Research Education Center (SERC), X-ray Powder Diffraction, **2013**.

224. Moeck, P.; X-ray diffraction, Portland State University, **2004**.

225. James, R. X-ray Diffraction Http:// Spark.parklands.edu.ah/115, **2014**.

226. Fultz, B.; Howe, J. M. Transmission electron microscopy and diffractometry of materials, Springer, **2012**

227. Alem, N.; Erni, R.; Kisielowski, C.; Rossell, M.D.; Gannett, W.; Zettl, A. Atomically thin hexagonal boron nitride probed by ultrahigh-resolution transmission electron microscopy, *Physical review B* **2009**, 80, 155425.

228. Huang, P.Y.; Ruiz-Vargas, C.S.; van der Zande, A.M.; Whitney, W.S.; Levendorf, M.P.; Kevek, J.W.; Garg, S.; Alden, J. S.; Hustedt, C.J.; Zhu, Y. Grains and grain boundaries in single-layer graphene atomic patchwork quilts. *Nature* **2011**, 469, 389-392.

229. Straumal, B.B.; Mazilkin, A.A.; Baretzky, B.; Schuetz, G.; Rabkin, E.; Valiev, R. Z. Accelerated diffusion and phase transformations in Co-Cu alloys driven by the severe plastic deformation. *Materials Transactions* **2012**, 53, 63-71.

230. Jiang, W.; Atzmon, M. The effect of compression and tension on shear-band structure and nanocrystallization in amorphous Al₉₀Fe₅Gd₅: a

high-resolution transmission electron microscopy study. *Acta materialia* **2003**, 51, 4095-4105.

231. Yuk, J.M.; Park, J.; Ercius, P.; Kim, K.; Hellebusch, D.J.; Crommie, M.F.; Lee ,J.Y.; Zettl, A.; Alivisatos, A.P. High-resolution EM of colloidal nanocrystal growth using graphene liquid cells. *Science* **2012**, 336, 61-64.

232. Wells, O.C.; Joy, D.C. The early history and future of the SEM. Surface and interface analysis **2006**, 38, 1738-1742.

233. Hummers, W. s.; Offeman, R.E.; *J. Am. Chem. Soc*, **1958**, 80, 1339-1339.

234. Yang, D.; velamakanni, A.; Bozoklu, G.; Park, S.; Stoller, M.; Piner, D.R.; Stankovich, S.; Jung, I; Field, D.A.; Ventrice Jr, C.A.; Ruoff, R.S.; Chemical analysis of graphene oxide films after heat and chemical treatments by X-ray photoelectron and Micro-Raman spectroscopy, *Carbon*,47, 145-152, **2009**.

235. Shen, J.; Hu, Y. Shi, M., Lu, X.; Qin, C.; Ye, M.; Fast and facile preparation of graphene oxide and reduced graphene oxide nanoplatelets, *Chem. Matter*, 21, 3514-3520, **2009**.

236. Muvundla, S.E.; malgas, g.F.; Baker, P.B.; Iwuoha, E.I.; Synthesis and Characterisation of Novel Nanophase Hexagonal poly (2,5-dimethoxy aniline), *Electroanalysis*, 21, 2347-2353, **2008**.

237. Li, Z.; Zhang, H.; Liu, Q.; Sun, L.; Stanciu, l.; Xie, J.; fabrication of High-Surface- Area Graphene/Polyaniline Nanocomposites and their Appliactions in Supercapacitors, *Appl. Mater.interfaces*, 5, 2658-2691, **2013**.

238. Hu, S.; Wu, K.; Yi, H.; cui, D.; Voltammetric behaviour and determination of estrogens at nafion-modified glassy carbon electrode in the presence of cetyltrimethyl ammonium bromide, *Analytical Chimica Acta*, 464,209-216, **2002**.

239. Thema, F.T.; Moloto, M.J.; Dikio, E.D.; Nyangiwe, N.N.; Kotsedi, L.; Maaza, M.; Khenfouch, M.; Synthesis and characterization of graphene thin films by chemical reduction of exfoliated and intercalated graphite oxide. Hindawi Publishing Corporation, *Journal of Chemistry*, **2013.**

240. Pulchamy, B; Arthi, G; Lingesh, B.D.; A simple approach to stepwise synthesis of graphene oxide nanomaterial. *Journal of Nanomedicine and Nanotechnology*, 6, 2157-7439, **2015**.

241. Ferrari, A.C.; Robertson, J.; Interpretation of Raman spectra of disordered and amorphous carbon. *Phys, Rev. B* 61, 14095- 14107, **2000**.

242. Tuinstra, F.; Koenig, J.L.; Raman spectrum of graphite *J. Chem. Phys*. 53, 1126-1130, **1970.**

243. Ferrari, A.C; Meyer, J.C.; Scardaci, V.; Casiraghi, C,; Lazzeri, M.; Mauri, F.; Piscanec, S.; Jiang, D.; Novoselov, K.S.; Roth, S.; Geim, A.K.;Raman spectrum of graphene and graphene layers. *Phys. Rev. Lett* 97, 187401, **2006**.

244. Graf, D.; Molitor, F.; Ensslin, K.; Stampfer, C.; Jungen, A.; Hierold, C, Wirtz, L.; Spatially Resolved Raman spectroscopy of single- and few-layer graphene, Nano Lett. 7, 238-242, **2007**.

245. Shahriary, L.; Athawale, A.A.; Graphene oxide synthesized by using modified hummers approach, International Journal of Renewable Energy and Environmental Engineering, 2, 58-63, **2014**.

246. Stankovich, S.; Dikin, D.A.; Piner, R.D.; Kolhaas, K.A.; Kleinhammes, A.Jia, Y.; Wu, Y.; Nguyen, S.T.; ruoff, R.S.; Synthesis of graphene-based nanosheets via chemical reduction of exfoliated graphite oxide, Carbon, 45, 1558-1565, **2007**

247. Iwuoha, E.I.; Mavundla, S.E.; Somerset, V.S.; Petrik, L.F.; Klink, M.J.; Sekota, M.; Baker, P.; *Microchim Acta*, **2006**, 155, 453.

248. Bavastrello, V.; Stura, E.; Carrara, S.; Erokhin, V.; Nicolini,; *Sens. Actuators* **2004**, 98, 247.

249. Huang, J.; Kaner, R.B.; *J. Am. Chem.Soc*. **2004**, 4, 141.

250. Yin, P.; Kilmartin, P.A.; *Curr. Appl. Phys*. **2004**, 4, 141

251. Huang, J.; Wen, T.; Gopalan, A.; *Mater. Lett*. **2003**, 57, 1765.

252. Palys, B.; Kudelski, A.; Stankiewicz, K.; Jackowska, K.; *Synth. Met*. **2000**, 108, 111.

253. Chandrakanthi, M.; Careem, M.A.; *Polym. Bull*. **2000**, 45, 113.

254. Masikini, M.; Stephen, N.M.; Tsegaye, A.; Ikpo, C.O.; Njomo, N.; Waryo, T.; Baker, P.G.L.; Iwuoha, E.I.; In situ electrochemical synthesis, microscopic and spectroscopic characterisation of electroactive poly(2,5-dimethoxyaniline)- multiwalled carbon nanotubes composite films in neutral media.*Int. J. Electrochem. Sci*. **2014**, 9, 7003-7020.

255. Subrahman, K.; Vivekchand, S.; Gonvindaraj, A.; Rao, C. A study of graphenes prepaed by different methods: characterization, properties and solubilisation. *Journal of Materials Chemistry*. **2008**, 49, 4413-4419.

256. Lian, P.; Zhu, X.; Liang, S.; li, Z.; Yang, W.; wang, H.; Large reversible capacity of high quality graphene sheets as an anode material for lithium ion batteries. *Electrochim Acta*. **2010**, 55, 3909-3914.

257. Ehret, R,; Baumann, W.; Brischwein, M.; Scwinde, A.; Stegbauer, K.; Wolf, B.; Monitoring of cellular behaviour of impedance measurements on interdigitated electrode structures. *Biosensors and Bioelectronics*, **1997**, 12, 29-41.

258. Kang, X.; Mai, Z.; Zou, X.; Cai,P.; Mo, J.; a novel glucose biosensor based on immobilization of glucose oxidase in chitosan on a glassy carbon electrode modified with gold-platinum alloy nanoparticles/multiwall carbon nanotubes. *Analytical Biochemistry*. **2007**, 369, 71-79.

259. Wang, L.; Wang, E.; direct electron transfer between cytochromec and gold nanoparticles modified electrode. *Electrochemistry Communications*, **2004**, 6, 49-54.

260. Piro, B.; Haccoun, J.; Pham, M.C.; Tran, L.; Rubin, A.; Perrot, H.; Gabrielli, C.; Study of the DNA hybridisation transduction behaviour of aquinone-containing electroactive polymer by cyclic voltammetry and electrochemical impedance spectroscopy. *Journal of electroanalytical Chemistry*, **2005**, 577, 155-165.

261. Nian, Y.R.; Teng, H.; Nitric acid modification of activated carbon electrodes for improvement of electrochemical capacitance. *Journal of Electrochemical Society*. **2002**, 149, A1008-A1014.

262. Shah, A.H.A.; holze, R.: Spectroelectrochemistry of two layered composites of polyaniline and poly(o-aminophenol). *Eletrochimica Acta*. **2008**, 53, 4642-4653.

263. Brett, C.M.A.; Oliveira-Brett, A.M.; Electrochemistry Priciples, Methods and Applications. 2nd Ed.; Oxford University Press. Oxford UK.

264. Mathebe, N.G.; Morrin, A.; Iwuoha, E.I.; Electrochemistry and scanning electron microscopy of polyaniline/peroxidase-based biosensor. *Talanta*, **2004**, 64, 115-120.

265. Mailu, S.N.; Waryo, T.; Ndangili, P.; Ngece, F.R.; Baleg, A.A.; Baker, P.G.; Iwuoha, E.I.; Determination of anthracene on Ag-Au alloy nanoparticles/overoxidizedpolypyrolle composite modified glassy carbon electrodes. *Sensors*, **2010**, 10, 9449-9465.

266. Somerset, V.; Iwuoha, E.I.; Hernandez, L.; Stripping voltammetric measurements of trace metal ions at screen-printed carbon electrodes. *Procedia Chemistry*, **2009**, 1, 1279-1282.

267. Lin, X.Q.; Li, X.Y.; *Biosensensors Bioelectronics*. **2006**, 22, 253-259.

268. Tao, H.; Wei, W.Z.; Zeng, X.Y.; Liu, X.J.; Zhang, Y.M.; *Michrochim Acta*, **2009**, 166, 53-59.

269. Song, J.C.; Yang, X.M.; Hu, J.; *Apll. Electrochemistry*, **2008**, 38, 833-836.

270. Batista, M.V.; Lanz, M.R.V.; Dias, I.L.T.; Tanaka, A.A.; Sotomayor, M.; *Analyst*, **2008**, 133, 1692-1699.